

**T.C.
REPUBLIC OF TURKEY
HACETTEPE UNIVERSITY
GRADUATE SCHOOL OF HEALTH SCIENCES**

**PARENCHYMAL NEUROINFLAMMATION IN
FAMILIAL HEMIPLEGIC MIGRAINE TYPE 1
TRANSGENIC MOUSE MODEL AFTER CORTICAL
SPREADING DEPRESSION**

MSc. Anisa Dehghani Mohammadi

**Program of Basic Neuroscience
DOCTOR OF PHILOSOPHY THESIS**

ANKARA

2019

**T.C.
REPUBLIC OF TURKEY
HACETTEPE UNIVERSITY
GRADUATE SCHOOL HEALTH SCIENCES**

**PARENCHYMAL NEUROINFLAMMATION IN FAMILIAL
HEMIPLEGIC MIGRAINE TYPE 1 TRANSGENIC MOUSE
MODEL AFTER CORTICAL SPREADING DEPRESSION**

Anisa Dehghani Mohammadi (MSc.)

**Program of Basic Neuroscience
DOCTOR OF PHILOSOPHY THESIS**

**ADVISOR OF THE THESIS
Associate Prof. Dr. Hülya KARATAŞ-KURŞUN**

**ANKARA
2019**

PARENCHYMAL NEUROINFLAMMATION IN FAMILIAL
HEMIPLEGIC MIGRAINE TYPE 1 TRANSGENIC MOUSE MODEL
AFTER CORTICAL SPREADING DEPRESSION

Anisa Delghani Mohammadi

Supervisor: Associate Prof. Dr. Hülya KARATAŞ-KURŞUN

This thesis study has been approved and accepted as a PhD dissertation in "Basic Neuroscience Program" by the assesment committee, whose members are listed below, on 08/01/2019.

Chairman of the Committee:

Professor Dr. Turgay Dalkara (Signature)
Hacettepe University.



Member:

Professor Dr. Arn M.J.M. van den Maagdenberg (Signature)
Leiden University Medical Center



Member:

Professor Dr. Saban Remzi Erdem (Signature)
Baskent University



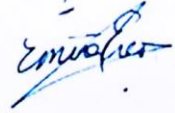
Member:

Professor Dr. Aygun Ertugrul (Signature)
Hacettepe University



Member:

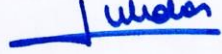
Professor Dr. Emine Eren Kocak (Signature)
Hacettepe University
Psychiatry



This dissertation has been approved by the above committee in conformity to the related issues of Hacettepe University Graduate Education and Examination Regulation.

Prof. Dr. Diclehan ORHAN

Institute Manager



15 Ocak 2019

YAYIMLAMA VE FİKRİ MÜLKİYET HAKLARI BEYANI

Enstitü tarafından onaylanan lisansüstü tezimin/raporumun tamamını veya herhangi bir kısmını, basılı (kağıt) ve elektronik formatta arşivleme ve aşağıda verilen koşullarla kullanıma açma iznini Hacettepe Üniversitesine verdiğimi bildiririm. Bu izinle Üniversiteye verilen kullanım hakları dışındaki tüm fikri mülkiyet haklarım bende kalacak, tezimin tamamının ya da bir bölümünün gelecekteki çalışmalarda (makale, kitap, lisans ve patent vb.) kullanım hakları bana ait olacaktır.

Tezin kendi orijinal çalışmam olduğunu, başkalarının haklarını ihlal etmediğimi ve tezimin tek yetkili sahibi olduğumu beyan ve taahhüt ederim. Tezimde yer alan telif hakkı bulunan ve sahiplerinden yazılı izin alınarak kullanılması zorunlu metinlerin yazılı izin alınarak kullandığımı ve istenildiğinde suretlerini Üniversiteye teslim etmeyi taahhüt ederim.

Yüksekoğretim Kurulu tarafından yayınlanan "*Lisansüstü Tezlerin Elektronik Ortamda Toplanması, Düzenlenmesi ve Erişime Açılmasına İlişkin Yönerge*" kapsamında tezimin aşağıda belirtilen koşullar haricinde YOK Ulusal Tez Merkezi / H.Ü. Kütüphaneleri Açık Erişim Sisteminde erişime açılır.

- Enstitü / Fakülte yönetim kurulu kararı ile tezimin erişime açılması mezuniyet tarihinden itibaren 2 yıl ertelenmiştir. ⁽¹⁾
- Enstitü / Fakülte yönetim kurulunun gerekçeli kararı ile tezimin erişime açılması mezuniyet tarihinden itibaren 6 ay ertelenmiştir. ⁽²⁾
- Tezimle ilgili gizlilik kararı verilmiştir

7.12.2018
(İmza)
Öğrencinin Adı SOYADI
Ayşe Değirici

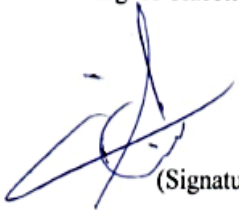
¹"*Lisansüstü Tezlerin Elektronik Ortamda Toplanması, Düzenlenmesi ve Erişime Açılmasına İlişkin Yönerge*"

- (1) Madde 6.1. Lisansüstü teze ilgili patent başvurusu yapılmış veya patent alma sürecinin devam etmesi durumunda, tez danışmanının önerisi ve enstitü anabilim dalının uygun görüşü üzerine enstitü veya fakülte yönetim kurulu iki yıl süre ile tezin erişime açılmasının ertelenmesine karar verebilir.
- (2) Madde 6.2. Yeni teknik, materyal ve metodların kullanıldığı, henüz makaleye dönüşmemiş veya patent gibi yöntemlerle korunmamış ve internetten paylaşılmış durumda 3. şahıslara veya kurumlara haksız kazanç imkanı oluşturabilecek bilgi ve bulguları içeren tezler hakkında tez danışmanının önerisi ve enstitü anabilim dalının uygun görüşü üzerine enstitü veya fakülte yönetim kurulunun gerekçeli karar ile altı ayı aşmamak üzere tezin erişime açılması engellenebilir.
- (3) Madde 7.1. Ulusal çıkarları veya güvenliği ilgilendiren, emniyet, istihbarat, savunma ve güvenlik, sağlık vb. konulara ilişkin lisansüstü tezlerle ilgili gizlilik kararı, tezin yapıldığı kurum tarafından verilir *. Kurum ve kuruluşlarla yapılan işbirliği protokolü çerçevesinde hazırlanan lisansüstü tezlerle ilişkin gizlilik kararı ise, ilgili kurum ve kuruluşun önerisi ile enstitü veya fakültenin uygun görüşü üzerine üniversite yönetim kurulu tarafından verilir. Gizlilik kararı verilen tezler Yükseköğretim Kuruluna bildirilir. Madde 7.2. Gizlilik kararı verilen tezler gizlilik süresince enstitü veya fakülte tarafından gizlilik kuralları çerçevesinde muhafaza edilir, gizlilik kararının kaldırılması halinde Tez Otomasyon Sistemine yüklenir

* Tez danışmanının önerisi ve enstitü anabilim dalının uygun görüşü üzerine enstitü veya fakülte yönetim kurulu tarafından karar verilir.

ETHICAL DECLARATION

In this thesis study, I declare that all the information and documents have been obtained in the base of the academic rules and all audio-visual and written information and results have been presented according to the rules of scientific ethics. I did not do any distortion in data set. In case of using other works, related studies have been fully cited in accordance with the scientific standards. I also declare that my thesis study is original except cited references. It was produced by myself in consultation with supervisor (Associate Prof. Dr. Hülya KARATAŞ-KURŞUN) and written according to the rules of thesis writing of Hacettepe University Institute of Health Sciences.



(Signature)

Student Name SURNAME

Anisa Delghai
Mohammed

To Khosrow, Homa, and Arash

ACKNOWLEDGEMENTS

I would like to express my sincere thanks to my supervisor Associate Prof. Dr. Hülya Karataş-Kurşun who strongly supported me during the course of my dissertation and for providing open-minded scientific environment and support, and her cooperative guidance till the end of this thesis. Further, I am deeply grateful to Prof. Dr. Turgay Dalkara, my mentor and director of the Institute of Neurological Sciences and Psychiatry, who deeply supported me during the course of my Ph.D. with his profound knowledge, and thought-provoking impulses. I could always rely on their supporting forces in securing scholarships and facilitating the way to realizing experiments and dealing with writing scientific concepts and analysis.

Sincere thanks are given to Prof. Dr. Arn M.J.M. van den Maagdenberg and Dr. Else A. Tolner for their precious advice and discussion on my thesis and providing the transgenic mice from their lab in Leiden University Medical Center, Human Genetic Department to our lab in Ankara. Thanks to Thas Phisonkunkasem for his help with the quantifications.

I would like to thank my other mentors in the Institute and Lab including Prof. Dr. Müge Yemişçi-Özkan and Associate Prof. Dr. Emine Eren-Koçak for their scientific contributions during my Ph.D. Many thanks to Dr. Sinem Yılmaz Özcan for her significant contribution in doing Western blotting part of this thesis, thanks to Dr. Buket Demir, Dr. Aslıhan Taşkıran, Assistant Prof. Dr. Gül Yalçın Çakmaklı, and Dr. Canan Çakır Aktaş, each for their great responsiveness and cooperative attitudes. My sincere thanks to all the Ph.D. students in the lab including Burak Uzay, Aslıhan Bahadır Varol, Gökhan Uruk, Gülce Küreli, Özlem Hökelekli, Zeynep Kaya, and Erknaz Ecehan Erk for their endless kindness and support in the lab, special thanks to our technician Mesut Fırat for all his sincere help in the Institute of Neurological Sciences and Psychiatry. I also thank Nursel İlikli, the secretary of the institute, for all her help and contributions in the logistic. I would like to thank Hacettepe University Research Projects Department for its support of my thesis project (HUBAP-Project no: THD-2018-15457).

ABSTRACT

Anisa D. M. Parenchymal neuroinflammation in familial hemiplegic migraine type 1 transgenic mouse model after cortical spreading depression. Hacettepe University Graduate School Health Sciences, Ph.D. Thesis in Basic Neuroscience, Ankara, 2019. Cortical spreading depression (CSD) is the likely cause of the migraine aura. CSD causes a signaling pathway between stressed neurons and trigeminal afferents via transient opening of neuronal Pannexin-1 (Panx1) mega-channels followed by high mobility group box 1 (HMGB1) release from neurons and nuclear factor kappa B (NF- κ B) relocation in astrocytes. Familial hemiplegic migraine type 1 (FHM1) is a rare monogenic subtype of migraine with aura caused by mutations in the *CACNA1A* gene. Transgenic knock-in mice that carry human FHM1 missense mutations R192Q or S218L exhibit an increased susceptibility to CSD and other features relevant to migraine. Here, we investigated the basal and experimentally CSD-induced parenchymal neuroinflammation in female mutant mice and wild-type (WT), and studied whether CSD-induced inflammation shows a particular regional pattern, which may highlight areas that are particularly relevant to disease pathology. Our data revealed a basal parenchymal neuroinflammatory state in R192Q mutant mice as revealed by higher neuronal HMGB1 release and NF- κ B activation in astrocytes. There was a different regional distribution pattern in the inflammatory signaling upon CSD in the frontal/parietal cortices and striatum/thalamus of both R192Q and WT mice. In addition, in mutant mice this inflammatory pattern was bilateral. There was a rise in HMGB1 release in subcortical areas of mutant mice compared to that in WT mice which was particularly pronounced in thalamus compared to striatum. Immunohistochemical data was supported by Western blotting in which cerebrospinal fluid (CSF) HMGB1 amount and brain nuclear translocation of NF- κ B was studied. S218L mutant mice showed more HMGB1 in CSF compared to WT and brain NF- κ B translocation was increased in mutant and WT CSD and mutant sham-operated groups compared to WT sham. Electrophysiological analysis showed that CSD speed is higher in mutant groups, however CSD half maximum amplitude duration and CSD frequency did not change significantly between groups. Derivative of CSD depolarisation phase demonstrated that both derivative of the first CSD and subsequent CSDs were increased in FHM1 mutant groups compared to WT mice reflecting the hyperexcitability of mutant ones. Here for the first time in the literature, we presented that there is basal parenchymal neuroinflammation in R192Q mutant mice brain both in cortical and subcortical levels. Our findings indicate that CSD triggers parenchymal inflammatory processes in both WT and mutant mouse brains, which is mostly ipsilateral to the side of CSD induction in WT mice, and bilateral in the mutant mice. Future studies may indicate if basal neuroinflammation contributes to cortical hyperexcitability seen in FHM1 mutants in addition to the increased neuronal calcium influx or increased calcium and glutamate cause basal neuroinflammation. These findings indicate that CSD-induced parenchymal neuroinflammation spreads through cortex, striatum, and thalamus of both hemispheres in genetically susceptible brains, which may explain the prolonged hemiplegia, coma, and seizure phenotype in this variant of migraine with aura.

Key Words: Migraine, Aura, Cortical spreading depression, Familial hemiplegic migraine type 1, Inflammation, HMGB1, NF- κ B

OZET

Anisa D. M. Familial hemiplejik migren tip 1 transgenik fare modelinde kortikal yayılan depresyona bağlı parankimal nöroinflamasyon. Hacettepe Üniversitesi, Sağlık Bilimler Enstitüsü, Temel Nörolojik Bilimler Doktora Tezi, Ankara, 2019. Kortikal yayılan depresyon (KYD) migren aurasının nedeni olarak kabul edilmektedir. KYD stres altındaki nöronlar ile trigeminal aferentler arasında bir sinyalizasyon yolağını başlatır, bu yolak nöronal Panneksin-1 (Panx1) mega kanallarının geçici olarak açılması ile 'high mobility group box 1' (HMGB1)'in nörondan salıverilmesi ve astrositlerde nükleer faktör kappa B (NF- κ B)'nin nükleusa yer değiştirmesinden oluşur. Ailevi hemiplejik migren tip 1 (AHM1) *CACNA1A* genindeki bir mutasyonun neden olduğu migrenin nadir görülen bir monogenik alt tipidir. İnsan AHM1 mutasyonu taşıyan dişi transgenik knock-in fareler (R192Q veya S218L) KYD oluşumuna yatkınlık ve migrenin diğer özelliklerini sergiler. Bu çalışmada, AHM1 mutasyonu olan ve yabancı farelerde bazal ve KYD'nin tetiklediği parankimal nöroinflamasyon incelenmiştir, ayrıca KYD'nin tetiklediği inflamasyonun hastalığın patofizyolojisi ile ilişkili olabilecek bölgesel farklılığı olup olmadığı çalışılmıştır. Sonuçlara göre R192Q mutasyonu olan farelerde bazalde bir parankimal nöroinflamatuvar durum olduğu nöronal HMGB1 salınımı ve astrositik NF- κ B translokasyonu ile gösterilmiştir. KYD hem R192Q mutasyonu olan hem de yabancı fare gruplarında frontal/pariyetal korteks ve striatum/talamusta farklı bölgelerde inflamatuvar sinyal yolağını tetiklemektedir. Ayrıca mutasyonu olan farelerde bu inflamatuvar paternin bilateral sergilendiği saptanmıştır. AHM1 mutasyonu olan farelerde subkortikal alanlarda HMGB1 salınımı yabancı gruba göre artmıştır ve bu artış talamusta striatuma göre daha belirgindir. Western blotlama ile immünohistokimyasal tekniklerle saptanan bulgular desteklenmiştir. S218L mutasyonu taşıyan farelerde beyin omurilik sıvısında HMGB1 protein miktarında artış olduğu ve beyin parankiminden yapılan nükleer NF- κ B translokasyonu deneylerinde KYD tetiklenen yabancı grup ve mutant grupta NF- κ B translokasyonunun yabancı kontrole göre anlamlı olarak arttığı gösterilmiştir. Elektrofizyolojik analizlerde literatürle benzer şekilde mutant fare gruplarında KYD hızının yabancı gruba göre artmış olduğu, yarı maksimum amplitüd süresi ve KYD frekansının iki grup arasında anlamlı olarak değişmediği görülmüştür. İlk ve diğer KYD'lerin depolarizasyon fazının türevi alındığında R192Q mutasyonu taşıyan farelerde yabancı gruba göre anlamlı artış olduğu saptanmıştır, bu bulgu mutant gruptaki hipereksitabiliteyi desteklemektedir. Bu çalışmada literatürde ilk kez R192Q mutasyonu taşıyan farelerde bazalde bir parankimal nöroinflamatuvar durum olduğu, KYD'nin AHM1 mutant farelerde bilateral kortikal ve subkortikal, yabancı farelerde unilateral parankimal inflamatuvar süreci tetiklediği söylenebilir. KYD'ye yatkınlığı artıran AHM1 mutasyonunda görülen kortikal hipereksitabiliteye, artmış nöronal kalsiyumun yanısıra bazal inflamatuvar durumun katkıda bulunup bulunmadığı veya artmış kalsiyum ve glutamatın bazal inflamasyona yol açıp açmadığı daha sonraki çalışmaların konusu olabilir. Bulgularımız genetik olarak yatkın beyinde KYD'nin tetiklediği parankimal nöroinflamasyonun her iki hemisferde korteks, striatum ve talamusa yayıldığını göstermiş ve auralı migrenin bu alt grubunda uzamış hemipleji, koma ve nöbet fenotipinin nasıl ortaya çıktığını anlamamıza katkıda bulunmuştur.

Anahtar Kelimeler: Migren, Aura, Kortikal yayılan depresyon, Ailevi hemiplejik migren tip 1, İnflamasyon, HMGB1, NF- κ B.

CONTENTS

	Page
APPROVEMENT PAGE	i
YAYIMLAMA VE FİKRİ MÜLKİYET HAKLARI BEYANI	ii
ETHICAL DECLARATION PAGE	iii
ACKNOWLEDGEMENTS	V
ABSTRACT	Vi
OZET	Vii
CONTENTS	Viii
ABBREVIATIONS	Xii
FIGURE INDEX	Xiv
TABLE INDEX	Xvii
1. INTRODUCTION	1
2. BACKGROUND	4
2.1. Epidemiology	4
2.2. History	5
2.3. Economic Impact	7
2.4. Migraine: A Noblesse and Challenge for Social Coexistence	8
2.5. Migraine Classification	11
2.6. Migraine Without Aura	12
2.7. Migraine With Aura	13
2.8. Familial and Sporadic Hemiplegic Migraine	13
2.9. Familial Hemiplegic Migraine Mutations as a Model for Disease	14
2.10. Functional Consequences of FHM Mutations	18
2.11. Ca _v 2.1 Gain of Function and CSD Susceptibility Enhancement in FHM1 Mice	19
2.12. Neuronal Network Dependent Synaptic Plasticity in FHM1 Mutant Mice	20
2.13. The Effect of FHM1 Mutations on Neuroinflammation	21
2.14. Cortical Spreading Depression	23
2.15. High Mobility Group Box 1 (HMGB1) Protein	24
2.16. The Role of Nuclear Factor κ B in Neuroinflammation	27

3. MATERIALS AND METHODS	30
3.1. Materials Used	30
3.2. Methods	31
3.2.1. Ethics	31
3.2.2. Animals	31
3.2.3. Surgical Procedure and Electrophysiological Recordings	33
3.2.4. Experimental Design	34
3.2.5. Immunohistochemistry	35
3.2.6. Western Blotting	36
3.2.6.1. Subcellular Fractionation and NF- κ B Western Blotting	36
3.2.6.2. CSF Collection After CSD and HMGB1 Western Blotting	37
3.2.7. Electrophysiological Analysis	38
3.2.8. Quantification of HMGB1 Release and NF- κ B Activation	38
3.2.9. Statistical Analysis	39
4. RESULTS	40
4.1. Parenchymal Neuroinflammation in Naïve Wild-type and R192Q Mutant Mice	40
4.1.1 HMGB1 release in naïve Wild-type and R192Q Mutant Mice	40
4.1.2 NF- κ B Cytoplasm–To–Nucleous Translocation In Astrocytes of Naïve Wild-type and R192Q Mutant Mice	43
4.2. Effect of a Non-invasive Confounding Stimulus, Drilling the Skull, on Parenchymal Neuroinflammation and HMGB1 Release	46
4.3. Pinprick-induced CSD Causes Parenchymal Neuroinflammation in Wild-type and R192Q Mutant Mice: Does CSD Cause a Regional Specific Distribution Pattern and Increase in HMGB1 Release?	48
4.3.1 Laterality in HMGB1 Release in WT and R192Q Mutant Mouse Brains	48
4.3.2 Laterality in HMGB1 Release in Cortical Areas of Wild-type and R192Q Mutant Mouse Brains	52

4.3.3 Laterality in HMGB1 Release In Subcortical Areas of Wild-type and R192Q Mutant Mouse Brains	56
4.3.4. Laterality in Cortical and Subcortical HMGB1 Release of Wild-type and R192Q Mutant Mouse Brains	60
4.4. Pinprick-induced Parenchymal Neuroinflammation in Wild-type and R192Q Mutant Mouse Brains: A Regional Distribution Pattern and Increase in NF- κ B Translocation in Astrocytes	64
4.5. Neuroinflammation After Multiple CSD Events Induced By KCl in Wild-type and S218L Mutant Mouse Brains	66
4.5.1. HMGB1 Release in CSF in Wild-type and S218L Mutant Mice After KCl-induced Multiple CSDs	66
4.5.2. Translocation of NF- κ B from Cytoplasm to Nucleus in Astrocytes of Wild-type and S218L Mutant Mice Assessed by Western Blotting	67
4.6. Electrophysiological Characterization of Cortical Spreading Depolarization Events	73
4.6.1. CSD amplitude was not significantly different in wild-type mice compared to that in R192Q or S218L mutant mice	77
4.6.2. Speed of CSD was higher in R192Q and S218L mutant mice compared to that in wild-type mice	77
4.6.3. Total CSD duration was not significantly changed in R192Q and S218L mutant mice compared to that in wild-type mice	79
4.6.4. CSD half-maximum duration was not statistically different in R192Q and S218L mutant mice compared to wild-type mice	79
4.6.5. Frequency of CSD events in R192Q and S218L mutant mice compared to that in wild-type mice	80
4.6.6. The first component of the CSD derivative was higher in the first CSD event compared to subsequent events in R192Q and S218L mutant mice compared to that in wild-type mice	81
5. DISCUSSION	83
6. CONCLUSION	94

7. REFERENCES

95

8. ADDITORY

Add-1: Ethical Approval-1

Add-2: Ethical Approval-2

Add-3: Turnitin Ekran görüntüsü

Add-4: Digital Makbuz

9. ACADEMIC CV

ABBREVIATIONS

ATP1A2	ATPase, alpha 2 polypeptide
Ca_v2.1	Subunit of brain-specific voltage-gated P/Q-type calcium channel
CACNA1A	Calcium channel, alpha 1A subunit
CSF	Cerebrospinal fluid
CGRP	Calcitonin gene-related peptide
CSD	Cortical spreading depression
Cox-2	Cyclooxygenase-2
DAMPs	Damage-associated molecular patterns
DALYs	Disability-adjusted life years
DC	Direct current
EAAT1	Excitatory amino acid transporter 1
EAAT2	Excitatory amino acid transporter 2
FHM	Familial hemiplegic migraine
GABA	γ -aminobutyric acid
GWAS	Genome wide association studies
HM	Hemiplegic migraine
HOM	Homozygous
HET	Heterozygous
HMGB1	High mobility group box 1
IL-1β	Interleukin -1 β
IHC	Immunohistochemistry
ICHD	International classification of headache disorders
IRAK	Interleukin-1 receptor-associated kinase
NIK	NF-kappa-B-inducing kinase
IκB	I-kappa-B
IHS	International headache society
iNOS	Inducible nitric oxide synthase
KI	Knock in
KCl	Potassium chloride
MA	Migraine with aura

MO	Migraine without aura
MAPK	Mitogen activated protein kinases
MYD88	Myeloid differentiation primary response protein 88
NF-κB	Nuclear factor kappa B
NGS	Normal goat serum
NMS	Normal mouse serum
NSAIDs	Nonsteroidal anti-inflammatory drugs
PAMPs	Pathogen-associated molecular patterns
RAGE	Receptor for advanced glycation endproducts
SHM	Sporadic hemiplegic migraine
SCN1A	Voltage gated sodium channel, type 1 alpha subunit
TG	Trigeminal Ganglion
TLR	Toll-like receptor
TVS	Trigemino-vascular system
TNFα	Tumor necrosis factor alpha
TRAF	Tumor necrosis factor associated factors
WT	Wild type
WHO	World Health Organization

FIGURES

Figure	Page
2.1. The percentage of migraine prevalence in different genders and age groups.	3
2.2. "The Extraction of the Stone of Madness".	5
2.3. Neuron–microglia communication signaling pathways.	10
2.4. Schematic diagram of the NF- κ B pathway.	12
2.5. A common pathway demonstrating the mutations influences in familial hemiplegic migraine genes.	19
2.6. Migraine may be a promoter for artistry.	27
3.1. Schema shows the number and design of wild-type and transgenic animals with R192Q and S218L mutations in each experimental group.	30
3.2. A schematic showing the location of the position of drilling, pinprick and KCl-induced CSDs, intracerebroventricular (i.c.v.) cannula and CSF collection, and non-invasive DC recordings	32
4.1. HMGB1 Release in cortical and subcortical areas of naïve WT and R192Q mutant mice brains.	39
4.2. Basal neuroinflammation in naïve WT and R192Q mutant mice.	40
4.3. NF- κ B translocation from cytoplasm to nucleus in astrocytes in naïve WT and R192O mutant mice.	42
4.4. NF- κ B translocation.	43
4.5. HMGB1 release after drilling the skull in WT and R192Q mice.	45
4.6. HMGB1 release after pinprick-induced single CSD in WT and R192Q mutant brains.	47
4.7. HMGB1 release after pinprick-induced single CSD in WT mice brain.	48
4.8. HMGB1 release after pinprick-induced single CSD in R192Q mutant mice brain.	49
4.9. HMGB1 release after pinprick-induced single CSD in cortical areas of R192Q mice compared to those WT mice.	51
4.10. HMGB1 release after pinprick-induced single CSD in cortical areas of WT mice brain.	52
4.11. HMGB1 release after pinprick-induced single CSD in cortical	

areas of R192Q mutant mice brain.	53
4.12. HMGB1 release after pinprick-induced single CSD in subcortical areas of WT and R192Q mutant mice brain.	55
4.13. HMGB1 release after pinprick-induced single CSD in subcortical areas of WT mice brain.	56
4.14. HMGB1 release after pinprick-induced single CSD in subcortical areas of R192Q mice brain.	57
4.15. HMGB1 release after pinprick-induced single CSD in cortical and subcortical areas of WT and R192Q mutant mice brains.	59
4.16. HMGB1 release after pinprick-induced single CSD in cortical and subcortical areas of WT mice brains.	60
4.17. HMGB1 release after pinprick-induced single CSD in cortical and subcortical areas of R192Q mutant mice brains.	61
4.18. NF- κ B translocation from cytoplasm to nucleus in astrocytes after pinprick-induced CSD in WT and R192O mutant mice.	63
4.19. HMGB1 release during 1 hour KCl-induced multiple CSDs detected in CSF collected through i.c.v. cannula in S218L mutant mice compared to its wild-type.	64
4.20. NF- κ B translocation from cytoplasm to nucleus in astrocytes shown by nuclear subtraction Western blotting.	65
4.21. NF- κ B translocation from cytoplasm to nucleus in astrocytes shown by nuclear subtraction Western blotting.	66
4.22. Scheme showing neuronal HMGB1 release distribution pattern and amount in frontal section of the brain of WT and R192Q mutant mice	70
4.23. Scheme showing neuronal HMGB1 release distribution pattern and amount in posterior section of the brain of WT and R192Q mutant mice	71
4.24. Scheme showing neuronal NF- κ B relocation distribution pattern and amount in frontal section of the brain of WT and R192Q mutant mice	72
4.25. CSD recordings monitored after CSD induction in R192Q mouse.	73
4.26. CSD speed is increased in both R192Q and S218L mutant strains after both pinprick- and KCl-induced CSDs compared to WT mice.	78
4.27. CSD frequency is increased in R192Q and S218L mutant mice compared to WT mice.	80

- 4.28.** CSD derivatives (first component) difference between R192Q, S218L KI mice and WT. 82

TABLES

Table		PAGE
3.1.	Antibodies for Immunohistochemistry and Western Blotting.	30
3.2.	Experimental Facilities	31
4.1.	Electrophysiological characteristics of Pinprick-induced CSD in R192Q strain HOM/HOM	74
4.2.	Electrophysiological characteristics of 1 hr KCl- induced multiple CSDs in R192Q strain HOM/HOM.	75
4.3.	Electrophysiological characteristics of 1 hr KCl- induced multiple CSDs in S218L strain HET/WT.	76

INTRODUCTION

Migraine, one of the most common human diseases (1), is a brain disorder that is characterized by attacks of throbbing often unilateral headache that can be accompanied by neurological symptoms such as nausea and vomiting, as well as hypersensitivity to light and sound (2). There are two main types of migraines: migraine with aura and migraine without aura (2). Migraine with aura affects one-third of migraine patients. The aura is characterized by gradually developing neurological symptoms such as sensory, motor, and visual or speech difficulties that last 5–60 minutes before the onset of headache.

Despite much progress, the molecular pathophysiology of migraine is only partly understood. Animal studies may help better understand how migraine is brought about and how it affects the brains (3, 4). Cortical spreading depression (CSD) underlies the migraine aura (5). CSD is a wave of depolarization of neuronal and glial cells that starts slowly and spreads over the cortex with a speed of 2-6 mm/min. CSD activates parenchymal neuroinflammatory cascade by opening neuronal Pannexin1 (Panx1) channels followed by the release of neuroinflammatory molecules such as high mobility group box-1 (HMGB1) and activation of nuclear factor- κ B (NF- κ B), which ultimately results in the stimulation of the trigeminovascular system, as was demonstrated in experimental animals (6). CSD can reach subcortical areas (7), and affect meninges and brainstem leading to the activation of headache mechanisms (6, 8), although evidence in humans is essentially lacking.

HMGB1 acts as a nuclear and cellular danger signal (9). Endogenous danger signals released from necrotic or stressed cells that trigger the inflammatory response after trauma have been termed alarmins or danger-associated molecular patterns (DAMPs). The subcellular localization of HMGB1 depends on the type and activation state of the cell. The HMGB1 is mainly localized in the cell nucleus. HMGB1 can exert different functions depending on its cellular localization. HMGB1 can be released from the nucleus to the extracellular space in response to different stimuli in two ways: following cellular injury it is passively released during cellular

apoptosis or necrosis; or it is released actively following inflammatory signals from activated immune cells or neuronal cells (10). Nuclear Factor κ B (NF- κ B) is a ubiquitous transcription factor which can be found in almost all the cells of an organism. NF- κ B regulates the cytokines and chemokines expression, including interleukins, interferons, lymphokines and tumor necrosis factors. Microglial cells have membrane receptors such as toll-like receptors (TLRs), nucleotide-binding oligomerization domain proteins (NLRs), and receptor for interferons and cytokines (11). TLRs specifically recognize pro-inflammatory ligands including pathogen-associated molecular patterns (PAMPs) and damage-associated molecular patterns (DAMPs).

Migraine is considered a complex disorder, which implies that migraine is brought about by an interplay of multiple genetic and environmental factors, except for the few monogenic types in which one genetic mutation is sufficient to bring about the disease (12). Various transgenic mouse models have been generated in which human mutations causing monogenic types of migraine have been introduced as an instrumental tool to study disease neurobiology in much detail exhibiting features and symptoms relevant to those of migraine in humans (3). One of transgenic mouse models, familial hemiplegic migraine type 1 (FHM1), a rare monogenic subtype of migraine with aura characterized by motor weakness during the aura (2), is caused by specific missense mutations in the *CACNA1A* gene that codes for the pore-forming α_{1A} subunit of neuronal voltage-gated $\text{Ca}_v2.1$ channels (13), and is considered a relevant model for the common forms of migraine (3). Transgenic knock-in (KI) mice that express mutated $\text{Ca}_v2.1$ channels containing either the FHM1 R192Q or S218L mutation in the α_{1A} subunit exhibit an increased susceptibility to CSD due to an increased neuronal calcium influx through $\text{Ca}_v2.1$ channels and increased cortical glutamatergic excitatory neurotransmission (14-16). Investigations of an epilepsy rodent model have provided hints about the close interplay between increased excitation and inflammation (17, 18) suggesting that elevated glutamatergic activity in FHM1 mutant mice may initiate an enhanced inflammatory response, especially in response to CSD events when neuronal activity is increased.

Therefore, in the current study we aimed to provide an in-depth analysis of parenchymal neuroinflammation in FHM1 mutant mice. Not only we investigated to what extent the mutant mice exhibit a basal neuroinflammation phenotype but also whether CSD can induce a specific parenchymal inflammatory pattern in the mutant mice. Basal parenchymal inflammation was assessed by neuronal HMGB1 release and astrocytic NF- κ B activation, both in naïve mutant and wild-type (WT) mice. Next, we tested the effect of different paradigmes of CSD induction on inflammation and investigated whether CSD led to regional differences of HMGB1 release in mutant and WT mice. To this end, we investigated frontal/parietal cortices and striatal/thalamic subcortical areas, both ipsilateral and contralateral to the side of CSD induction in the various genotypes. We also studied whether drilling the skull may be a confounding factor in triggering HMGB1 release in mice and whether it showed a genotypic difference. The basal parenchymal neuroinflammation in FHM1 mutant mice, and the regional differences in the neuroinflammatory response revealed in this study may provide further insight into the routes and mechanisms that are affected by CSD in mutant and WT mice, which help our understanding of the exact role of CSD in migraine pathophysiology.

2. BACKGROUND: Migraine at a glance

2.1. Epidemiology

Migraine affects nearly 10 % of people in the world (19). In the United States about 18 % of women and 6 % of men suffer from migraine yearly with a corresponding lifetime prevalence of 43 % and 18 % respectively (20). According to Europe declarement 12-28 % of people at some time in their lives suffer from migraine (21) which rises during adolescence and falls in the early 50s (22). According to studies, the range of one-year prevalence of migraine is 14-35 % in adult women and 6-15 % in adult men (Figure 2.1.) (21). Beside specific differences between genders, the life time prevalence also significantly differs with age; about 5 % of children under 12 suffer from migraine, with nearly no difference between girls and boys (23).

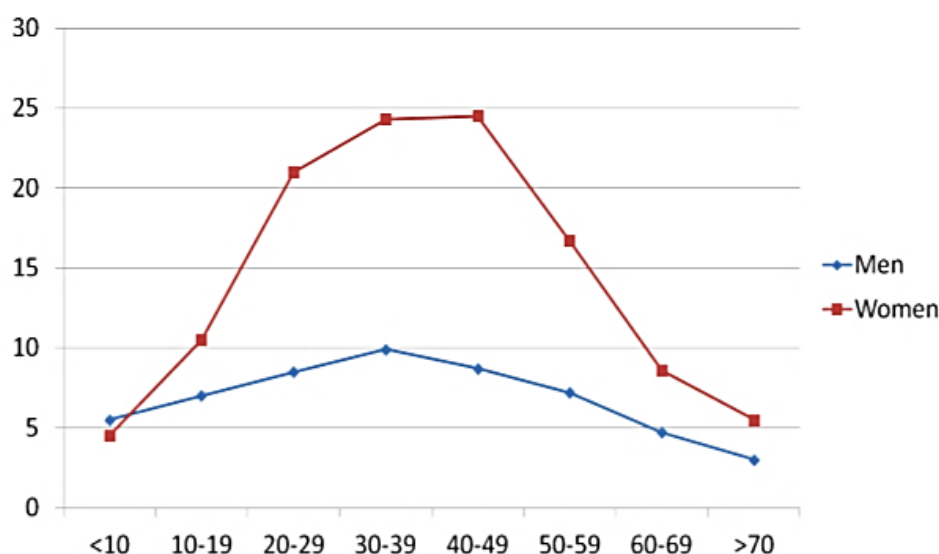


Figure 2.1. The percentage of migraine prevalence in different genders and age groups (average of 10 studies)(21).

After puberty, a significant rapid raise in incidence, especially in girls, is evident (Figure 2.1.) and goes on throughout early adult life. The disease picks to its highest prevalence during the most productive years of working life, between 20 to

50 (21). As a result, the economic relevance of migraine should not be underestimated; this will be discussed separately. After menopause, migraine attacks decrease radically in women, reaching nearly equal numbers in women and men (21).

Regarding geographic distribution, migraine was considered to be more prevalent in the industrialized regions and countries through the past decades. Studies in Asia and South America demonstrated lower prevalence rates compared to Europe (24, 25). However, recently the current epidemiologic researches of headache in Asia was reviewed using International Headache Society (IHS) classification criteria (25). The differences specific to gender in migraine prevalence were comparable in these studies (25). Although the economic situations, cultural background and social features vary significantly, the mentioned research indicated that migraine is as evidential in Asia and its prevalence rate is very much close to the reported ones in Western countries (25).

Migraine subclasses also show epidemiologic variations. In this regard, two thirds of migraineurs suffer from migraine without aura (MO), the most common type of migraine. Incidence data collections show that the surfeit of migraine headache in women in reproductive ages is mainly because of migraine without aura (26).

It is important to mention that migraine occurrence is related to the epilepsy occurrence in families. A study showed that the risk of migraine is significantly higher in all sub-types of epileptics as well as in all unaffected and first-degree relatives. The data indicates to a strong comorbidity of migraine and epilepsy, in an independent manner to etiology, seizure type and age of onset (27).

2.2. History

Evidence from medical practices in the field of head pain and migraine can be traced back to the Stone Age, the time in which even medical surgery on the skull was well established. Evidence of trepanation, a method including drilling a hole on the human skull, has been found from prehistoric human skulls. One study from the 1960s indicates that people believed trepanation can heal migraine, epileptic

seizures, and mental illnesses showed by cave paintings (Figure 2.2.)(28). The well-known ancient Greek physician Hippocrates, introduced the aura as a potential underlying cause of headache at 400 BC, and described it as vapors ascending from the stomach to the head (29). However, it was Aretaios who first distinguish migraine with other headaches and gave the name "heterocrania", the parent of today's word migraine, to the first migraine characterization as a unilateral and pulsating nature, associated with nausea and vomiting, in the 2nd century (30).

When searching for resources from modern history, the migraine neurovascular characteristics were documented in 1684. Dr. Willis in his "Practice of Physike" considered the headache to be a result of blood flow exceeding to the head, which "distends the vessels", and "blows up the membranes", and "pulls the nervous corrugation or wrinkling" (31). In the 1940s and 1950s, Wolff, performed brain surgery with local anesthesia on conscious patients; he also insisted on the cranial blood vessels importance as the pain source (32).



Figure 2.2. "The Extraction of the Stone of Madness", a painting by Hieronymus Bosch expounding trepanation (1488-1516), Netherlands Institute for Art History.

The observation that mechanical stimulation of the skull, dura mater, and brain not associated with blood vessels did not cause pain, but, large meningeal, cerebral, and temporal arteries stimulation evoked a throbbing pain was so striking at that time (33, 34). Although Wolff's data have never been replicated, for about 60 years, the vascular headache theory has been well established (35). Currently, vascular changes and headache relationship is strongly debated because of the lack of evidence for greater vasodilation through headache attacks than during headache-free intervals could not confirm the theory (32, 36). Contrary to Wolff description for migraine as a result of vasodilation, Moskowitz showed that headache occurrence is not in correlation with vessel diameter alterations. Vessel dilation may occur during migraine headache, not as the pain source, but as a part of central activity and neurogenic inflammation coupled to raise the brain metabolism. Headache is suggested to be the consequence of trigeminovascular afferents activation which causes neurogenic inflammation and stimulation of brainstem nuclei and trigeminal nucleus caudalis which have been recognized to be important for pain perception (37-40). The neurogenic inflammation in the meninges has been studied in animal models after trigeminal nerve terminals experimental activation (41). Neurogenic inflammation in the dura mater causes the release of vasodilating neuropeptides from sensitive nerve fibers (41) which initiates a cascade of events including vasodilation, edema, and the release of proinflammatory mediators such as bradykinin and prostanoids (42). It is also shown that after CSD, the putative cause of aura, parenchymal neuroinflammatory cascades are triggered, Panx1 channels in neurons are opened and neuroinflammatory molecules such as high mobility group box-1 (HMGB1) are released and nuclear factor- κ B (NF- κ B) are translocated to the nucleus of astrocytes, and in the end trigeminovascular system is activated (6).

2.3. Economic Impact

The economic importance of migraine is related to its great prevalence. According to the World Health Organization (43), migraine is among the three disorders with the highest prevalence (43). Prevalence rates of migraine, as mentioned earlier, is different with age and gender, but irrespective of all these

variabilities, migraine is to be seen a common disease affecting much people at some points in their lives. However, not each prevalent disease has such a great economic influence, in reverse, very rare diseases put high costs on patients. Various categories of costs have to be taken into consideration when considering the economic effect of a disease:

- costs for the individual
- costs for medical care
- costs for the economy of the country

The costs to the individual mainly is because of spending on OTC drugs (basically NSAIDs) and deductibles on prescribed drugs (44). For migrainers, these costs should be bearable, because especially NSAIDs are mostly accessible as generic drugs. Nevertheless, the considerable costs of migraine are because of the medical care system and economy detraction. The smaller portion of these socio-economic costs is the result of the hospitalization, health care provider visits, medication. Researches evaluate the economic impact of migraine as an annual total direct costs of 696 € per patient with episodic migraine (about 15 days of headache per month) in Germany. Figures for other countries such as Italy, UK, Spain and France is in a comparable range (45).

Migraine can impair patients' ability to do their job properly, it can force affected persons to go home earlier or even become absent from work. Absence from workplace due to migraine may extend from few days to several weeks or even a month in each year. A British research reports the average of 5.7 working days which are lost per year for every student or working migraineur (22). In another study, the indirect financial impact of migraine on US employers was evaluated to be nearly \$12 billion per year (mainly as a result of absenteeism) (46).

2.4. Migraine: A Noblesse and Challenge for Social Coexistence

There is a fact that there are very famous migraineurs in history including Julius Caesar, Napoleon Bonaparte, Frédéric Chopin, Charles Darwin, Wilhelm Busch, Claude Monet, Alfred Nobel, Friedrich Nietzsche, Vincent van Gogh, Marie Curie and Sigmund Freud. Characteristically, migraine has been more often

associated with sentimental artists, prestigious individuals, and aristocratic ladies. As migraine has the obligatory implication of vulnerability and weakness, people suffering from migraine need to rest, retreat and recreate. In another word, migraine may provide individuals with the chance to highlight the vulnerable and weak features of their character (44)(Figure 2.6).

Definitely, this perception of migraine is considered for the diseased people who experience the strong disabling nature of migraine attacks several days in each month. Nobody disregards the disease of these patients, but the particular issue with this sickness is that it is not provable. This is the reason, why migraine perfectly suits as a fad of the aristocratic ladies and gentlemen (44). And this is also the reason, why migraine became the prototype of excuses.

Indeed, it is hard to make a balance in the perception of migraine pain and its impact, due to a broad spectrum of severity. WHO announces that in high-income countries migraine ranges among the 10 leading causes of the sickness burden for women between 15-44 years, causing close to 5 disability-adjusted life years (DALYs), that is a measure of general disease burden) in 1000 women (43).



Figure 2.3. Migraine may be a promoter for artistry. These collages and photographs from the artist and migraineur Deborah Leigh demonstrate her emotions related to migraine. This artistry expresses an implication of noblesse, as it is usual for many artworks dealing with migraine. Titles: (upper row, left to right) “Migraine mood #10”, “Migraine Moods #11”, “Migraine Moods-Cloudy Day”, (middle row, left to right) “Migraine Aura Club-What Do You See?”, “Coffee headache”, (bottom row, left to right) “Butterflies of pain”, “Migraine Barbie has Snapped!”, “Migraines Moods”.

2.5. Migraine Classification

Classification and diagnosis criteria for migraine were established by the International Headache Society (IHS). Its International Classification of Headache Disorders, 3rd edition (ICHD-3), clarified a basis to make the nomenclature for different types of headache and migraine standardized; it provides a well explanation of symptoms for each type of migraine. The categorization distinguishes six subclasses of migraine (47) .

The primary headaches

1. Migraine

1.1. Migraine without aura (MO)

1.2. Migraine with aura (MA)

1.2.1. Migraine with typical aura

1.2.1.1. Typical aura with headache

1.2.1.2. Typical aura without headache

1.2.2. Migraine with brainstem aura

1.2.3. Hemiplegic migraine

1.2.3.1. Familial hemiplegic migraine (FHM)

1.2.3.1.1. Familial hemiplegic migraine type 1 (FHM1)

1.2.3.1.2. Familial hemiplegic migraine type 2 (FHM2)

1.2.3.1.3. Familial hemiplegic migraine type 3 (FHM3)

1.2.3.1.4. Familial hemiplegic migraine, other loci

1.2.3.2. Sporadic hemiplegic migraine (48)

1.2.4. Retinal migraine

1.3. Chronic migraine

1.4. Complications of migraine

1.5. Probable migraine

1.6. Episodic syndromes that may be associated with migraine

Migraine with and without aura, are the most common types that themselves are divided into various subtypes. Their characteristics are described below.

2.6. Migraine without aura

Migraine without aura is a recurrent headache disorder manifesting in attacks lasting 4–72 hours. Typical characteristics of this kind of headache are pulsating quality, unilateral location, moderate or severe intensity, getting aggravated by ordinary physical activity and association with nausea and/or phonophobia and photophobia (47).

Diagnostic criteria:

- A. At least five attacks, fulfilling criteria B–D
- B. Headache attacks lasting 4–72 hours (when untreated or unsuccessfully treated)
- C. Headache has at least two of the following four characteristics:
 - 1. Unilateral location
 - 2. Pulsating quality
 - 3. Moderate or severe pain intensity
 - 4. Aggravation by or causing avoidance of routine physical activity (e.g. walking or climbing stairs)
- D. During headache at least one of the following:
 - 1. Nausea and/or vomiting
 - 2. Photophobia and phonophobia
- E. Not better accounted for by another ICHD-3 diagnosis.

Migraine attacks may also be associated with cranial autonomic symptoms and cutaneous allodynia symptoms. In young children, phonophobia and photophobia may be inferred from their behavior (47). A minority of women (<10%) have migraine attacks in association with the majority of their menstrual cycles; most of them are without aura. Attacks during menstruation are usually longer and accompanied by more severe nausea than attacks outside the menstrual cycle (47).

2.7. Migraine with Aura

Migraine with aura is described as recurrent attacks, which last minutes, of unilateral reversible sensory, visual or other symptoms of central nervous system that usually develop gradually and are followed by headache and associated migraine symptoms(47).

Diagnostic criteria:

- A. At least two attacks fulfilling criteria B and C
- B. One or more of the following fully reversible aura symptoms:
 - 1. Visual
 - 2. Sensory
 - 3. Speech and/or language
 - 4. Motor
 - 5. Brainstem
 - 6. Retinal
- C. At least three of the following six characteristics:
 - 1. At least one aura symptom spreads gradually over ≥ 5 minutes
 - 2. Two or more aura symptoms occur in succession
 - 3. Each individual aura symptom lasts 5–60 minutes
 - 4. At least one aura symptom is unilateral
 - 5. At least one aura symptom is positive
 - 6. The aura is accompanied, or followed within 60 minutes, by headache
- D. Not better accounted for by another ICHD-3 diagnosis (47).

2.8. Familial and Sporadic Hemiplegic Migraine

IHCD-3 classified the hemiplegic types of migraine as subtypes of migraine with aura. The symptoms are similar to MA, but with preceding or associating hemiplegic symptoms, such as sensory disturbances and motor weakness during the aura. The IHS classifies cases of hemiplegic migraine without any affected relatives as sporadic (48), whereas the cases with at least one affected person as a first or second degree relative are called familial hemiplegic migraine (FHM)(47).

Therefore, familial hemiplegic migraine has a very strong genetic component; in fact, it is the only type of migraine which inherits in an autosomal dominant mode. Because of its monogenic appearance, FHM is of special interest for migraine studies. The affected neuronal ion channels give us a considerable knowledge of mechanisms in migraine.

2.9. Familial Hemiplegic Migraine Mutations as a Model for Disease

Genes and pathways for migraine vulnerability have been revealed by investigating the mutations influence in the rare monogenic forms of migraine. Mutations leading to FHM type 1, 2, and 3 shaped the basis for the available transgenic mouse models for monogenic disorders accompanied with migraine (13, 49, 50). CSD susceptibility enhancement has been reported in these transgenic mouse models with different underlying mutations and mechanisms (51). This increased CSD susceptibility may be due to the enhanced cortical glutamatergic transmission, which has been shown for FHM1 mouse models (16). The importance for the role of neuronal excitability in determining CSD susceptibility has been revealed after the indirect evidence of experiments showing that antiepileptic drugs suppressing neuronal excitability (52, 53) also decrease CSD susceptibility (54). Clinical studies in patients with FHM1 (55) and common migraine (56, 57) and genome-wide association studies (GWAS) in patients with common migraine (3) confirm that cortical hyperexcitability may be an underlying base for migraine.

FHM is a rare subtype of monogenic MA with the characteristic of transient hemiparesis during the aura phase of attacks (2). Most of FHM patients also experience classic migraine attacks beside hemiplegia (58) so, FHM can be considered part of the migraine spectrum and a valid model to study migraine. Three FHM genes have been recognized: voltage-dependent, calcium channel, alpha 1A subunit (CACNA1A)(FHM1); Na⁺/K⁺ transporting ATPase, alpha 2 polypeptide (ATP1A2)(FHM2); and voltage-gated sodium channel, type 1 alpha subunit (SCN1A)(FHM3)(Figure 2.5).

FHM1 gene, CACNA1A, is located on chromosome 19p13 and codes for a subunit of voltage-gated Ca_v2.1 Ca²⁺ channels in neurons (13). These channels

regulate neurotransmitter release at central synapses in brain (59). FHM1 mutations show gain-of-function of human $\text{Ca}_v2.1$ channels in heterologous cell systems (38) and neuronal $\text{Ca}_v2.1$ channels in FHM1 KI mice (14) revealed by biophysical analysis. This gain-of-function effect increases action-potential evoked Ca^{2+} influx and raises glutamate release in the synaptic cleft (16, 60). Upon this enhancement in neuronal network activity, CSD can be facilitated (51) and this may explain symptoms of migraine aura and headache in FHM1. In clinical practice, the variability of FHM1 mutations ranges from pure hemiplegic episodes, as reported for R192Q mutation carriers (13), to FHM with severe neurological deficits such as cerebellar ataxia, epilepsy, or fatal coma, as observed in S218L mutation carriers (61).

FHM2 gene, ATP1A2, is located on chromosome 1q23. The gene encodes a $\alpha 2$ subunit of the Na^+/K^+ pump ATPase (49) which binds Na^+/K^+ , and ATP, and uses ATP hydrolysis to force Na^+ ions out of the glial cell in exchange for K^+ ions. By this mechanism, the ATPase regulate potassium and glutamate re-uptake from the synaptic cleft into glial cells. FHM2 mutations cause a loss-of-function of Na^+/K^+ ATPase in glial cells at the cellular level, leading to increase in extracellular levels of glutamate and K^+ , and could indirectly cause hyperexcitability in neuronal networks (62, 63). However, the roles of the three types of cerebral Na^+/K^+ ATPases in potassium and glutamate clearance is not clear yet (64). From a clinical point of view, FHM2 mutations have been associated with pure hemiplegic features in association with FHM attacks (49, 65, 66) or a combination of FHM features with other neurological disorders, including cerebellar ataxia, aphasia, recurrent coma, and behavioral changes (67-69). New missense mutations in the ATP1A2 gene may explain the co-occurrence of migraine with childhood epilepsy (70) in some patients.

FHM3 gene, SCN1A, is located on chromosome 2q24 and encodes a voltage-gated $\text{Na}_v1.1$ sodium channel subunit (50) that has an essential role in the action potential generation and propagation. FHM3 mutations are sometimes associated with more severe clinical symptoms including childhood epilepsy, transient blindness and generalized tonic-clonic epilepsy (50, 71-73) apart from migraine and hemiplegia. There is a shared molecular pathway between FHM and epilepsy suggested by seizures which were observed independently from hemiplegic migraine

attacks in FHM3 cases with epilepsy comorbidity (71). FHM3 could be associated with Nav1.1 channels gain-of-function leading to hyperexcitability of inhibitory interneurons. But, there are conflicting data on the influence of FHM3 mutations on recombinant Nav1.1 channels, suggesting either gain- or loss-of-function effects depending on the mutation and/or the study. These data suggest that FHM3 has a complex spectrum of Nav1.1 defects (74). More studies are needed both *in vitro* and *in vivo* to clarify neuronal mechanisms by which FHM3 mutations, with their loss- or gain-of-function effects, cause epilepsy and migraine comorbidity in some patients (74, 75).

The conceivable hypotheses of FHM subtypes are outlined in the following schema (Figure 2.5.):

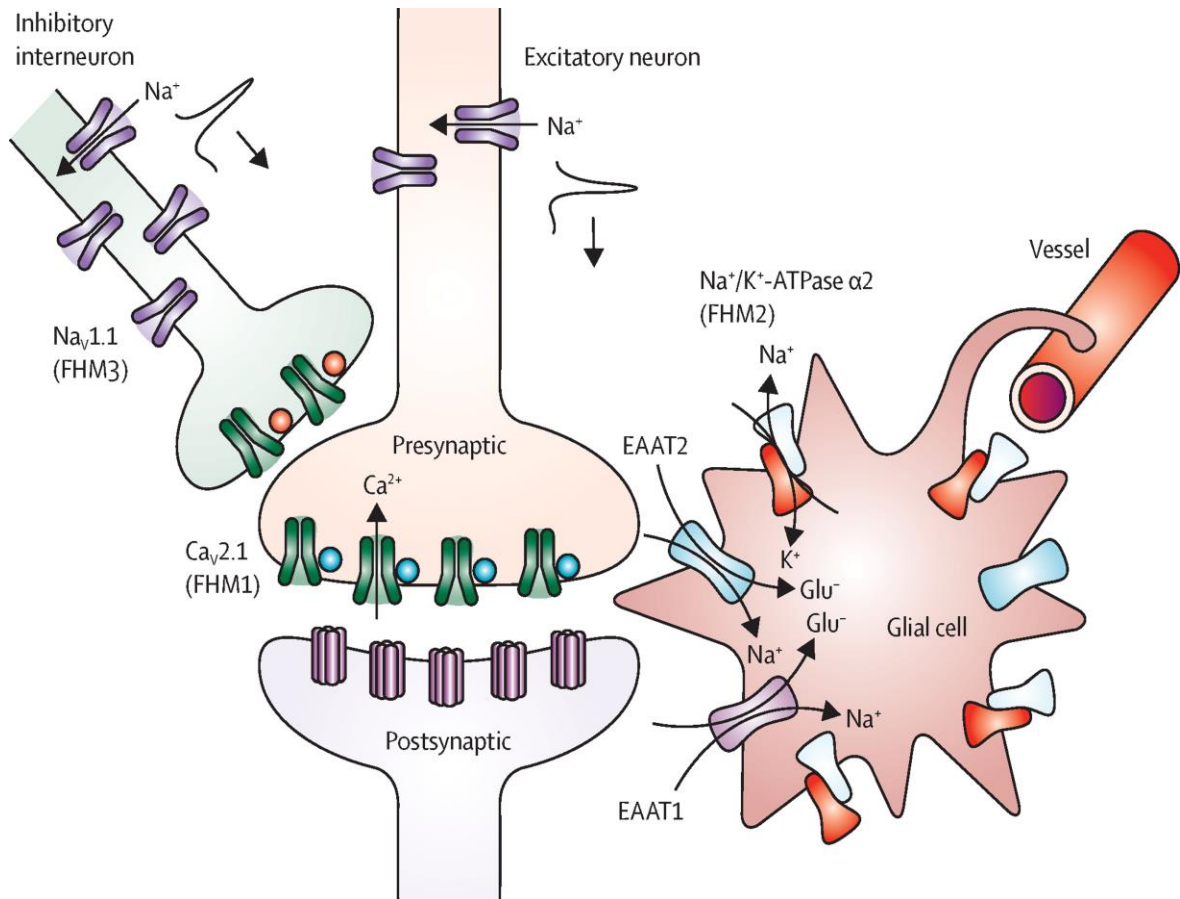


Figure 2.4. A common pathway demonstrating the mutations influences in familial hemiplegic migraine genes. The functional influences of FHM1, FHM2, and FHM3 gene mutations all result in raised levels of glutamate in the synaptic cleft. FHM1 gain-of-function mutations in the *CACNA1A* gene encoding presynaptic $Ca_v2.1$ calcium channels causes an increase in calcium influx and rise in glutamate release in the synaptic cleft by action potentials. Normally glutamate is taken up from the synaptic cleft into the glial cells by a glial cell Na^+/K^+ ATPase pump-dependent manner. FHM2 loss-of-function mutations in the *ATP1A2* gene encoding Na^+/K^+ -ATPase in the glial cell causes a decreased reuptake of glutamate, and leads to an increase in concentrations of glutamate in the synaptic cleft. Higher activity of excitatory glutamatergic neurons in normal condition is compensated by increased activity of inhibitory γ -aminobutyric acid (GABA)-ergic interneurons. FHM3 loss-of-function mutations in the *SCN1A* gene encoding $Na_v1.1$ sodium channels on inhibitory interneurons leads to decreased inhibitory activity, which eventually leads to uncompensated increased excitatory neuronal activity and increased glutamate release. FHM= familial hemiplegic migraine. EAAT1= excitatory amino acid transporter 1. EAAT2= excitatory amino acid transporter 2 (3).

2.10. Functional Consequences of FHM Mutations

Increase in CSD susceptibility has been reported in all of these transgenic mouse models having multiple various underlying mutations and mechanisms. This may be due to the enhanced cortical glutamatergic transmission shown for FHM1 mouse models (16). Antiepileptic drugs suppressed neuronal excitability showing the importance of neuronal excitation in determining CSD susceptibility (52, 53). Beside this, many clinical studies in patients with FHM1 (55) and common migraine (56, 57) and also GWAS in patients with common migraine (3) confirm the hyperexcitability of cortex to be an underlying base for migraine.

There is a comprehensive characterization of clinical symptoms in migraine but its precise molecular and neurobiological pathophysiology and its association with comorbidities is not known well. Nevertheless, with the help of animal studies a better understanding of migraine base has been achieved in order to have a better therapeutic targeting (3, 4, 76, 77)

So far, two transgenic FHM1 mutant mouse models have been produced, with the gain-of-function missense mutations R192Q or S218L in the CACNA1A gene (14, 78). While mice with the milder R192Q mutation do not show a severe phenotype (14), mice with the S218L mutation display an overt phenotype with cerebellar ataxia and seizures (78), consistent with the clinical phenotype in FHM1 S218L patients. Functional studies of FHM1 mutant mice reveal that beside enhancement in susceptibility to experimentally induced CSD (14, 15, 78-80), as triggering mechanism underlying migraine aura, there are changes in excitation/inhibition balance (16, 81, 82), synaptic plasticity (83) and calcitonin gene-related peptide (CGRP)-mediated pain signaling in trigeminal nuclei (84-86) as well.

2.11. Ca_v2.1 Gain of Function and CSD Susceptibility Enhancement in FHM1 Mice

FHM1 mutations lead to a Ca_v2.1 gain of function, the potential cause of cerebral hyperexcitability seen in FHM1 patients (55). FHM1 R192Q (16, 81) and S218L (82) mutations revealed an enhancement in excitatory but not inhibitory release of neurotransmitters in brain slices of cortex and neuronal cultures. The enhanced glutamatergic synaptic transmission in cortex and increased CSD susceptibility were shown for R192Q mutant mice *in vitro* in brain slices (16). By reducing excitatory transmission to wild-type (WT) level in cortex by partially inhibiting Ca²⁺ channels, the CSD susceptibility facilitation was normalized (16). This may provide a link between raised Ca²⁺ influx, glutamatergic synaptic transmission and enhanced susceptibility to CSD. FHM1 S218L mutant mice revealed an increase in neuronal Ca²⁺ levels at rest, together with a change in synaptic morphology as shown in a recent *in vivo* Ca²⁺ imaging study in the somatosensory cortex of these mutants (87) which suggest increased synaptic strength and a hyperexcitable phenotype. These findings indicate a facilitated state of S218L mutant channels at rest. Increase in the miniature excitatory postsynaptic currents (mEPSCs) frequency in cortical slices of S218L (82) but not R192Q mutant mice (16) indicates that the rise in resting Ca²⁺ levels may be characteristic for S218L mutant mice, underlying the specific neurological symptoms including epilepsy in S218L mice. CSD susceptibility was also increased (15, 78-80) more in S218L compared to R192Q mutant mice *in vivo* under anesthesia, and further modulated by hormones of stress and sex (79, 88). The stronger CSD susceptibility of homozygous in comparison to heterozygous S218L mutant *in vivo* (15, 78) is suggested to be due to a fraction of cortical Ca_v2.1 channels in S218L homozygous mutant synapses already being opened at membrane potentials below the needed threshold for generating action potential (82). The more severe neurological deficits in patients with the S218L mutation compared to the R192Q mutation confirms these experimental observations.

2.12. Neuronal Network Dependent Synaptic Plasticity in FHM1 Mutant Mice

Cortical synapse proteomes of FHM1 R192Q mutant mice and WT mice was analyzed by iTRAQ reagent-based Liquid chromatography-mass approach to identify the proteins and their different expression. Except few alterations in presynaptic active zone or postsynaptic density proteins, rest of them were subtle (89). R192Q mutation does not have a functional effect on synaptic molecular architecture which is consistent with the earlier findings in the same mutant mice reporting no changes in the abundance level of several kinds of Cav channels (14) or any change in the releasable pool of neurotransmitters at cortical synapses (16). However, there was a significant difference in abundance levels of 19 proteins involved in vesicle turnover, neurite outgrowth and actin molecule dynamics, and finally, glutamate transporters between genotypes. These data imply the possibility of compensatory mechanisms to counter-balance a dysregulated glutamatergic signaling and as an adaptation mechanism at the level of synapse (89). An enhancement of synaptic depression for R192Q (16) and S218L mutant mice (82) has been reported at the cortical level, in *in vitro* studies, indicating a decline in synaptic transmission efficacy after repetitive stimulation. Findings from *in vitro* and *in vivo* studies of the brainstem Calyx of Held synapse in homozygous S218L mutant demonstrated a faster rate of recovery after synaptic depression in comparison with WT (90); this finding also was shown *in vitro* for R192Q mutant mutant (91). In the cerebellum of R192Q and S218L mutant mice slices, a short-term synaptic facilitation reduction at the parallel fiber-to-Purkinje cell synapses was observed which may be related to a facilitated state of mutant presynaptic Cav2.1 channels (60) that impair the balance in Purkinje cell firing tuning, and by this causing cerebellar ataxia associated with FHM1. The hippocampal function in R192Q and S218L mutant recently shown in an *in vivo* study demonstrated that enhancement in long-term potentiation with no change in long-term depression were associated to impaired learning and memory behavior, and this could be as a result of imbalance between potentiation and depression at the neuronal circuit level (83).

How neuronal network modifications in the brainstem, hippocampus and cerebellum lead to functional FHM1 features of migraine-relevant neuronal networks remains to be investigated. The same mutation in the cortex has different effects compared to the trigeminal ganglion (TG) (85) and brainstem (92), and this leads to the idea that functional influences of FHM1 mutations can be neuron type dependent. For instance, there is a strong FHM1 mutations gain-of-function effect seen for excitatory pyramidal neurons in contrast to the absence of any influence of these mutations on cortical fast-spiking interneurons and this may be due to the expression of some interneuron-specific Cav2.1 channels with gating properties that are not altered by the FHM1 mutation (81). Functional differences between various types of neurons in healthy networks in the cortex (93) could be the reason for distinct FHM1 mutations effects on different neuronal networks that may lead to dynamic perturbations in the excitatory/inhibitory balance in specific neuronal networks in the brain.

2.13. The Effect of FHM1 Mutations on Neuroinflammation

The first pro-inflammatory profile evidence of *in vivo* and *in vitro* studies in R192Q mutant TG indicates that neuroinflammation may occur in this migraine mouse model. In mutant or WT TG, most of neurons co-express P2X3 and tumor necrosis factor alpha (TNF α) receptors making them potentially susceptible to inflammation mediated by TNF α and the pain signaling related to it (94, 95). R192Q mutant TG have been reported to be enriched in activated macrophages, showed by both immunoreactivity to the CD11b (an adhesion molecule marker to mark active macrophages and microglia), Iba1 and macrophage antigen ED1, and also by macrophage morphology, compared to WT mice (95). R192Q mutant TG expressed increased levels of mRNA of IL6, IL1b, and IL10 and the MCP-1 chemokine and TNF α cytokines (95). In accordance with the study investigating that TNF α is a major factor in TG sensitization, following an inflammatory reaction induced by LPS injection, expression of TNF α and macrophage occurrence were significantly higher in ganglia of R192Q mutant compared to WT ganglia (95). The complex molecular and cellular environment in mutant TG reveals a novel tissue phenotype consistent

with a neuroinflammatory profile. In FHM patients, this can contribute to pathophysiology of trigeminal pain by release of soluble mediators such as TNF α , establishing a crosstalk between resident glia and sensory neurons, underlying the process of neuronal sensitization (95).

In a recent study, gene expression profile analysis from isolated cortical tissue of FHM1 R192Q mutant mice revealed the molecular pathways affected by CSD (96). CSD-induced up-regulation of a group of genes specifically, in FHM1 R192Q mutant brains was striking data of the study. These genes show a strong functional enrichment for inflammatory signaling genes (96) including several genes in cluster 1 (Cd53, Anxa2, Ms4a6d, Ccl2, C3ar1, Vim and Timp1) which are main drivers of inflammatory reactions (97). Pathway analyses indicate that the exacerbated inflammatory reaction is interferon related (96). However, the way that this interaction between R192Q mutation and CSD result in a definite inflammatory profile should be more studied. Epilepsy model investigations have some hints about the close interplay between increased excitation and inflammation (17, 18), which suggest that the elevated activity in glutamatergic pathways in R192Q KI mice (16) being more severe during CSD episodes, may start an enhanced inflammatory response specifically. On the other hand, it can be interpreted that the CSD-induced elevation of inflammatory response can be due to a pro-inflammatory state in the FHM1 R192Q brains which may already exist in naïve animals (96). Therefore, naïve TG of R192Q KI mice could exhibit a pro-inflammatory phenotype with increased activated macrophages and microglia and also elevated levels of cytokine expression (86, 98-100). As reported in wild type mice, CSD caused a signaling pathway between stressed neurons and trigeminal afferents via opening of neuronal Panx1 megachannel and caspase-1 activation followed by HMGB1 release from neurons and nuclear factor- κ B activation in astrocytes (6). Therefore, more studies are needed to investigate the CSD-induced parenchymal neuroinflammation pathway on FHM mutant mouse models.

2.14. Cortical Spreading Depression

Neurons and their proximal dendrites are the major active players of CSD (101). The brain is responsible for about 20 % of the body's resting metabolism (102), and beside this sodium pumps consume relatively half of that 20 % for maintaining homeostasis of the ion gradients. The term CSD describes the disturbance and breakdown of this homeostasis (103).

The characterization of CSD is near-complete breakdown of ion gradients (104), near-complete sustained depolarization in individual neuron recordings (105), loss of electrical activity (106), huge shunt of neuronal membrane resistance (105), and neuronal swelling and dendritic spines distortion (107). Therefore, CSD represents an electrical alteration with near-complete short circuit between neurons and extracellular space (103), and a morphological and biochemical change observed as neuronal cytotoxic edema (104, 107). Neurons cannot fire action potentials because the sustained depolarization is above the threshold at which the membrane channels which generate action potentials become inactivated (108). Consequently, CSD leads to the brain electrical silence that was termed cortical spreading depression of brain electrical activity by Aristides Leão in 1944 (106).

In the extracellular space, CSD is observed prominently as a negative change of the slow potential (109). This slow potential alteration may be the result of longitudinal gradients of depolarization along neurons, most probably due to dendritic opening of ion channels, which allows the large sustained influxes of small cations including sodium and calcium into the neurons (105).

There is substantial experimental and clinical data indicating to the pivotal role of CSD as a part of triggering headache initiation mechanism (6, 8, 110) mainly in migraine with aura attacks. CSD is called the wave of neuronal and glial depolarization with a spreading velocity of 3–6 mm/min through the cerebral cortex, and is known as the electrophysiological correlate of migraine aura (5). CSD initiates neuroinflammatory cascades associated with neuronal Panx1 mega channels opening and inflammatory mediators release including HMGB1, and finally trigeminovascular activation (7, (14)). CSD in animal models, initiates a cascade of events in cortex, subcortex (7), meninges and brainstem consistent with headache

development (6, 8, 110). Beside cortical structures, subcortical areas including diencephalic and brainstem nuclei are also affected by CSD (7), and might contribute to migraine pathophysiology by modulating the perception of activity in trigeminovascular system (TVS).

2.15. High Mobility Group Box 1 (HMGB1) Protein

HMGB1, a highly conserved nonhistone nuclear DNA-binding protein, is widely expressed in most eukaryotic cells including neural cells in several animal species including humans (111). Nuclear HMGB1 is able to bind to DNA to stabilize nucleosome formation and maintains nuclear homeostasis. HMGB1 enables bending of DNA and facilitates transcription to regulate gene expression (112).

HMGB1 acts as a nuclear and cellular danger signal (9). Endogenous danger signals released from necrotic or stressed cells that trigger the inflammatory response after trauma have been termed alarmins or danger-associated molecular patterns (DAMPs). The subcellular localization of HMGB1 depends on the type and activation state of the cell. The HMGB1 is mainly localized in the cell nucleus. HMGB1 can exert different functions depending on its cellular localization. HMGB1 can be released from the nucleus to the extracellular space in response to different stimuli in two ways: following cellular injury it is passively released during cellular apoptosis or necrosis; or it is released actively following inflammatory signals from activated immune cells or neuronal cells (10). Upon release, extracellular HMGB1 binds to its putative receptors and induces a series of signaling pathways in response to the original damage (9). Increasing evidence now suggests that HMGB1 is a key mediator in cerebral ischemic progression (10).

Released HMGB1 has recently been characterized as a key inflammatory mediator in response to infection, injury, and inflammation by binding to toll-like receptor 4 (TLR4) and/or receptor for advanced glycation endproducts (RAGE) (Figure 2.3.)(113); besides active secretion, HMGB1 can be released into extracellular space from damaged cells or necrotic cells. In this case, the membranes of necrotic or damaged cells become “leaky” and HMGB1, which is normally bound

loosely to chromatin, diffuses from nucleus to cytoplasm, then into the extracellular matrix (114).

Extracellular HMGB1 acts as a trigger or modulator that affects inflammation, proliferation, migration, and cell survival. High amounts of HMGB1 have been detected in the extracellular space in various inflammatory conditions (115).

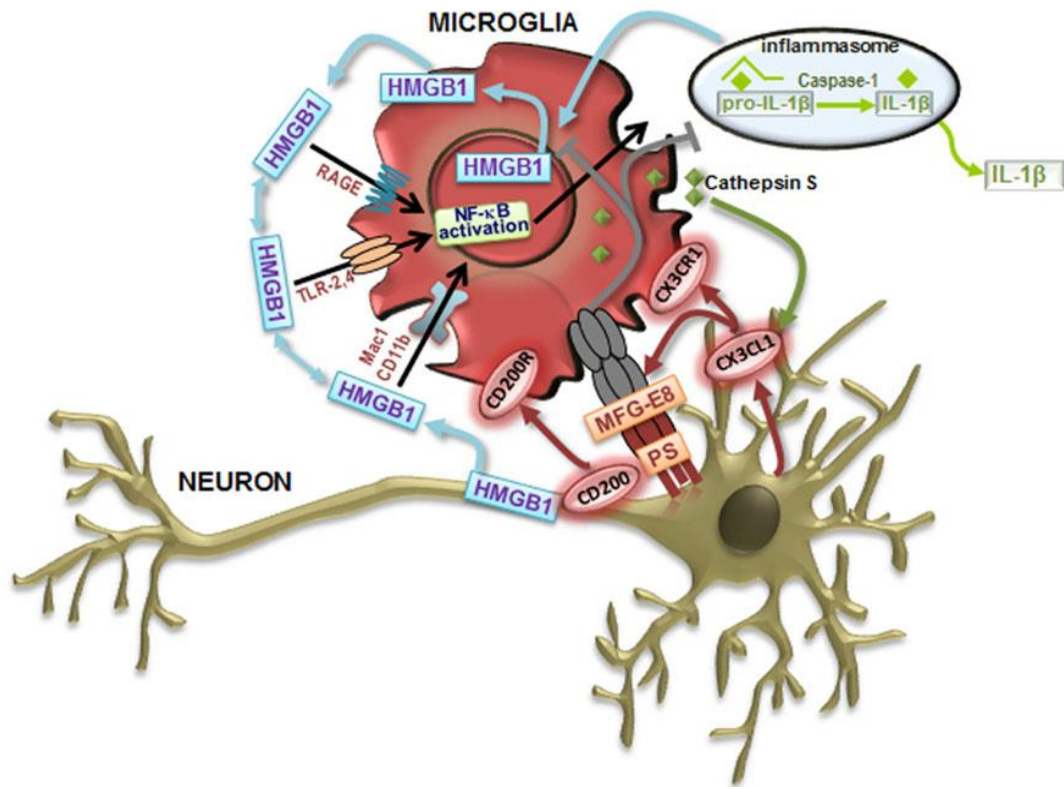


Figure 2.5. Neuron–microglia communication signaling pathways. After recognition of damage-associated molecular patterns (DAMPs), Toll-like receptors (TLR) activate downstream signaling cascades, then activate nuclear factor- κ B (NF- κ B) which induces the transcription of neuroinflammatory mediators associated with the microglia-like microglial cell phenotype, including the proinflammatory cytokines tumor necrosis factor (TNF)- α , and interleukin (IL)-1 β . High-mobility group box 1 (HMGB1) is associated to all these signaling events. HMGB1 released by stressed neurons and activated microglia concur for a vicious cycle mediating progressive, chronic neurodegeneration and neuroinflammation. HMGB1 may interact with receptors such as TLR-2, TLR-4, RAGE (receptor for advanced glycation end products), Mac-1 also known as CD11b, and possibly others (10).

2.16. The Role of Nuclear Factor κ B in Neuroinflammation

Nuclear Factor κ B (NF- κ B) is a ubiquitous transcription factor which can be found in almost all the cells of an organism. NF- κ B regulates the cytokines and chemokines expression, including interleukins, interferons, lymphokines and tumor necrosis factors. Microglial cells have membrane receptors such as toll-like receptors (TLRs), nucleotide-binding oligomerization domain proteins (NLRs), C-type lectin receptors (CLRs), the receptor for advanced glycation endproducts, RAGE and receptor for interferons and cytokines (11). TLRs specifically recognize pro-inflammatory ligands including pathogen-associated molecular patterns (PAMPs) and damage-associated molecular patterns (DAMPs)(Figure 2.4.). PAMPs include bacterial, parasitic, fungal, and viral molecules such as viral RNA and DNA, chitin, α - and β -glucans and microbial cell wall components (11). Examples of DAMPs can be blood-clotting factors, DNA and RNA, and different intracellular proteins that are released from damaged and dying cells (11).

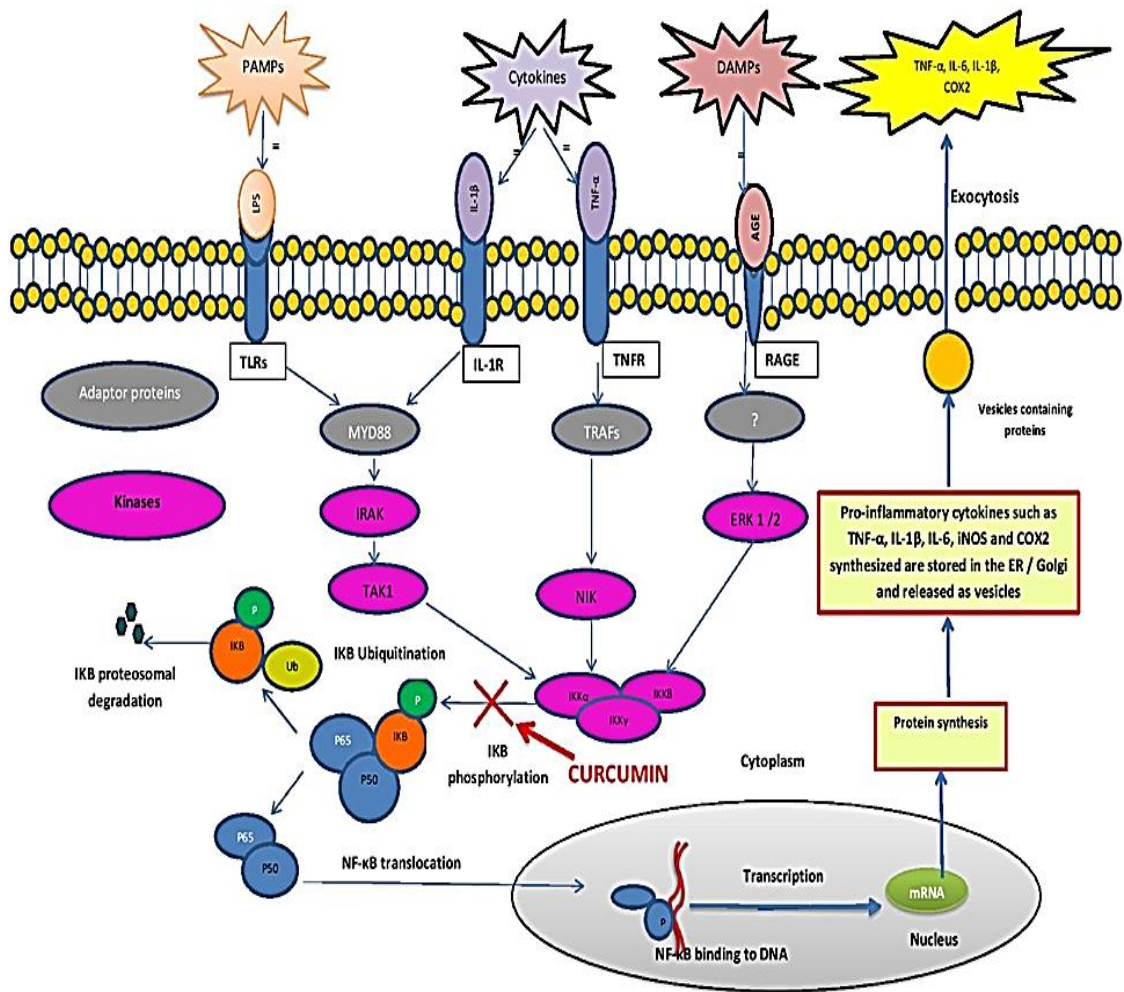


Figure 2.6. Schematic diagram of the NF- κ B pathway. Cells have membrane receptors such as toll-like receptors (TLRs), tumor necrosis factor receptors (TNFR), interleukin-1 β receptors (IL-1R), and receptor for advanced glycation end products (RAGE). These receptors distinguish pro-inflammatory ligands such as cytokines, pathogen-associated molecular patterns (PAMPs), damage-associated molecular patterns (DAMPs). Ligand binds activate downstream proteins such as tumor necrosis factor associated factors (TRAF). TRAF activates specific protein kinases including mitogen activated protein kinases (MAPK) such as interleukin-1 receptor-associated kinase 1 (IRAK), and NF-kappa-B-inducing kinase (NIK). These kinases activate I-kappa-B ($\text{I}\kappa\text{B}$) kinases which phosphorylate $\text{I}\kappa\text{B}-\alpha$. During cell stimulation, phosphorylation of $\text{I}\kappa\text{B}$ causes its dissociation from the complex, and its degradation, allowing NF- κ B to be activated and translocated to the nucleus, where it attaches to specific DNA sequences that are present in the promoters of several target genes, and finally leads to encoding the pro-inflammatory cytokines (IL-1, IL-6, TNF- α), chemokines (IL-8, MCP1, eotaxin), adhesion molecules (E-selectin), cyclooxygenase-2 (cox-2) and inducible nitric oxide synthase (iNOS) (11).

In an unstimulated cell, NF- κ B is located in the cytoplasm as an inactive heterodimer which is composed of two subunits, p50 and p65. The heterodimer make a complex together with the inhibitory proteins I κ B- α or I κ B- β , retaining it in the cytoplasm. When a cell is stimulated by a PAMP, cytokine or DAMP, a cascade of signaling events is triggered which is initiated by adapter proteins stimulation in the cytoplasm. In the case of many TLRs, myeloid differentiation primary response protein 88 (MYD88) is such an adaptor protein (116). MYD88 activates specific protein kinases downstream, such as I κ B kinase and mitogen activated protein kinase (MAPK) which phosphorylate I κ B- α . I κ B- α phosphorylation and its proteasomal degradation eventually leads to its dissociation from the NF- κ B complex. Then, NF- κ B translocates into the nucleus, where it binds to the promotor regions of specific genes (117, 118), and recruits other proteins, which lead to the expression of many proinflammatory cytokines (IL-1, IL-6 and TNF- α), chemokines (IL-8, MCP1, eotaxin), adhesion molecules (VCAM, E-selectin) and inducible pro-inflammatory enzymes (COX-2 and iNOS), that all lead to the exacerbation of the inflammatory process (11, 119) including CSD a putative cause of migraine aura.

3. MATERIALS AND METHODS

3.1. Materials Used

The antibodies and serums used for *in vitro* experiments are listed in Table 3.1. For mounting sections Polyl-lizin (Sigma) lamms were used. For IHC experiments following materials were used; Sucrose (Sigma), Hoechst 33258 (Thermofisher), Tris buffer powder (Thermofisher), PBS tampon powder (Biowest), Bovine Serum Albumin (Biowest), PFA, Isoflurane (Abbott), Isotonic Sodium Chloride (%0.9) (Polyfarma).

Table 3.1. Antibodies for Immunohistochemistry and Western Blotting

Primary antibodies	Origin	Aim	Polyclonal/ Monoclonal	Concentration	Company
HMGB1	Rabbit	Mouse	Polyclonal	1:200	Abcam
NeuN	Mouse	Mouse	Monoclonal	1:200	Calbiochem
NF-κB p65	Mouse	Mouse	Monoclonal	1:200	Cell Signaling
S100 beta	Mouse	Mouse	Monoclonal	1:100	Abcam
HMGB1	Mouse	Mouse	Monoclonal		Abcam
Secondary antibodies					
cy2 affini pure goat anti rabbit iga (H+L)	Goat	Rabbit		1:200	Jackson Immunoresearch
Cy3 affini pure goat anti mouse iga (H+L)	Goat	Mouse		1:200	Jackson Immunoresearch
cy3 secondary anti rabbit antibody (Fab)		Rabbit		1:100	Jackson Immunoresearch
Serums					
Normal Goat Serum				%10	Jackson Immuno Research
Normal Mouse Serum				%10	Jackson Immuno Research

Table 3.2. Experimental Facilities

Facility name	Company
Precision Scales	Shimadzu-AUX220
Vortex	Nüve-NM110
Distilled Water Machine	Mp Minipure Basic
Anesthesia and Oxygen Machine	AMS-Minor 612
Stereotaxic Frame	WPI
Homeothermic Blanket	Kent Scientific
pH Meter	Thermo-Orion3Star
Cryostat	Leica-CM1100
Fluorescent-Light Microscope	Nikon- E600
Stereomicroscope	Nikon SMZ 745T
Confocal Laser Scanning Microscope	Leica TCS SP8
Power Lab	AD Instruments
Perfusion Pump	MasterFlex console drive, Cole-Parmer Instrument Company, model 77800-60
High speed drill	World Precision Instruments

3.2. Methods

3.2.1. Ethics

All experimental procedures were carried out in accordance with the Guide for Care and Use of Laboratory Animals (NIH Publication No. 85-23, 1996), and were approved by Hacettepe University Animal Experiments Ethics Committee (2016/42 and 2018/57). All experimental procedures were held in the laboratories of Institute of Neurological Sciences and Psychiatry.

3.2.2. Animals

For this study, we used 46, 2- to 4-month-old, female WT mice (“WT mice”- C57BL/6J background) and transgenic FHM1 mice that carry either the human *CACNA1A* R192Q (homozygous) and S218L (heterozygous) missense mutation (“FHM1 R192Q and S218L mutant mice”)(Figure 3.1.). The mutant mice were generated by introducing the respective mutation in the endogenous *Cacna1a* gene

using a gene targeting approach (14, 78). Mice were obtained from Leiden University, Medical Centre as part of a collaboration with Prof. Dr. Arn van den Maagdenberg and Dr. Else Tolner. All mice were housed under a fixed 12-hours light/12-hours dark cycle in 24-26°C and 50-60% moisture in a special room for animal housing with fresh air and least stressful stimuli, and allowed free access to food and water at Hacettepe University, Institute of Neurological Sciences and Psychiatry animal facility. All animals were sacrificed immediately after completing the experimental procedures.

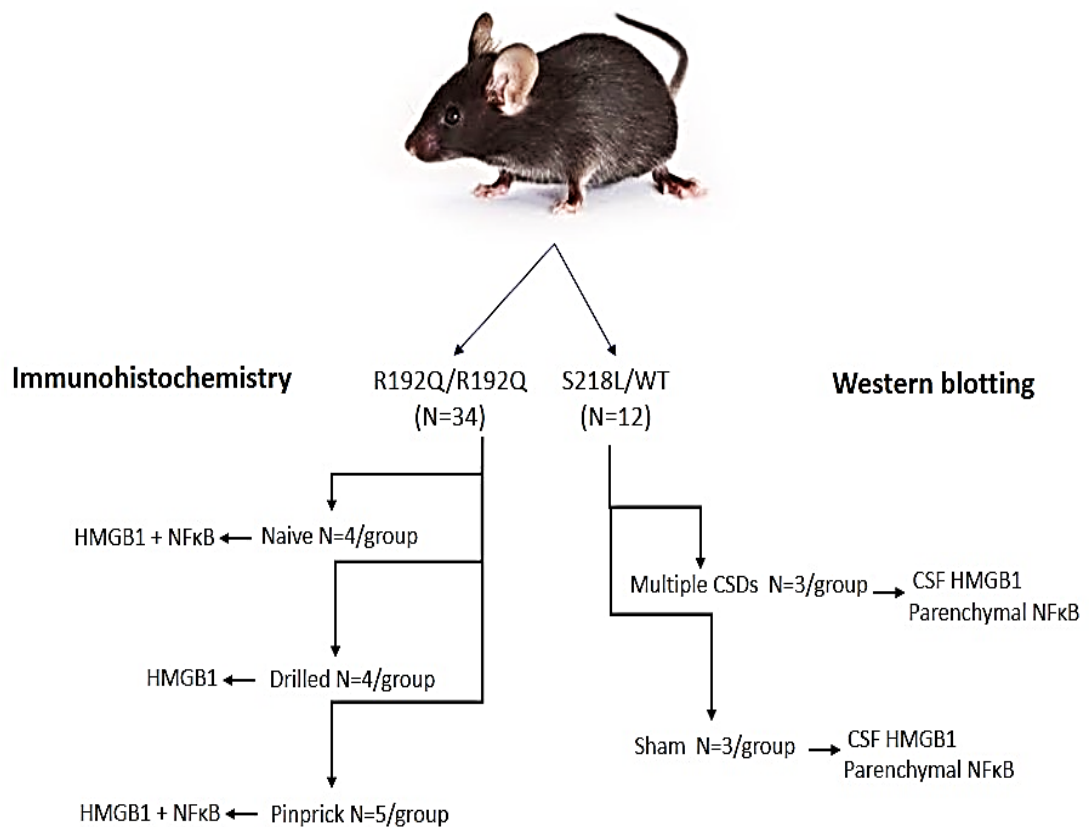


Figure 3.1. Schematic showing the number and design of wild-type (WT) and transgenic mutant mice with the R192Q or S218L missense mutation in each experimental group. A total of 46 mice was used for the different experiments that included pinprick-induced single CSD, KCl-induced multiple CSDs and CSF collection, drilling experiment as a non-invasive stimulus, and naïve control group.

3.2.3. Surgical Procedure and Electrophysiological Recordings

CSD experiments were performed under urethane (1.25 g/kg, i.p.), and xylazine (10 mg/kg, i.p) anesthesia. After deep anesthesia was achieved, mice were placed into a stereotaxic frame and allowed to breathe spontaneously under nasal oxygen support (2 L/min). The temperature was monitored by a rectal probe and maintained at $37 \pm 0.1^{\circ}\text{C}$ by a homeothermic blanket control unit. Surgery was performed under an operating stereo-microscope. Cranial sutures and bregma were exposed with a scalp incision. For pinprick and KCl-soaked cotton ball application a burr hole was drilled by using a high-speed drill while cooling with saline without removing dura mater above right frontal cortex (1.3 mm anterior; 1 mm mediolateral to bregma). For the drilling experiment a burr hole was drilled at the same coordinates without touching the dura. For some experiments a 1-mm-thick (Outer Diameter) polyethylene cannula was inserted 2 mm deep into the right lateral ventricle through a burr hole drilled over the right parietal bone (0.15 mm posterior, 0.65 mm lateral to bregma) under isoflurane anesthesia. CSF was collected one day after, by a 26 gauge hamilton syringe slowly inserted through the i.c.v. cannula during 1-hour topical application of a KCl-soaked cotton ball, in every 10 minutes interval.

Direct-current (DC) potentials were recorded with two Ag-AgCl pellet electrodes (1 mm diameter) placed over the thinned skull on either both the right and left parietal bone simultaneously (2 mm mediolateral; 1.5 mm posterior to bregma) for some experiments, or only the right parietal bone for others (Figure 3.2.). Good electrical contact was obtained with electrode gel applied to the electrode tip. An Ag-AgCl plated disk electrode placed under the neck muscles as the ground lead. Signals were digitized, displayed, and stored on a computer by a data acquisition and analysis system (Power Lab).

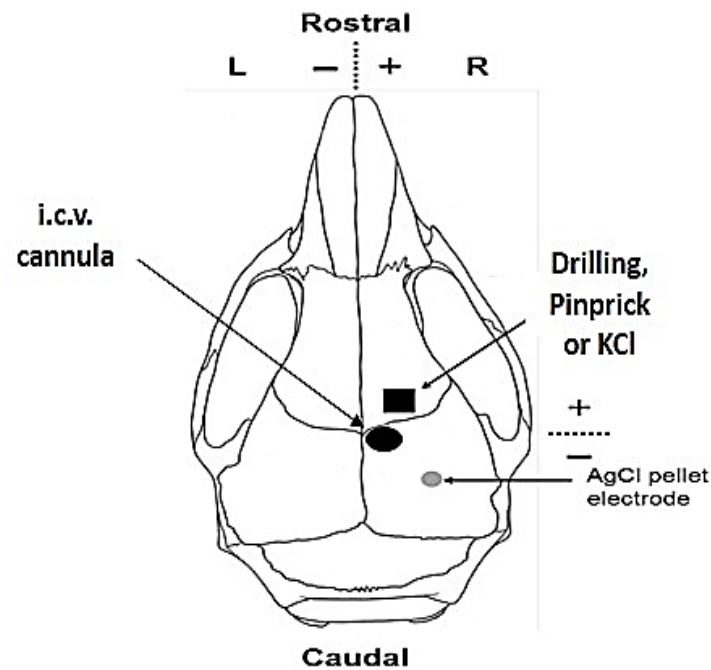


Figure 3.2. A schematic showing the location of the position of drilling, pinprick and KCl-induced CSDs, intracerebroventricular (i.c.v.) cannula and CSF collection, and non-invasive DC recordings.

3.2.4. Experimental Design

Two paradigms were used to assess cortical spreading depression (CSD)-induced parenchymal neuroinflammation (paradigms 1 and 2). Two further paradigms (paradigms 3 and 4) were performed to assess basal and confounding-factor induced neuroinflammation.

Paradigm 1: The pinprick method was used to induce *single* CSD to investigate neuronal HMGB1 release and glial NF- κ B activation (Figure 3.2.) for 30 minutes, as this time point has been reported to be the time of maximum amount of HMGB1 release in neurons after pinprick compared to 5 and 60 minutes which have been studied (6) Experiments ended by transcardial perfusion and immunohistochemistry for neuronal HMGB1 and NF- κ B activation in astrocytes.

Paradigm 2: Continuous topical application of a cotton ball soaked in 1 M KCl placed on the frontal cortex was used to induce *multiple* CSD-induced neuronal HMGB1 release in CSF and NF- κ B translocation in astrocytes of both brain

hemispheres (Figure 3.2). Experiments ended with euthanasia of the mouse by cervical dislocation in order to obtain fresh brain tissue for nuclear fractionation to assess NF- κ B translocation from cytoplasm to nucleus and for CSF, both assessed by Western blotting.

Paradigm 3: A burr hole was drilled over the right frontal cortex on the same location as the pinprick induction site without touching the dura to assess the effect of drilling the skull as a non-aversive stimulus on inflammation. Electrophysiological activity was recorded by an Ag-AgCl pellet electrode simultaneously to study if drilling also induced a CSD.

Paradigm 4: Naïve mice were anesthetized with intraperitoneal injection of 1 mg/g chloral hydrate to investigate basal neuroinflammation in the brain. After achieving deep anesthesia a transcardial perfusion was performed and the brain was extracted for further molecular experiments.

3.2.5. Immunohistochemistry

Mice were deeply anesthetized and transcardially perfused with heparinized saline and 4% PFA. Brains were quickly removed, post-fixed in the same solution overnight and cryoprotected in 30 % sucrose solution for two days. Twenty- μ m-thick coronal sections were cut on a cryostat. Sections were immunostained with rabbit polyclonal HMGB1 (1:200, Abcam) followed by secondary labeling with goat anti-rabbit Cy2 antibody (1:200, Jackson ImmunoResearch). Some sections were double-labeled with mouse monoclonal NeuN antibody (1:200, Chemicon) to identify neurons. Briefly, sections were rinsed after primary labeling with mouse monoclonal anti-NeuN and secondary labeling with goat anti-mouse Cy3 antibody (1:200, Jackson ImmunoResearch) and, then incubated with rabbit polyclonal anti-HMGB1 overnight followed by goat anti-rabbit Cy2 secondary antibody. Omission of the primary antibody from the blocking or PBS solution was performed to test the specificity of immunoreactivity. Sections were mounted in glycerol/PBS (1:1) medium containing 12.5 mg/mL sodium azide and 1 μ L/mL Hoechst-33258 and were examined under a wide-field fluorescence or laser-scanning confocal microscope with appropriate filter sets.

For astrocyte (S100-beta) and NF- κ B double-staining the following protocol was used: antigen retrieval for 10 minutes in 80°C in 10 mM Sodium citrate buffer in 0.05% Tween with pH 6, followed by washing the sections with PBS for 5 minutes three times each, and then blocking with 10% normal goat serum (NGS) with 0.5% TritonX100 in PBS with 0.3 M Glycine (to reduce background) for 90 minutes and incubating the sections overnight at +4°C with primary monoclonal anti-NF- κ B (P65) antibody (Cell Signaling) in 1:200 in blocking solution. On day 2, first a solution of 1 μ L primary anti-S100-beta (Abcam) with 1.5 μ L Cy3 secondary anti-rabbit antibody (Fab) with 10 μ L PBS was prepared in an aluminum folder and shaken for 1 hour, then 188 μ L of 10 % normal mouse serum (NMS) was added and incubated for 1 hour at room temperature (RT). Next, sections were blocked in this solution overnight at +4°C. On the third day, the sections were washed with PBS for 5 minutes three times each and mounted in glycerol/PBS (1:1) medium containing 12.5 mg/mL sodium azide and 1 μ L/mL Hoechst-33258 and examined under a wide-field fluorescence or laser-scanning confocal microscope with appropriate filter sets.

3.2.6. Western Blotting

3.2.6.1. Subcellular Fractionation and NF- κ B Western Blotting

Mice were euthanized under deep anesthesia of urethane and cervical translocation were done. Brains were quickly removed, dissected to several regions of interest including cortices, sub-cortices, cerebellum, and trigeminal ganglia from both CSD-induced hemisphere and contralateral hemisphere, then placed on ice, and prepared for nuclear and cytoplasmic extraction according to *NE-PER Nuclear and Cytoplasmic Extraction Reagents* (Thermo-Fisher Sci., USA) as indicated in the instructions. Brains were dissected into smaller pieces and weighed. Appropriate volume of CERI containing protease inhibitor cocktail was added to sample and homogenized using tissue grinder. Mixture was vortexed for 15 seconds and incubated on ice for 20 minutes. Ice cold CER II buffer was added to the tube and was vortexed for 5 seconds, incubated on ice for 5 minutes. Solution was centrifuged at 16000 g for 5 minutes and supernatant (Cytoplasmic fraction) was transferred

without touching the pellet immediately. Pellet was suspended in the appropriate amount of ice cold NER buffer with protease inhibitor cocktail and sample was incubated on ice for 40 minutes by vortexing 15 seconds every 10 minutes interval. Sample was centrifuged at 16000 g for 10 minutes and supernatant (Nuclear fraction) was transferred immediately to a clean pre-chilled tube. Protein extracts were stored at 80°C until use.

Protein amounts were quantified by Pierce BCA Protein Assay Kit (Thermo-Fisher Sci.). 30 µg protein was loaded to the gel for Western blotting. Primary antibody incubation was performed at +4°C for overnight (α -NF- κ B 1:1000, α -Histone-3 1:2000, α - β 3-Tubulin 1:2500) and secondary antibody (1:5000) incubation was performed at room temperature for 1 hour. Histone-3 and β 3-Tubulin proteins were used as nuclear and cytoplasmic fractions' loading controls.

The protein bands were detected by ECL based technique and were quantified with ImageJ analysis program.

3.2.6.2. CSF Collection after CSD and HMGB1 Western Blotting

For the detection of HMGB1 in CSF, this body fluid was collected through an i.c.v. cannula placed into right lateral ventricle a day before the experiment. In the 1 hour duration of CSD induction, CSF was collected every 10 minutes and stored immediately in -80°C. CSDs were induced by topical application of a 1 M KCl-soaked cotton ball placed on the right frontal burr hole for 1 hour. During this period, 3-5 µL CSF was collected from cannula (n = 3 mice). Sham experiments (n = 3 mice) were performed with application of saline-soaked cotton ball instead. CSD induction and CSF collection were performed as described above. A CSF sample was discarded if it was not crystal clear in order to be sure that blood contamination was not present. CSF was frozen immediately and stored at -80°C until use. Individual CSF samples were used at equal amounts for Western blotting. The blotted membrane was heated in boiling PBS for 5 minutes to enhance the signal. The other steps were performed with primary (mouse monoclonal anti-HMGB1, 1:500, Abcam) and secondary (HRP-conjugated anti-rabbit IgG, 1:3000, Cell

Signaling) antibodies as described above. HMGB1 protein bands were detected by ECL based technique and were quantified by ImageJ analysis program.

3.2.7. Electrophysiological Analysis

Total CSD duration was measured as the time from the beginning of the depolarization phase of the CSD to the end of the repolarization phase. To measure CSD half-maximum duration, the duration of CSD between half maximum amplitude of both depolarization and repolarization phase were assessed using Power Lab chart software. CSD derivative was measured for first component, the depolarizing phase, of CSD in KCl-induced multiple CSD experiments, for both the first CSD and all CSDs, using Power Lab software.

CSD velocity was calculated from the distance between the CSD induction site to the recording electrode (3 mm for pinprick experiments, 3.5 mm for KCl experiments), and the onset latency of the CSD, as mm/min. CSD frequency was calculated as the number of CSD events during the time course of the experiments (30 minutes in pinprick experiments and 1 hour in multiple CSD experiments).

3.2.8. Quantification of HMGB1 Release and NF- κ B Activation

HMGB1-labeled cells were counted at 200x magnification on 8 images obtained 2.5 mm apart from two frontal and two posterior coronal sections from each mouse, the studied brain areas were: frontal cortex (primary motor area), parietal cortex (primary somatosensory area), striatum, and thalamus, as these are the most studied areas for CSD in FHM1 mutant mice, of both ipsilateral and contralateral hemispheres to CSD induction site. Totally 13,062 neurons and 1,448 astrocytes were quantified in WT mice, and 13,740 neurons and 1,540 astrocytes were quantified in R192Q mutant mice. The NeuN-positive/HMGB1-negative signal was counted as total HMGB1 release. The HMGB1 immunoreactivity that extends the nucleus in NeuN-positive cells was considered as HMGB1 cytoplasmic signal. NeuN-positive/HMGB1-positive signal was regarded as no HMGB1 release. The quantification was done on different brain areas including ipsilateral and

contralateral frontal cortices, ipsilateral and contralateral parietal cortices, ipsilateral and contralateral striatum and ipsilateral and contralateral thalamus by two blinded researchers and the data were averaged.

For NF- κ B quantification the same method was performed at 400x magnification on 4 images obtained from frontal coronal sections of each mouse. S100-beta-positive cells (astrocytes) that were positive for nuclear NF- κ B in the nucleus that is confirmed with Hoechst-33258 staining, were counted out of the total S100-beta cells and the ratio reflected NF- κ B activated astrocytes.

3.2.9. Statistical Analysis

Data were expressed as mean and standard error of mean (mean \pm SEM) throughout the text. Non-parametric data was analyzed with Kruskal-Wallis test and the significant data was further analyzed by Mann-Whitney U test. All calculated p-values were two-tailed, and $p < 0.05$ was considered as statistically significant. Statistical analysis was performed using GraphPad Prism 5 (GraphPad Software, La Jolla, CA) and IBM SPSS Statistics version 23 (IBM, Armonk, NY).

4. RESULTS

4.1. Parenchymal Neuroinflammation in Naïve Wild-type and R192Q Mutant Mice

4.1.1. HMGB1 Release in Naïve Wild-type and R192Q Mutant Mice

In order to investigate to what extent basal neuroinflammation is present in the R192Q mutant brain compared to that of WT mice, the NeuN-positive/HMGB1-negative cells were counted as a readout of total HMGB1 release from neurons. The results indicated that in right frontal cortex the amount of HMGB1 release was 6.8 ± 0.4 % (mean \pm SEM) in R192Q mice whereas this amount in the same area in WT mice is 4.1 ± 0.4 %; in right striatum the amount of HMGB1 release was 8.7 ± 0.1 % in R192Q and 4.2 ± 0.1 % in WT mice; the amount in left frontal cortex was 6.9 ± 0.5 % in R192Q and 3.3 ± 0.4 % in WT mice; and in left striatum it was 7.5 ± 0.8 % in mutant and 4.1 ± 0.4 % in WT mice. In all four brain areas, there was a significantly higher amount of parenchymal neuroinflammation, as revealed by the neuronal total HMGB1 release, in R192Q mutant mice compared to WT (n=4/group; p<0.05) (Figure 4.1.).

HMGB1 Total Neuronal Release in Naive WT and R192Q mice

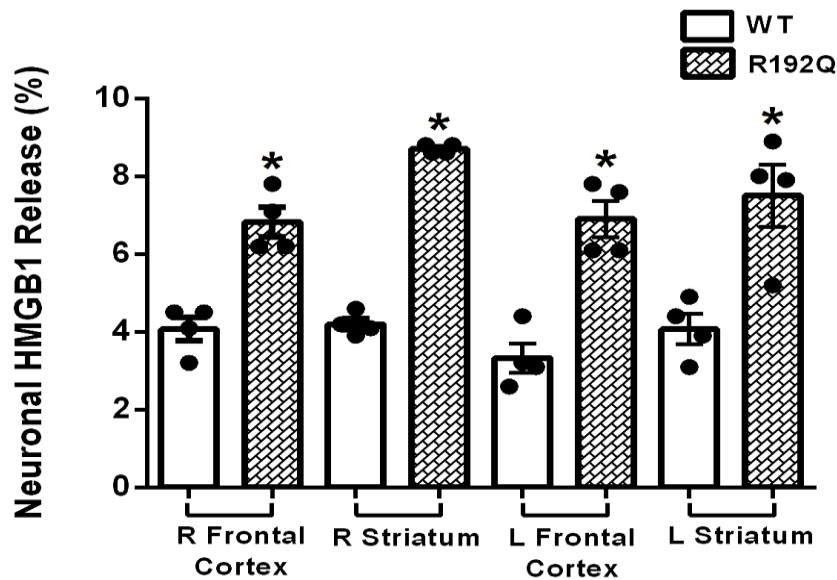


Figure 4.1. HMGB1 release in cortical and subcortical areas of naive WT and R192Q mutant mouse brains. NeuN-positive/HMGB1-negative cells were counted as total HMGB1 release. **R:** Right side. **L:** Left side. Bars show standard error of mean (SEM). $p=0.0005$ in Kruskal Wallis test. $*p=0.0286$ mutant *versus* WT in the same area; $n=4$ /group.

In confocal images taken from 20- μ m thick sections from the right parietal cortex, neuronal nuclei (NeuN) are shown in red and HMGB1 in green (Figure 4.2.). NeuN-positive/HMGB1-negative cells (triangles) were counted as total HMGB1 release. NeuN-positive/HMGB1-positive cells (arrows) were counted as no release. Total HMGB1 release was more prominent in the R192Q mutant mouse right parietal cortex.

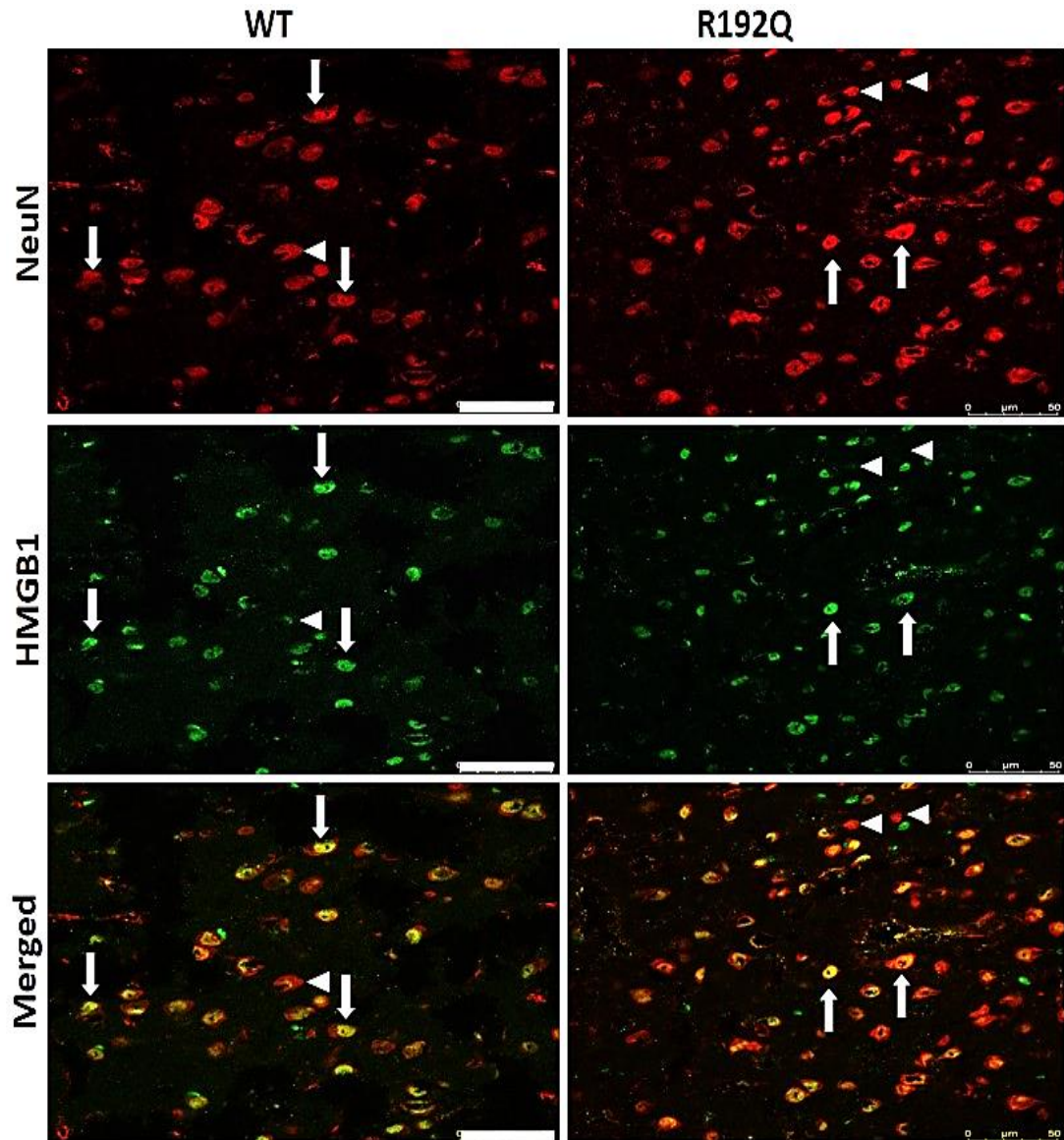


Figure 4.2. Basal neuroinflammation in naïve WT and R192Q mutant mice. Confocal images of the right parietal cortex show colocalization of neuronal nuclei (NeuN) (in red) with HMGB1 signal (in green). NeuN-positive/HMGB1-negative cells (arrowheads) were counted as total HMGB1 release (some are shown in the image as examples). NeuN-positive/HMGB1-positive cells (arrows) were counted as no release in HMGB1 (some are shown in the image as examples). Images were taken on 20- μ m-thick sections by laser scanning confocal microscope. Scale bars: 50 μ m.

4.1.2. NF- κ B Cytoplasm–To–Nucleous Translocation In Astrocytes of Naïve Wild-type and R192Q Mutant Mice

In an unstimulated cell, NF- κ B is located in the cytoplasm in an inactive form. Only upon stimulation NF- κ B translocates to the nucleus. Here we used S100-beta as an astrocyte marker, an NF- κ B antibody to show the immunoreactivity of these proteins, and Hoechst-33258 as a nuclear marker. To investigate the extent of basal neuroinflammation in R192Q mutant compared to WT mice, S100-beta positive/nuclear NF- κ B positive cells were counted as nuclear NF- κ B, which has been translocated from astrocytic cytoplasm as a parenchymal neuroinflammatory response. Results indicated that in the right frontal cortex the amount of NF- κ B translocation was 12.9 ± 3.3 % in R192Q mutant mice whereas the amount in the same area in WT mice was 7.1 ± 0.9 %; in right striatum the amount of NF- κ B translocation was 11.4 ± 1.5 % in R192Q mutant mice and 4.9 ± 0.1 % in WT mice; the amount in left frontal cortex was 10.6 ± 1.8 % in R192Q mutants and 6.5 ± 0.6 % in WT mice; and in left striatum it was 11.7 ± 2.1 % in mutant and 4.7 ± 0.2 % in WT animals. In all four brain areas there was a significantly higher amount of parenchymal neuroinflammation, as revealed by the astrocyte NF- κ B activation, in R192Q mutant mice compared to WT mice (n=4/group; p<0.05)(Figure 4.3. and 4.4.).

Nuclear NF- κ B Translocation in Astrocytes in Naive WT and R192Q mice

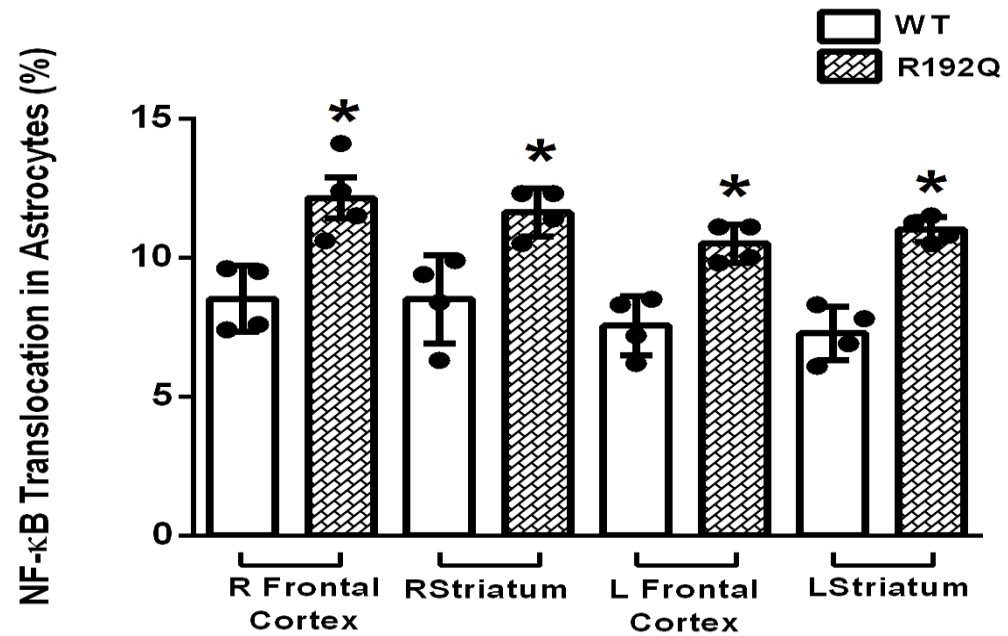


Figure 4.3. NF- κ B translocation from cytoplasm to nucleus in astrocytes in naive WT and R192O mutant mice. S100-beta positive/nuclear NF- κ B positive cells were counted as nuclear NF- κ B which had been translocated from astrocytic cytoplasm. **R:** Right side. **L:** Left side. Bars show standard error of mean (SEM). $p=0.0007$ in Kruskal Wallis test. $*p=0.0286$ mutant *versus* WT in the same area; $n=4$ /group.

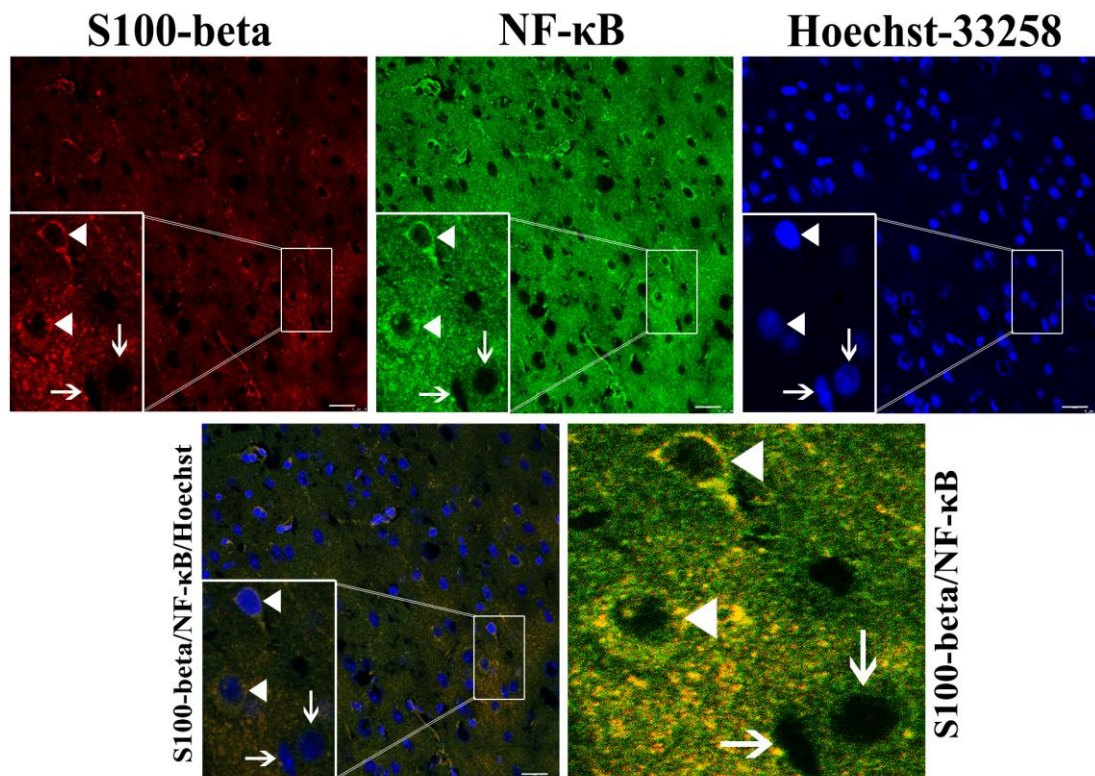


Figure 4.4. NF- κ B translocation. Confocal images show NF- κ B translocation from cytoplasm to nucleus in astrocytes of R192Q mutant mice as a demonstration (arrowheads in all images). Inset shows two astrocytes (arrowheads, S100-beta positive, in red) adjacent to two neurons (arrows, S100-beta negative, in red). NF- κ B immunoreactivity is shown in green, which is visible in the nuclei of astrocytes (arrowheads in green and merged image), but in neurons (arrows in green) NF- κ B is visible as a rim in cytoplasm and not in nuclei. Hoechst-33258 (blue) as a nuclear marker shows the colocalization of NF- κ B in nuclei of astrocytes (arrowheads, merged image). Images were taken on 20 μ m thick sections from right parietal cortex by laser scanning confocal microscope. Scale bars: 20 μ m.

4.2. Effect of a Non-invasive Confounding Stimulus, Drilling the Skull, on Parenchymal Neuroinflammation and HMGB1 Release

To investigate whether drilling the skull has a confounding effect on HMGB1 release and simultaneously investigate whether the effect acts as a non-invasive stimulus on the amount of parenchymal neuroinflammation in R192Q mutant mice compared to WT, the NeuN-positive/HMGB1-negative cells were counted as total HMGB1 release. Results of drilling the skull are represented as the amount of HMGB1 release from neurons in both frontal cortical and striatal areas of the brain. The right frontal cortex on which the drilling was performed, showed 14.6 ± 1.9 % HMGB1 release in R192Q mutant mice compared to 9.9 ± 0.8 % in the same area in WT mice; the difference is at the border of significance ($p=0.057$; $n=4/\text{group}$)(Figure 4.5.). The other regions of the brain act more or less the same with respect to HMGB1 release in R192Q mutant and WT mice. Data also showed that comparing naïve HMGB1 release to drilled groups, HMGB1 release is increased in both WT and R192Q mutant mice after drilling which was only significant in right cortex ($p=0.028$) compared to naïve mice.

HMGB1 Total Neuronal Release after Drilling the skull in WT and R192Q mice

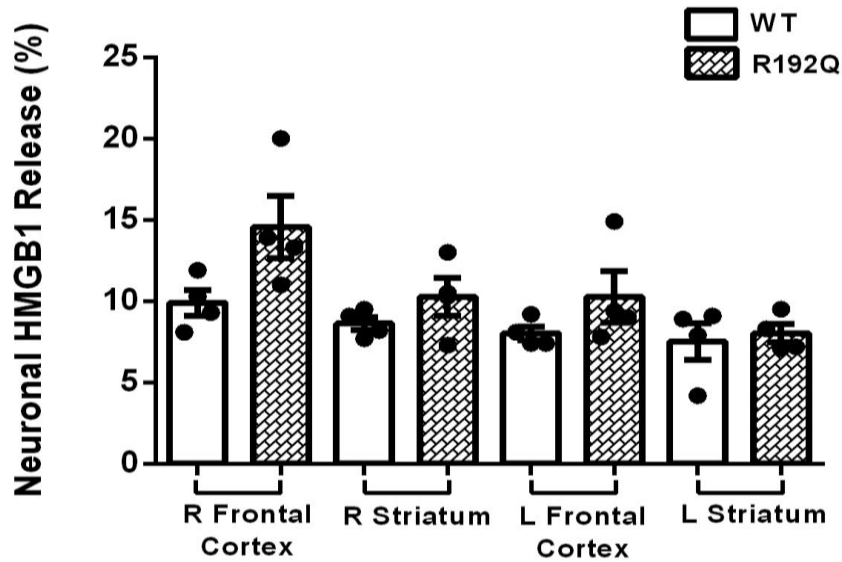


Figure 4.5. HMGB1 release after drilling the skull in WT and R192Q mutant mice. NeuN-positive/HMGB1-negative cells were counted as total HMGB1 release. Right frontal cortex was the site of drilling the skull. **R**: Right side. **L**: Left side. Bars show standard error of mean (SEM). $p=0.0386$ in Kruskal Wallis test. $p=0.057$ mutant *versus* WT in the right frontal cortex ; $n=4$ /group.

4.3. Pinprick-induced CSD Causes Parenchymal Neuroinflammation in Wild-type and R192Q Mutant Mice: Does CSD Cause a Regional Specific Distribution Pattern and Increase in HMGB1 Release?

4.3.1. Laterality in HMGB1 Release in Wild-type and R192Q Mutant Mouse Brains

To study the effect of a single CSD induced by pinprick on the amount of HMGB1 release indicating the parenchymal neuroinflammation in R192Q mutant compared to WT mice, NeuN-positive/HMGB1-negative cells were counted as total HMGB1 release by immunohistochemistry. Here both frontal and posterior cortical regions (primary motor and primary sensory cortices) and subcortical regions (striatum and thalamus) are included in the statistical analysis. In R192Q mutant mice, the amount of total neuronal HMGB1 release in the ipsilateral side was 54.3 ± 3.5 % compared to 55.0 ± 3.4 % for the same hemisphere in WT mice. However, HMGB1 release in the hemisphere contralateral to that in which CSD was induced was 59.4 ± 3.5 % for R192Q mutant mice and 34.5 ± 3.5 % for WT mice. Contralateral HMGB1 release was significantly higher in R192Q mutant mice than in WT mice ($p=0.0079$; $n=5/\text{group}$)(Figure 4.6.). In WT mice, the amount of HMGB1 release in the hemisphere in which CSD was induced (ipsilateral side) was 55.0 ± 3.4 % which was significantly higher than the amount of HMGB1 release in the contralateral hemisphere 34.5 ± 3.5 %, in the same animals ($P=0.0079$; $n=5/\text{group}$). Results show that there is no significant difference in HMGB1 release in CSD ipsilateral hemispheres between WT and R192Q mutant mice. However, in R192Q mutant mouse brains, HMGB1 release is *bilateral* and almost equally distributed, whereas in WT brains, there is more HMGB1 release *ipsilateral* to the side of CSD induction compared to the contralateral hemisphere.

Laterality in neuronal HMGB1 release in WT and R192Q mice brain

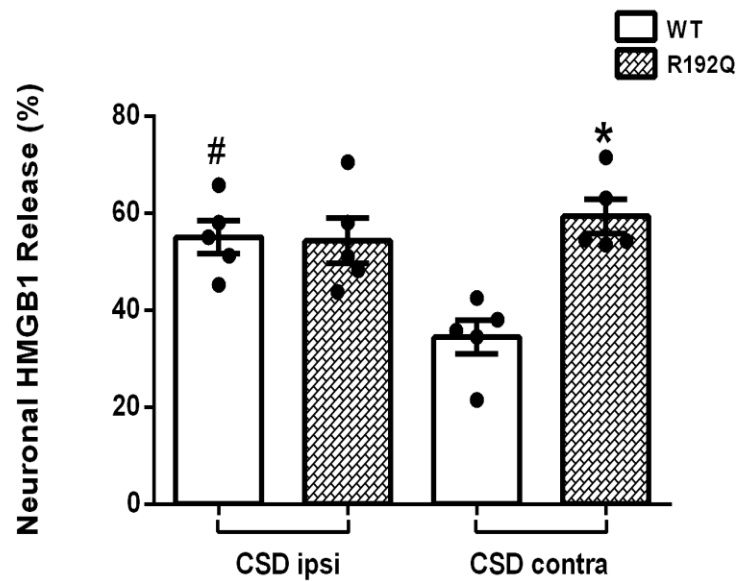


Figure 4.6. HMGB1 release after pinprick-induced single CSD in WT and R192Q mutant brains. NeuN-positive/HMGB1-negative cells were counted as total HMGB1 release. **CSD Ipsi:** the hemisphere, including cortex and subcortex, ipsilateral to CSD induction. **CSD Contra:** the hemisphere, including cortex and subcortex, contralateral to CSD induction. Outliers in R192Q group belongs to one animal which was monitored by 3 CSD after single pinprick. Bars show standard error of mean (SEM). $p=0.0097$ in Kruskal Wallis test. $*p<0.02$ mutant *versus* WT in the same area; $\#p<0.01$ WT CSD ipsilateral *versus* WT CSD contralateral; $n=5$ /group. In one of the R192Q mutant mice after pinprick, 3 CSDs were monitored so, for comparison of the effect of a single CSD, this mouse data was excluded from the analysis.

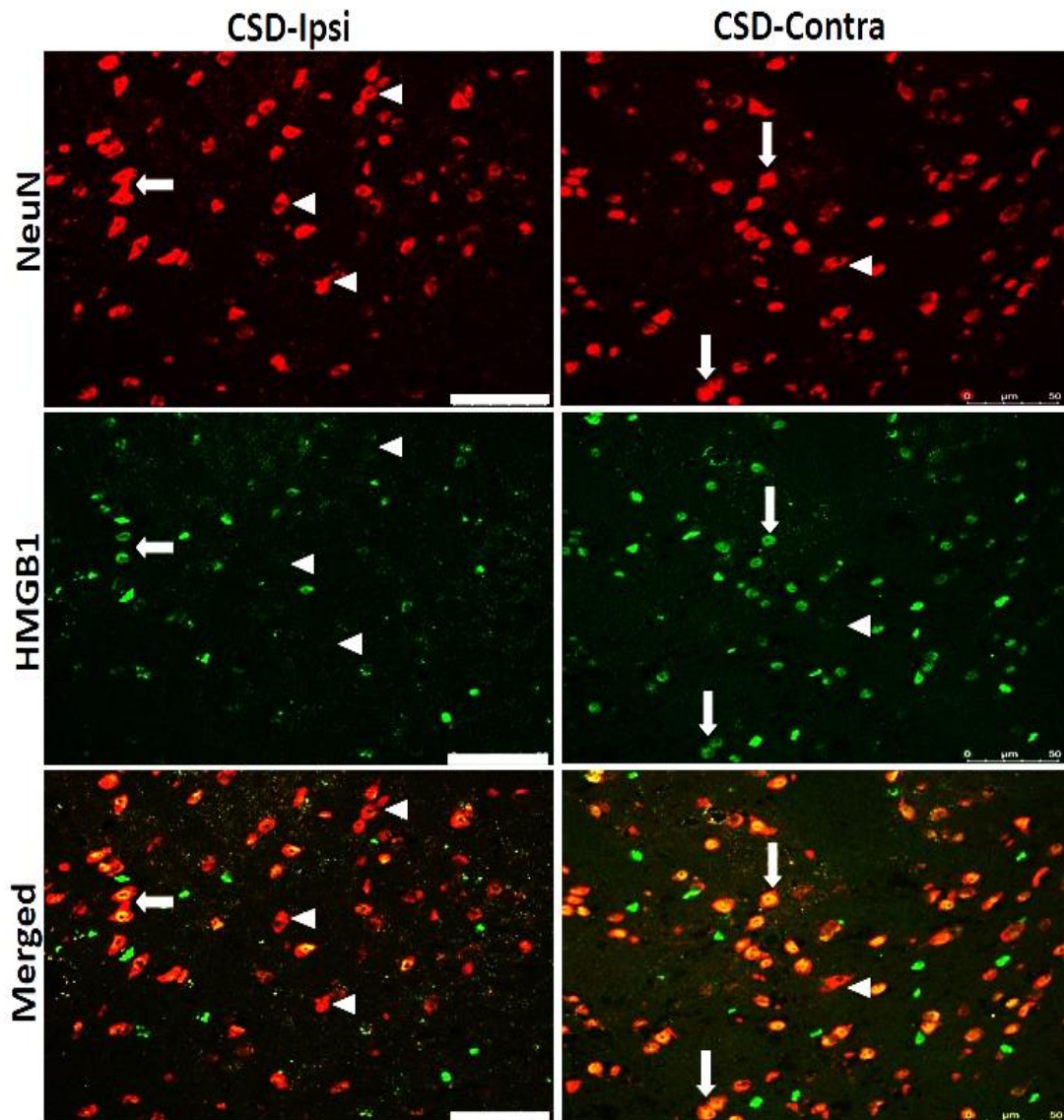


Figure 4.7. HMGB1 release after pinprick-induced single CSD in the WT mouse brain. Confocal images show colocalization of neuronal nuclei (NeuN) (in red) with HMGB1 signal (in green). NeuN-positive/HMGB1-negative cells (triangles) were counted as total HMGB1 release. NeuN-positive/HMGB1-positive cells (arrows) were counted as no release in HMGB1. **CSD-Ipsi:** brain cortex ipsilateral to CSD induction. **CSD-Contra:** brain cortex contralateral to CSD induction. Images were taken from 20- μ m-thick sections by laser scanning confocal microscope. Scale bars: 50 μ m.

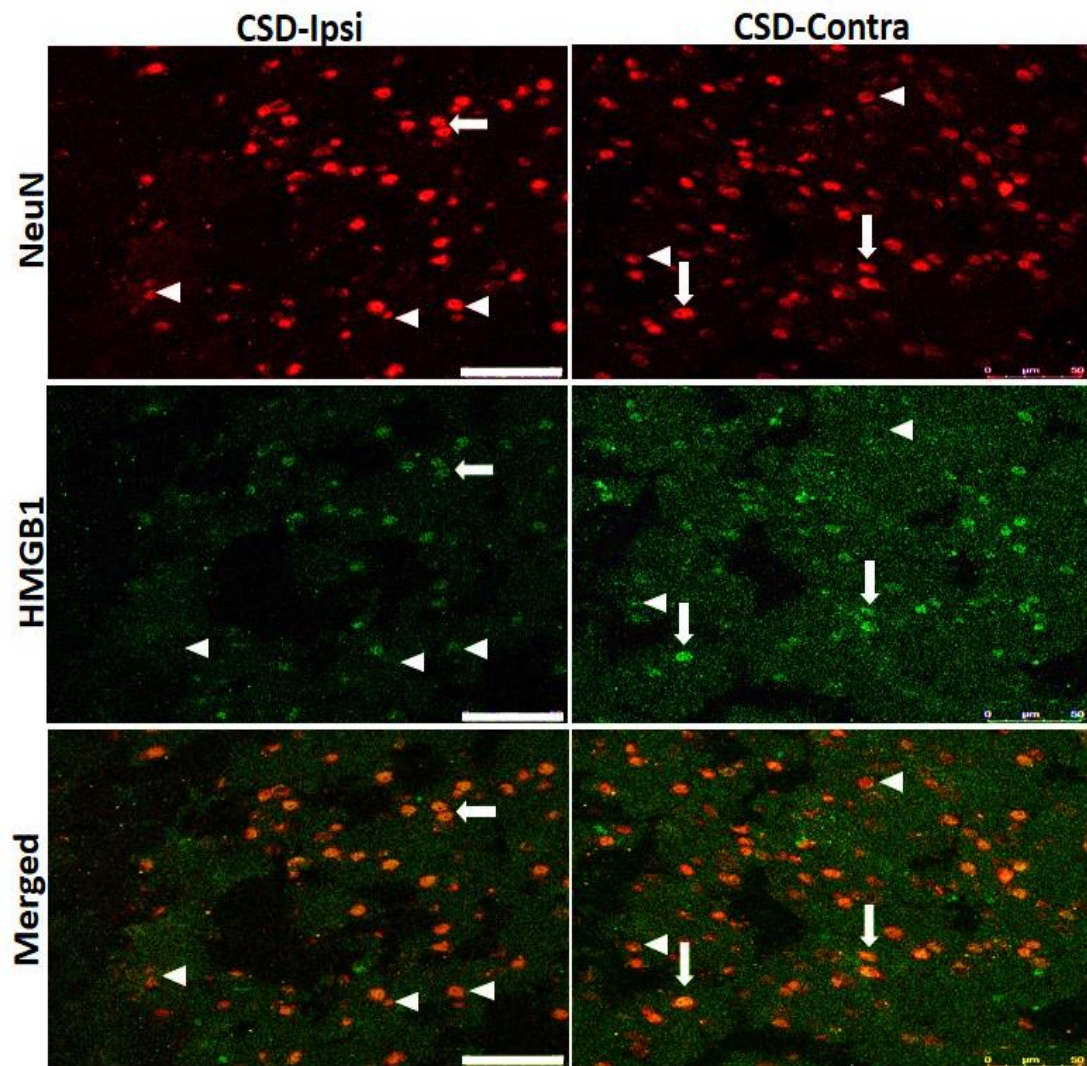


Figure 4.8. HMGB1 release after pinprick-induced single CSD in a R192Q mutant mouse brain. Confocal images show colocalization of neuronal nuclei (NeuN) (in red) with HMGB1 signal (in green). NeuN-positive/HMGB1-negative cells (triangles) were counted as total HMGB1 release. NeuN-positive/HMGB1-positive cells (arrows) were counted as no release in HMGB1. **CSD-Ipsi:** brain cortex ipsilateral to CSD induction. **CSD-Contra:** brain cortex contralateral to CSD induction. Images were taken from 20- μ m-thick sections by laser scanning confocal microscope. Scale bars: 50 μ m.

4.3.2. Laterality in HMGB1 Release in Cortical Areas of Wild-type and R192Q Mutant Mouse Brains

In order to study the effect of a single CSD, induced by pinprick, on the amount of HMGB1 release and parenchymal neuroinflammation in WT and R192Q mutant mice, NeuN-positive/HMGB1-negative cells were counted as total HMGB1 release. Results showed that HMGB1 release in ipsilateral frontal cortex was 43.2 ± 7.6 % in mutant mice and 38.6 ± 2.9 % in WT mice brain ($p > 0.05$). However, there was a significant increase in the amount of HMGB1 release (42.6 ± 7.3 %) from neurons in the R192Q contralateral frontal cortex compared to the same area in WT mice (13.0 ± 2.4 %)($p = 0.0079$; $n = 5/\text{group}$) (Figure 4.9). Moreover, WT ipsilateral frontal cortex had more HMGB1 release (38.6 ± 2.9 %) than WT contralateral frontal cortex (13.0 ± 2.4 %)($p = 0.0079$; $n = 5/\text{group}$). Results indicated there was a clear difference in ipsilateral and contralateral HMGB1 release of WT mice brain, as expected (6). However, in R192Q mutant mice this laterality was not seen as there was a *bilateral* parenchymal neuroinflammation. Neurons in right frontal cortex released more HMGB1 (43.20 ± 7.4 %) compared to right parietal cortex (35.80 ± 11.6 %) in the R192Q mutant mouse brain, this trend was followed in the left hemisphere as well (42.6 ± 7.1 %, 34.8 ± 10.3 % respectively) but the increases were not significant ($p = 0.5$, and $p = 0.3$ respectively). However, in WT mice, the HMGB1 release in frontal cortex was less than parietal cortex in both right (38.6 ± 2.9 %, 40.4 ± 9.2 %) and left hemisphere (13 ± 2.4 %, 31.6 ± 9.6 %) which was significant in the left side ($p < 0.05$; $n = 5/\text{group}$)(Figure 4.9.).

Laterality in HMGB1 release in CORTICAL areas of WT and R192Q mice brain

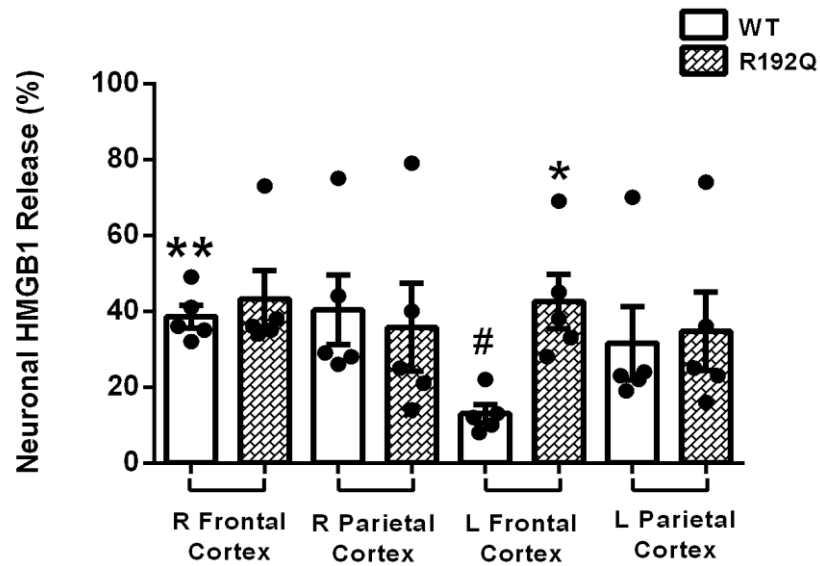


Figure 4.9. HMGB1 release after pinprick-induced single CSD in cortical areas of R192Q mutant mice compared to those WT mice. NeuN-positive/HMGB1-negative cells were counted as total HMGB1 release. **R**: Right side. **L**: Left side. Bars show standard error of mean (SEM). $p=0.0203$ in Kruskal Wallis test. * $p<0.01$ mutant versus WT in the same area; ** $p<0.01$ versus WT L Frontal Cortex; # $p<0.05$ versus WT L Parietal Cortex; $n=5$ /group.

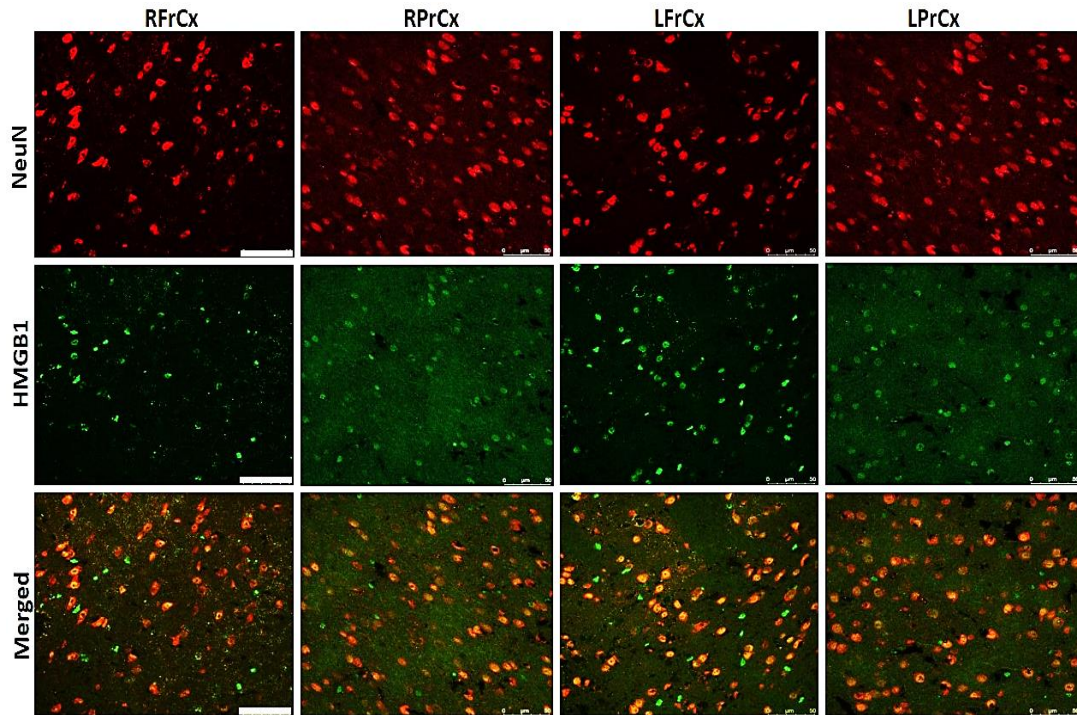


Figure 4.10. HMGB1 release after pinprick-induced single CSD in cortical areas of the WT mouse brain. Confocal images show NeuN-positive/HMGB1-negative cells that were counted as total HMGB1 release. **RFrCx:** Frontal cortex ipsilateral to CSD induction. **RPrCx:** Parietal cortex ipsilateral to CSD induction. **LFrCx:** Frontal cortex contralateral to CSD induction. **LPrCx:** Parietal cortex contralateral to CSD induction. Images were taken on 20- μ m-thick sections by laser scanning confocal microscope. Scale bars: 50 μ m.

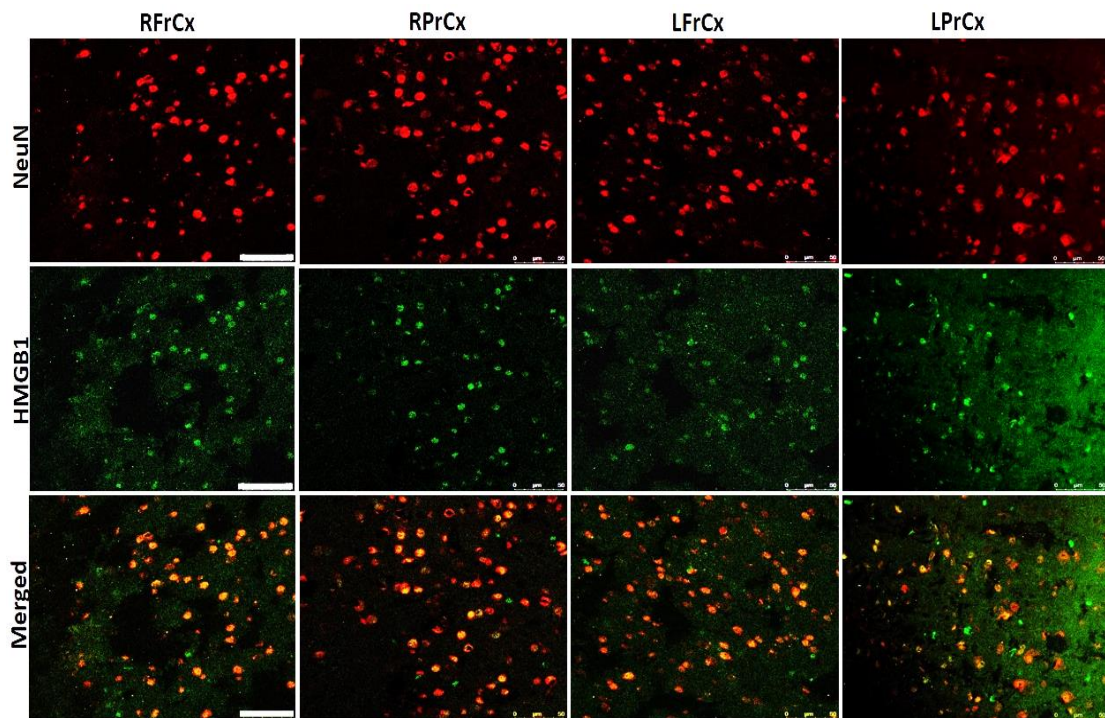


Figure 4.11. HMGB1 release after pinprick-induced single CSD in cortical areas of the R192Q mutant mouse brain. Confocal images show NeuN-positive/HMGB1-negative cells that were counted as total HMGB1 release. **RFrCx:** Frontal cortex ipsilateral to CSD induction. **RPrCx:** Parietal cortex ipsilateral to CSD induction. **LFrCx:** Frontal cortex contralateral to CSD induction. **LPrCx:** Parietal cortex contralateral to CSD induction. Images were taken on 20- μ m-thick sections by laser scanning confocal microscope. Scale bars: 50 μ m.

4.3.3. Laterality in HMGB1 Release In Subcortical Areas of Wild-type and R192Q Mutant Mouse Brains

The amount of HMGB1 release and parenchymal neuroinflammation in WT and R192Q mutant mice after a single CSD induced by pinprick was analyzed by the ratio of NeuN-positive/HMGB1-negative cells. Data demonstrated a higher increase in the amount of HMGB1 release from neurons in some subcortical areas of R192Q mutant mice compared to that in WT mice (Figure 4.12); however, in WT ipsilateral striatum the amount of HMGB1 release was 75.8 ± 7.1 % that was significantly more than the release in the same area in R192Q mutant mice (53.6 ± 5.7 %)($p=0.048$; $n=5$ /group). However, in R192Q mutants there was an increased amount of neuronal HMGB1 release in contralateral striatum: 55.2 ± 5.9 % compared to 26.0 ± 1.2 % in the same area in WT mice ($p=0.0079$; $n=5$ /group). Notably, the rise in HMGB1 release in R192Q mutant mice was significantly higher in ipsilateral (84.6 ± 4.5 %) and contralateral thalamic area (87.8 ± 3.5 %) than ipsilateral (53.6 ± 5.7 %) and contralateral striatal area (55.2 ± 5.9 %)($p= 0.016$; $n=5$ /group for thalamic area and $p= 0.0079$; $n=5$ /group for striatal area)(Figure 4.12). Comparing WT ipsilateral striatum to contralateral one revealed a significant increase in the release in ipsilateral striatal area (75.8 ± 7.1 %) compared to contralateral striatum (26.0 ± 1.2 %)($p=0.0079$; $n=5$ /group). Moreover, in the WT group, contralateral thalamic region shows significantly more HMGB1 release (59.6 ± 11.7 %) than contralateral striatal region (26.0 ± 1.2 %)($p=0.024$; $n=5$ /group) (Figure 4.12.).

Laterality in HMGB1 release in SUB-CORTICAL areas of WT and R192Q mice brain

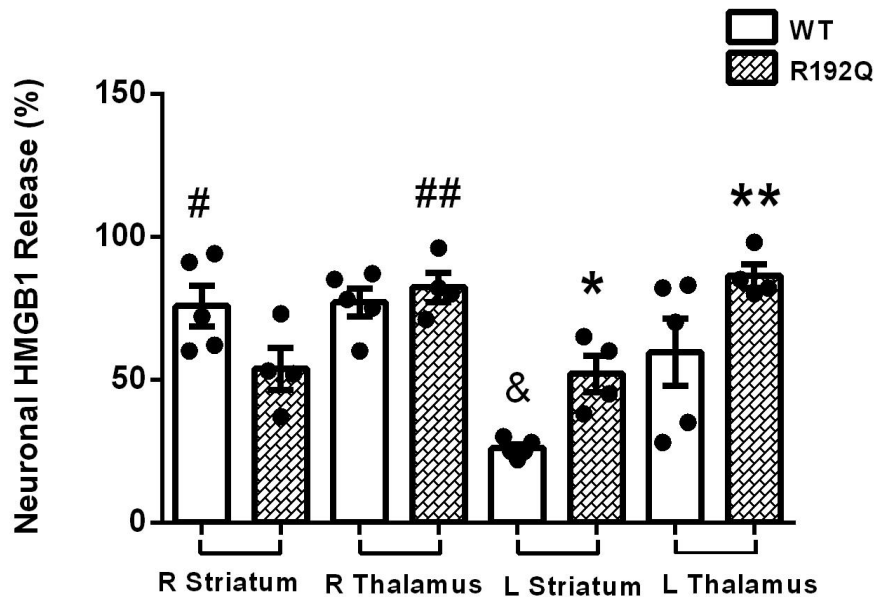


Figure 4.12. HMGB1 release after pinprick-induced single CSD in subcortical areas of WT and R192Q mutant mouse brains. NeuN-positive/HMGB1-negative cells were counted as total HMGB1 release. In R192Q mice neuronal HMGB1 release was higher in right and left thalamus and left striatum compared to WT mice. However right striatum of WT mice showed more HMGB1 release compared to R192Q mutant. **R**: Right side. **L**: Left side. Bars show standard error of mean (SEM). $p=0.0006$ in Kruskal Wallis test. * $p<0.05$ mutant *versus* WT in the same area; ** $p<0.05$ *versus* R192Q L Striatum; # $p<0.01$ *versus* WT L Striatum; & $p<0.05$ *versus* WT L Thalamus; ## $p<0.05$ *versus* R192Q R Striatum; $n=5$ /group.

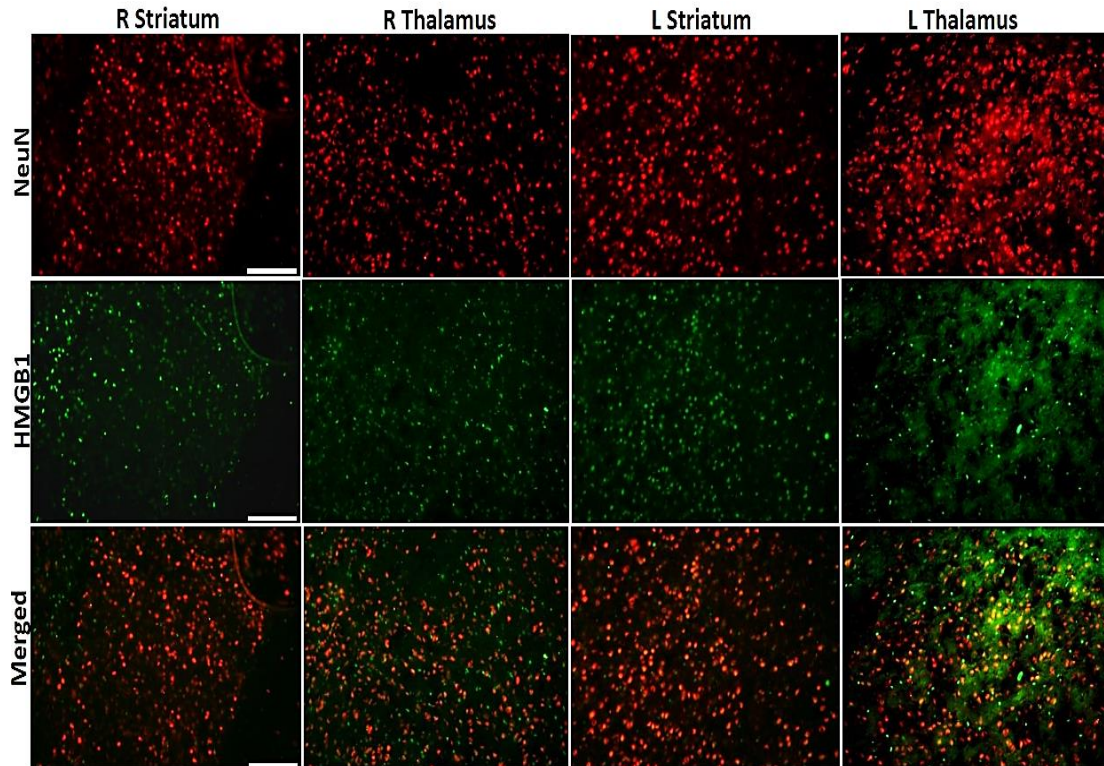


Figure 4.13. HMGB1 release after pinprick-induced single CSD in subcortical areas of a WT mouse brain. Confocal images show NeuN-positive/HMGB1-negative cells that were counted as total HMGB1 release. **R Striatum:** Striatal area ipsilateral to CSD induction. **R Thalamus:** Thalamic area ipsilateral to CSD induction. **L Striatum:** Striatal area contralateral to CSD induction. **L Thalamus:** Thalamic area contralateral to CSD induction. Images were taken on 20- μ m-thick sections by laser scanning confocal microscope. Scale bars: 50 μ m.

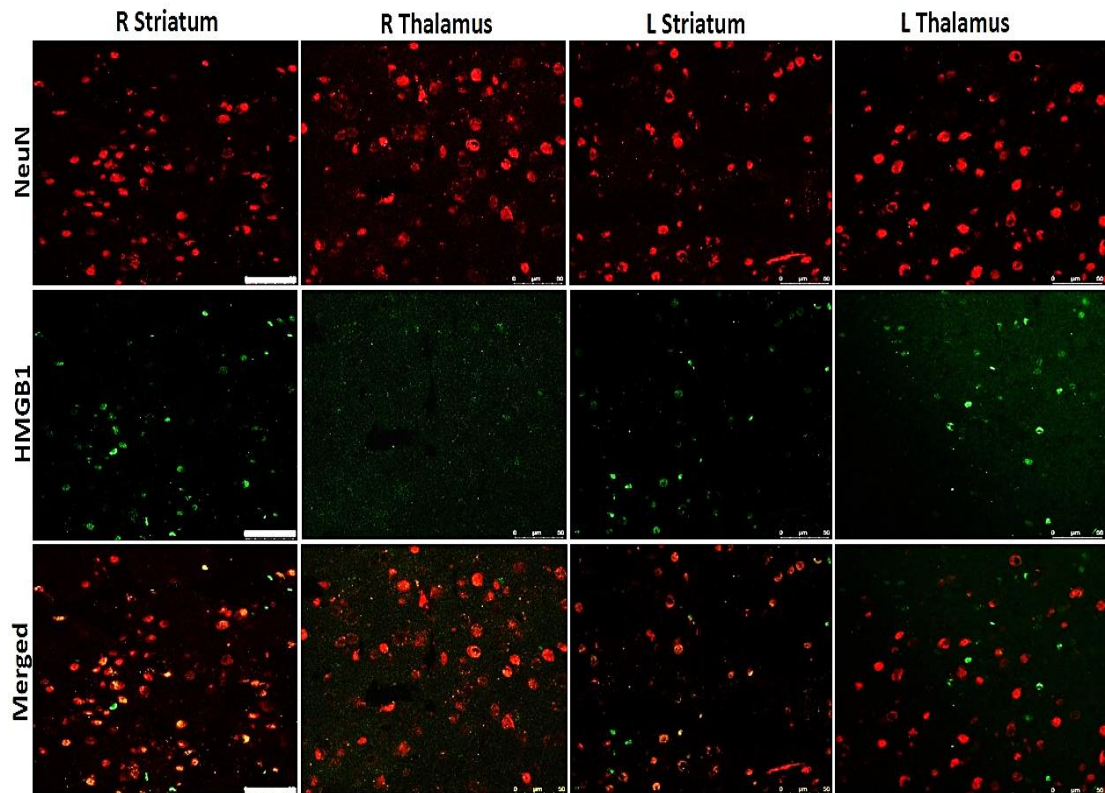


Figure 4.14. HMGB1 release after pinprick-induced single CSD in subcortical areas of an R192Q mouse brain. Confocal images show NeuN-positive/HMGB1-negative cells that were counted as total HMGB1 release. **R Striatum:** Striatal area ipsilateral to CSD induction. **R Thalamus:** Thalamic area ipsilateral to CSD induction. **L Striatum:** Striatal area contralateral to CSD induction. **L Thalamus:** Thalamic area contralateral to CSD induction. Images were taken on 20- μ m-thick sections by laser scanning confocal microscope. Scale bars: 50 μ m.

4.3.4. Laterality in Cortical and Subcortical HMGB1 Release of Wild-type and R192Q Mutant Mouse Brains

To study the effect of a single CSD induced by pinprick on the amount of HMGB1 release and parenchymal neuroinflammation in WT and R192Q mutant mice, NeuN-positive/HMGB1-negative cells were counted as total HMGB1 release. Data demonstrated that in WT, ipsilateral frontal cortical and striatal HMGB1 release was more than on the contralateral side; for example, ipsilateral striatum had significantly more HMGB1 release ($79.2 \pm 3.8 \%$) compared to contralateral striatum ($42.8 \pm 5.8 \%$) in WT ($p=0.0079$; $n=5/\text{group}$)(Figure 4.15.).

Generally, striatal release was higher than cortical release in both the mutant and the WT group. In WT mice, ipsilateral striatum showed significantly more amount of HMGB1 release ($79.2 \pm 3.8 \%$) than ipsilateral frontal cortex ($39.4 \pm 3.9 \%$)($p=0.0079$; $n=5/\text{group}$). R192Q mutant mice followed the same trend with significantly more release but in *both* ipsilateral ($69.1 \pm 4.5 \%$) and contralateral ($71.5 \pm 4.0 \%$) striatum compared to ipsilateral ($39.5 \pm 6.9 \%$) and contralateral ($38.7 \pm 5.3 \%$) frontal cortices ($p=0.0079$; $n=5/\text{group}$ for both). Notably, in R192Q mutant mice there was no such side difference present in WT group (Figure 4.15.). Comparing WT with R192Q mutant mice, data showed a significant rise in the amount of HMGB1 release in mutant contralateral striatum ($71.5 \pm 4.0 \%$) compared to the same area in WT mice ($42.8 \pm 5.8 \%$)($p=0.0079$; $n=5/\text{group}$)(Figure 4.15.).

Laterality in Neuronal HMGB1 release when comparing CORTEX with SUB-CORTEX of R192Q/WT mice

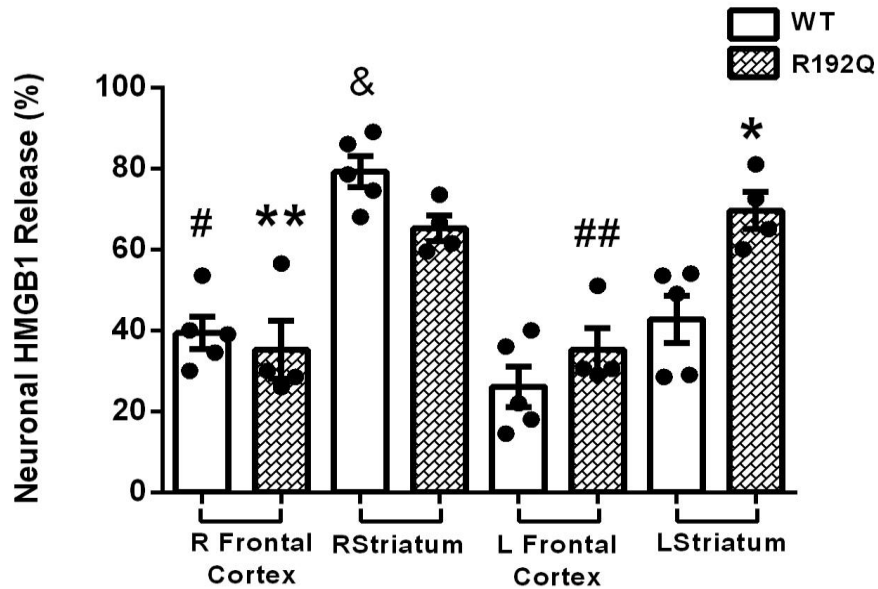


Figure 4.15. HMGB1 release after pinprick-induced single CSD in cortical and subcortical areas of WT and R192Q mutant mouse brains. NeuN-positive/HMGB1-negative cells were counted as total HMGB1 release. **R**: Right side. **L**: Left side. Bars show standard error of mean (SEM). $p=0.0001$ in Kruskal Wallis test. * $p<0.01$ mutant *versus* WT in the same area; ** $p<0.01$ *versus* R192Q R Striatum; # $p<0.01$ *versus* WT R Striatum; & $p<0.01$ *versus* WT L Striatum; ## $p<0.01$ *versus* R192Q L Striatum; $n=5$ /group.

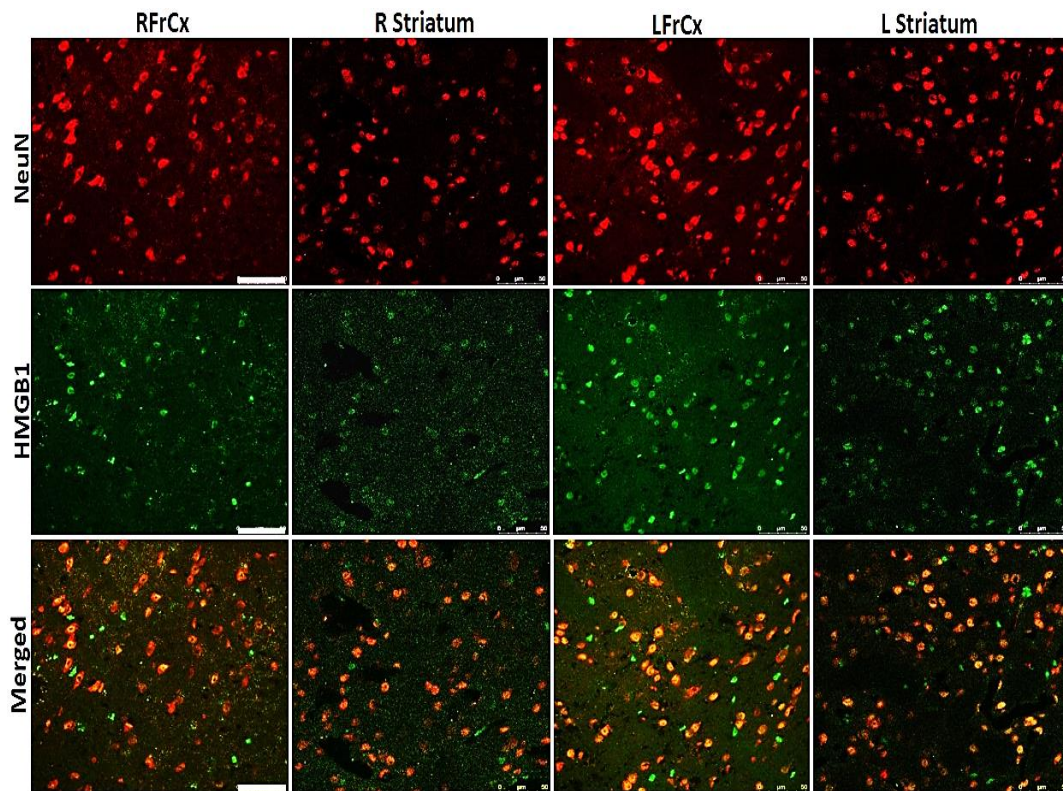


Figure 4.16. HMGB1 release after pinprick-induced single CSD in cortical and subcortical areas of a WT mouse brain. Confocal images show NeuN-positive/HMGB1-negative cells that were counted as total HMGB1 release. **RFrCx:** Frontal cortex ipsilateral to CSD induction. **R Striatum:** Striatal area ipsilateral to CSD induction. **LFrCx:** Frontal cortex contralateral to CSD induction. **L Striatum:** Striatal area contralateral to CSD induction. Images were taken on 20- μ m-thick sections by laser scanning confocal microscope. Scale bars: 50 μ m.

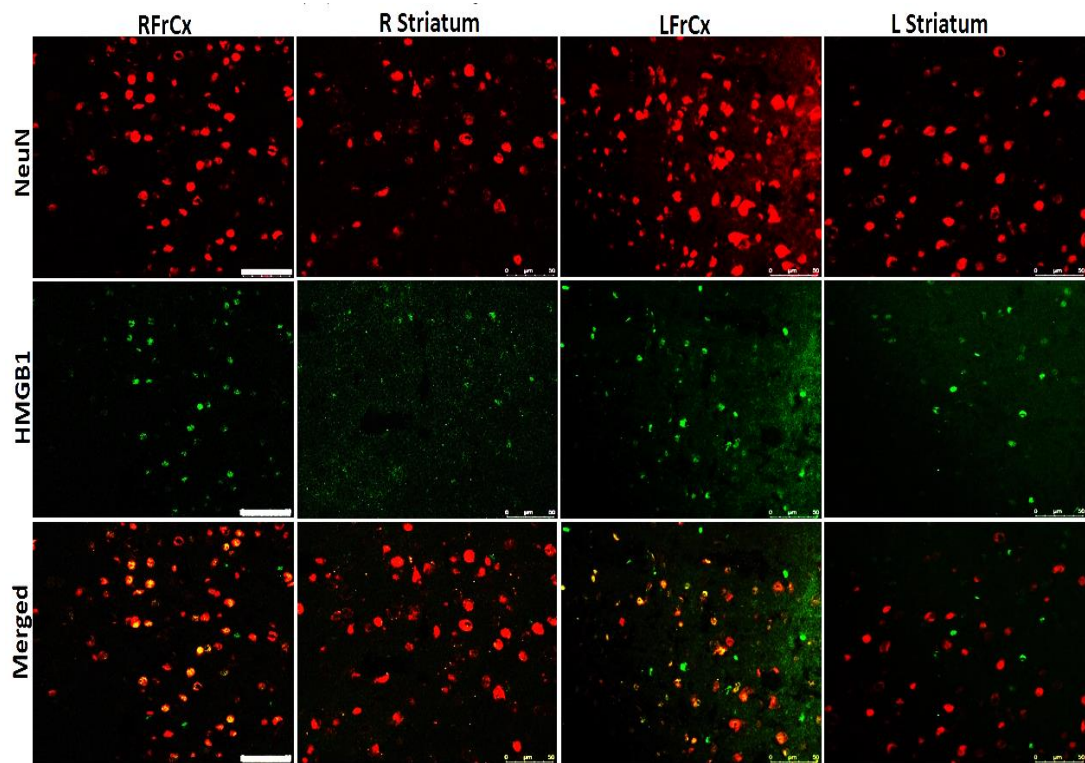


Figure 4.17. HMGB1 release after pinprick-induced single CSD in cortical and subcortical areas of an R192Q mutant mouse brain. Confocal images show NeuN-positive/HMGB1-negative cells that were counted as total HMGB1 release. **RFrCx:** Frontal cortex ipsilateral to CSD induction. **R Striatum:** Striatal area ipsilateral to CSD induction. **LFrCx:** Frontal cortex contralateral to CSD induction. **L Striatum:** Striatal area contralateral to CSD induction. Images were taken on 20- μ m-thick sections by laser scanning confocal microscope. Scale bars: 50 μ m.

4.4. Pinprick-induced Parenchymal Neuroinflammation in Wild-type and R192Q Mutant Mouse Brains: A Regional Distribution Pattern and Increase in NF- κ B Translocation in Astrocytes

To study the effect of a single CSD induced by pinprick on the amount of parenchymal neuroinflammation, NF- κ B translocation from cytoplasm to nucleus in astrocytes was investigated. In this set of experiments S100-beta was used as an astrocyte marker, an NF- κ B antibody to show the immunoreactivity of these proteins, and Hoechst-33258 as a nuclear marker. To show the extent of basal neuroinflammation in R192Q mutant compared to WT mice, S100-beta positive/nuclear NF- κ B positive cells were counted as nuclear NF- κ B, which has been translocated from astrocytic cytoplasm as a parenchymal neuroinflammatory response. Results indicated an increase in NF- κ B activation in all investigated brain regions of R192Q mutant mice compared to activation in WT mice (Figure 4.18.). The laterality in NF- κ B activation was shown in the graph for WT mice with more translocation in ipsilateral frontal cortex (89.1 ± 1.4 %) and striatum (93.1 ± 2.1 %) compared to the respective contralateral areas (64.5 ± 10.4 % and 61.8 ± 11.4 %, respectively)($p < 0.05$; $n = 4$ /group). However, in R192Q mutant mice the activation was *bilateral*. The rise in NF- κ B nuclear translocation was significantly higher in R192Q mutant ipsilateral frontal cortex (97.5 ± 1.0 %) and contralateral striatum (87.8 ± 5.1 %) compared to WT ipsilateral frontal cortex (89.1 ± 1.4 %) and contralateral striatum (61.8 ± 11.4 %)($p < 0.05$; $n = 4$ /group)(Figure 4.18.). Contralateral frontal cortex in R192Q mutant mice also showed more NF- κ B activation compared to the same area in WT mice, although the increase did not reach statistical significance.

Nuclear NF- κ B Translocation in Astrocytes after Pinprick-induced CSD in WT and R192Q mice

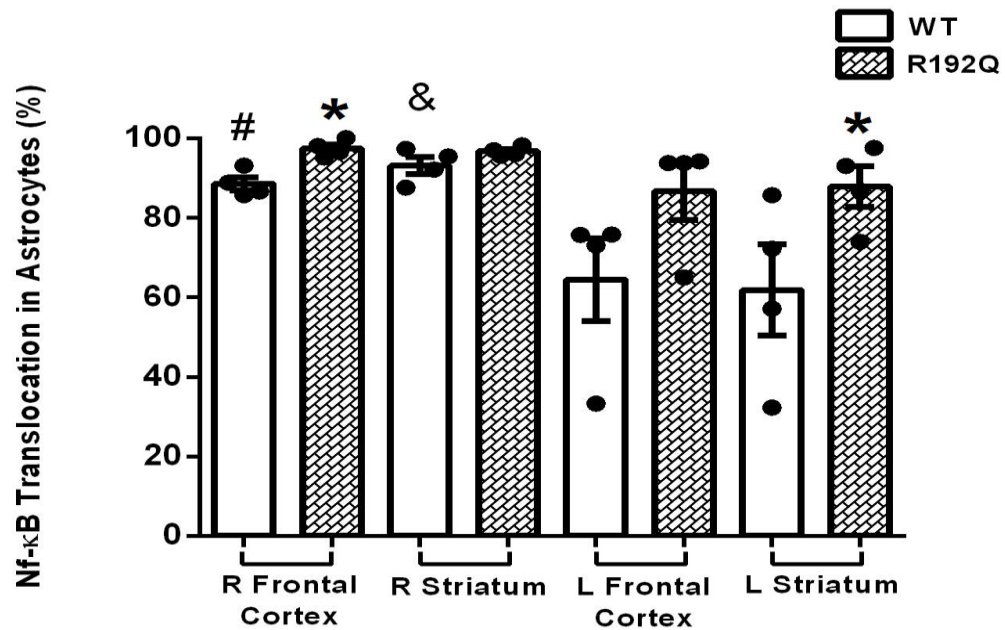


Figure 4.18. NF- κ B translocation from cytoplasm to nucleus in astrocytes after pinprick-induced CSD in WT and R192O mutant mice. S100-beta-positive/nuclear NF- κ B-positive cells were counted as nuclear NF- κ B that had been translocated from astrocytic cytoplasm. **R:** The brain area ipsilateral to CSD induction. **L:** The brain area contralateral to CSD induction. Bars show standard error of the mean (SEM). $p=0.0024$ in Kruskal Wallis test. * $p<0.05$ mutant *versus* WT in the same area; # $p<0.05$ *versus* WT L Frontal Cortex; & $p<0.05$ *versus* WT L Striatum; $n=4$ /group).

4.5. Neuroinflammation After Multiple CSD Events Induced by KCl in Wild-type and S218L Mutant Mouse Brains

4.5.1. HMGB1 Release in CSF in Wild-type and S218L Mutant Mice After KCl-induced Multiple CSDs

During the course of multiple CSDs induced by a KCl-soaked (saline for the sham group) cotton ball for 1 hour, CSF was collected through an i.c.v. cannula in the right lateral ventricle of each brain, individual and pooled CSF samples were studied in each group (2 μ l/mouse, n=2/group). According to Western Blot bands, for released HMGB1 protein to CSF, there was almost 2-fold increase in WT CSD group compared to WT sham; there was almost 2.5-fold increase in S218L CSD group compared to S218L sham, and there was 0.66 fold increase in S218L CSD group compared to WT CSD group, however none of them was significant (Figure 4.19.). For R192Q group the same procedure was performed but due to technical problems, data was not regarded as reliable.

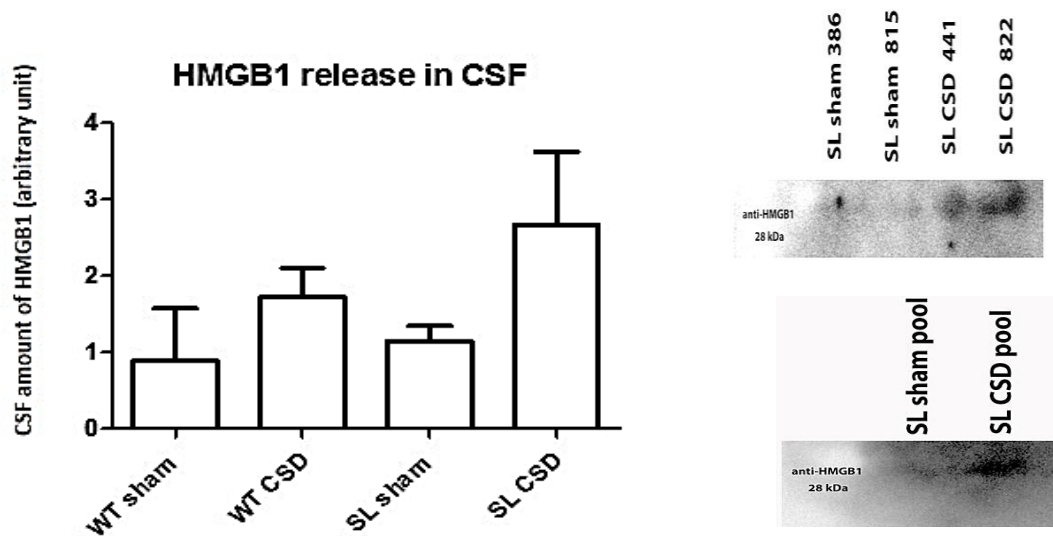


Figure 4.19. HMGB1 release during 1 hour KCl-induced multiple CSDs/saline application for sham group, detected in CSF collected through i.c.v. cannula in S218L mice compared to its WT, (n=2/group).

4.5.2. Translocation of NF- κ B from Cytoplasm to Nucleus in Astrocytes of Wild-type and S218L Mutant Mice Assessed by Western Blotting

Immediately after finishing the multiple CSDs induced by a KCl or saline (for sham group) soaked cotton ball for 1 hour, fresh brains were extracted and sliced to different cortical and subcortical areas, then nuclear and cytoplasmic parts were separated and NF- κ B translocation from cytoplasm to nucleus was detected by nuclear subtraction Western blotting in S218L and its wild-type mice in right frontal cortical areas, and left subcortical areas (n=3/group, except S218L sham group which was 2). We preferred left subcortical area as another area to show the NF- κ B activation, because in immunohistochemistry experiments of this area was the one that had the most prominent difference between mutant and WT groups. Results showed that CSD causes an increased NF- κ B activation in WT CSD group (85.2 ± 5.1 %) compared to WT sham group (60.7 ± 6.5 %) in frontal cortex ipsilateral to CSD (p=0.04) (Figure 4.20.). Interestingly, both in S218L CSD (90.9 ± 2.1 %) and S218L sham-operated (84.7 ± 4.7 %) groups there was similar amount of NF- κ B activation in right frontal cortices (p=0.25). These results were similar to WT CSD group (p=0.35) and more than WT sham group (p=0.07). In subcortex contralateral to CSD there was significant increase of NF- κ B activation in WT CSD group (63.1 ± 0.9 %) compared to sham-operated ones (48.3 ± 5.8 %)(p=0.06). In S218L mutant mice groups, CSD (83.1 ± 6.9 %) caused an increased NF- κ B activation compared to sham operated group (79.6 ± 2.6 %)(p=0.72). NF- κ B activation in both S218L mutant mice groups (CSD and sham-operated) was more compared to WT CSD and WT sham-operated ones in contralateral subcortical areas (p=0.04, p=0.02, respectively)(Figure 4.21.).

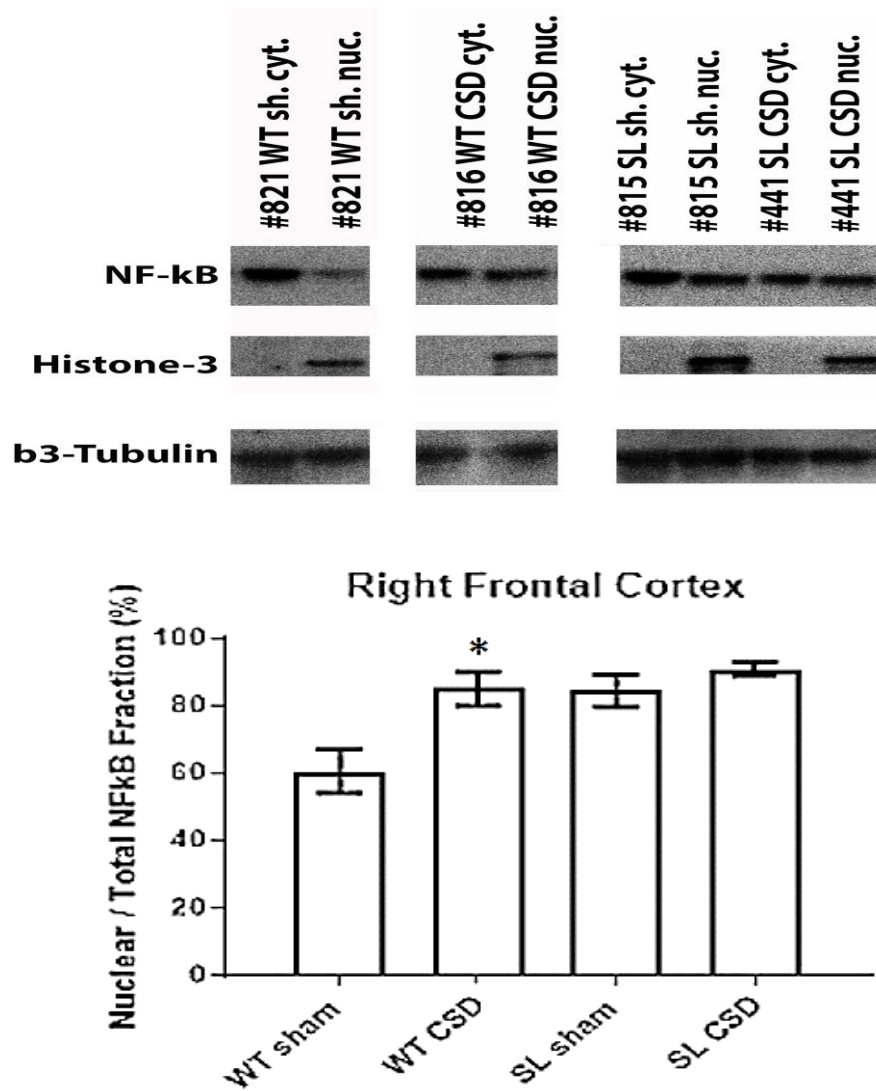


Figure 4.20. NF- κ B translocation from cytoplasm to nucleus in astrocytes shown by nuclear subtraction Western blotting. After KCl-induced multiple CSDs NF- κ B is translocated from cytoplasm to nucleus of the astrocytes shown in ipsilateral cortical area of the brains of S218L mutant mice compared to WT mice and sham groups of each (For sham group saline was applied); * $p=0.04$ versus WT sham; (n=3/group, except S218L sham group which was 2).

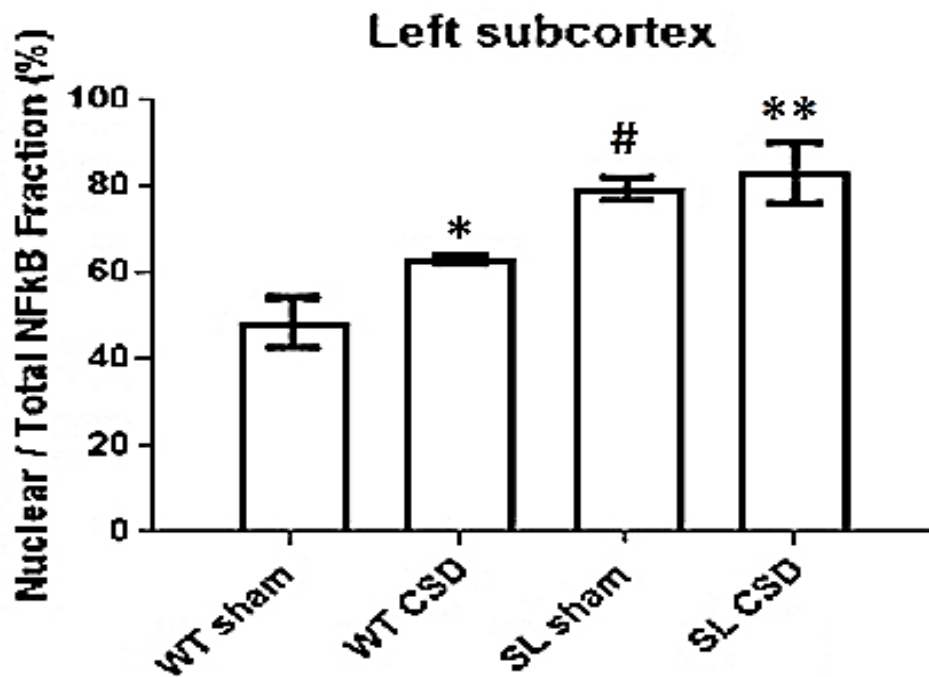


Figure 4.21. NF- κ B translocation from cytoplasm to nucleus in astrocytes shown by nuclear subtraction Western blotting. After KCl-induced multiple CSDs NF- κ B is translocated from cytoplasm to nucleus of the astrocytes shown in contralateral subcortical area of the brains of S218L mutant mice compared to WT mice and sham groups of each (For sham group saline was applied); * $p=0.02$ versus WT sham; ** $p=0.04$ versus WT CSD; # $p=0.02$ versus WT sham ($n=3$ /group, except S218L sham group which was 2).

Frontal brain neuronal HMGB1 release in wild-type and R192Q mutant mice

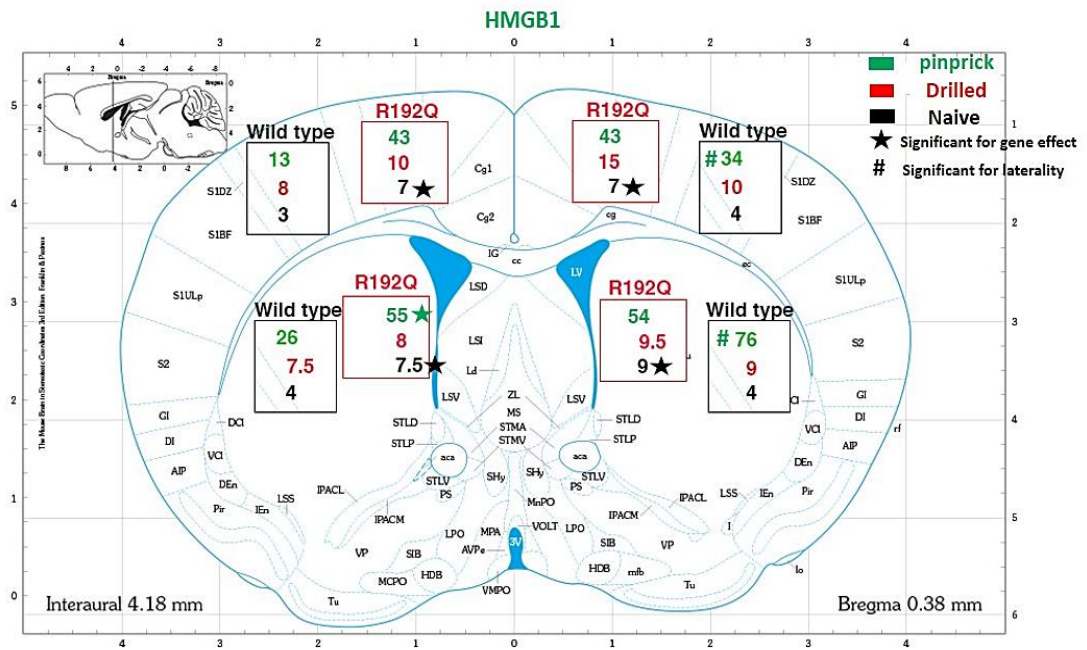


Figure 4.22. Scheme showing neuronal HMGB1 release distribution pattern and amount in frontal section of the brain of WT and R192Q mutant mice.

Posterior brain neuronal HMGB1 release in wild-type and R192Q mutant mice

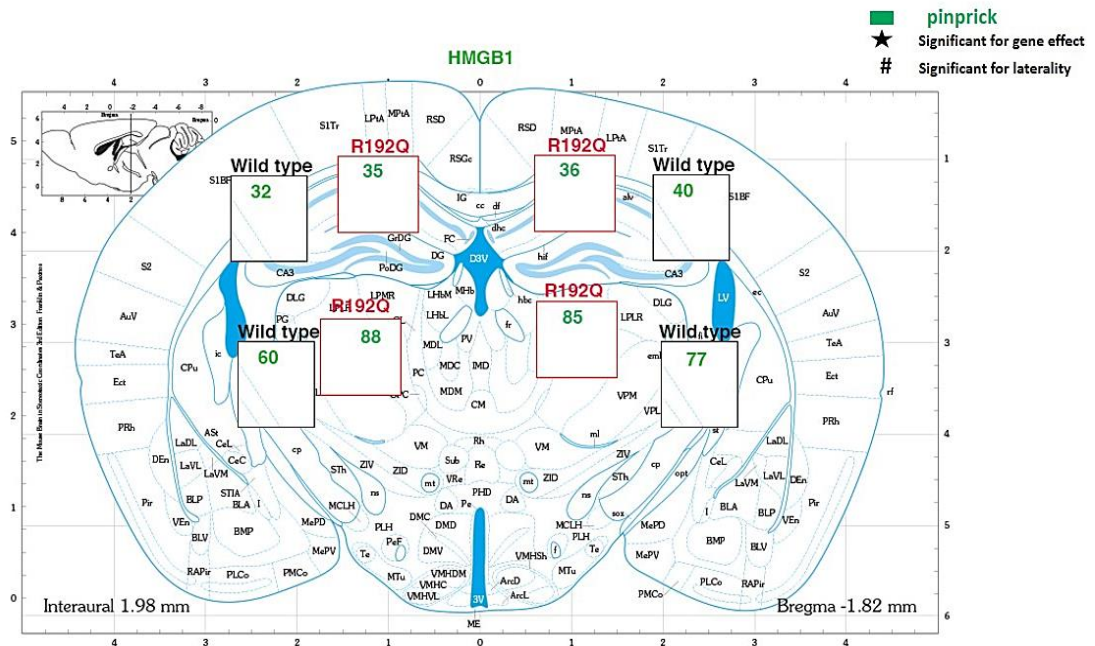


Figure 4.23. Scheme showing neuronal HMGB1 release distribution pattern and amount in posterior section of the brain of WT and R192Q mutant mice.

Frontal brain astrocytic NF- κ B translocation in wild-type and R192Q mutant mice

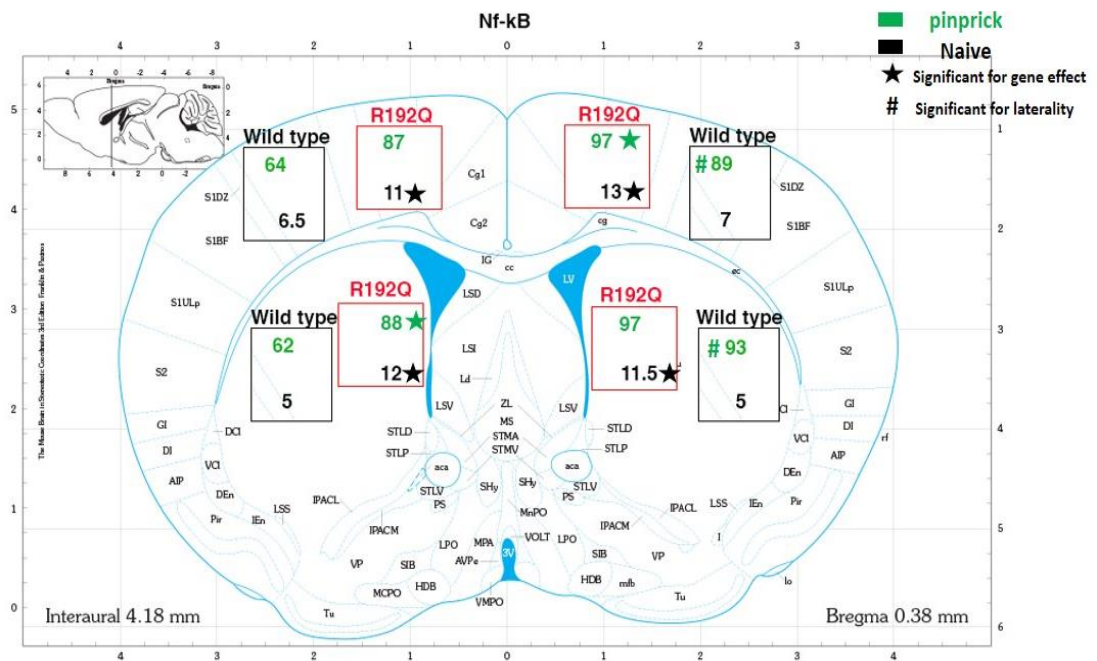


Figure 4.24. Scheme showing astrocytic NF- κ B translocation distribution pattern and amount in frontal section of the brain of WT and R192Q mutant mice.

4.6. Electrophysiological Characterization of Cortical Spreading Depression Events

Electrophysiological characterization of CSD events that were induced by either pinprick which causes a single CSD event or topical application of a KCl-soaked cotton ball which induces multiple CSD events, was investigated in WT, R192Q or S218L mutant mice. For this purpose, frequency, amplitude, total duration, half-maximum amplitude duration, derivative (rising rate) and speed of CSDs were analyzed from DC-potentials of the electrophysiological recordings in *in vivo* experiments. For two mice (numbers: 298 R192Q and 587 WT), CSD recordings were monitored on *both* hemispheres simultaneously. In the left hemisphere, CSDs had very low amplitude of 2-3 mV, with a very short (less than 1 minute) delay of detection on the contralateral hemisphere. In one of the R192Q mice, there were three CSDs after one pinprick (number 394, Figure 4.25.).

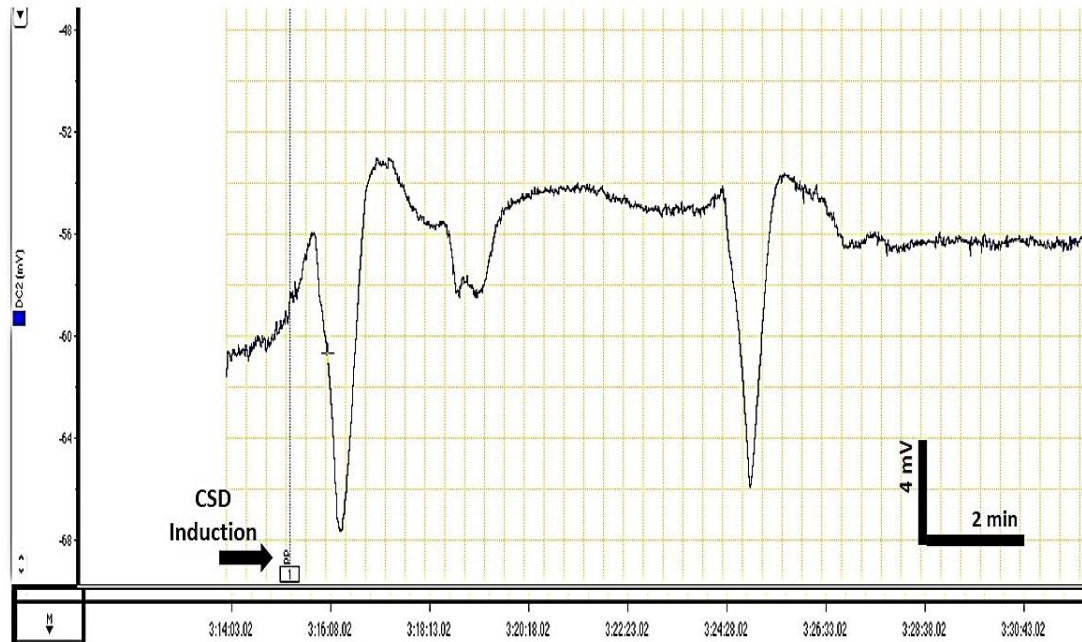


Figure 4.25. CSD recordings monitored after CSD induction in R192Q mouse. In this mouse there were 3 CSDs after one pinprick which were monitored on right parietal bone of the brain.

Table 4.1. Electrophysiological Characteristics of Pinprick-induced CSD in R192Q strain HOM/HOM

Pinprick-induced CSD in R192Q strain HOM/HOM Mouse last 3 digits	Number of CSDs	CSD Amplitude (mV)	CSD Total Duration (s)	Derivative (mV/s)	CSD Half Maximum Duration (s)	Speed (mm/min)
389 RQ	1	21	78	1.8	50	4.6
*394 RQ	3	10.2, 6, 11.9	61	0.6	38	4.2
298 RQ	1	19.1	102	0.1	60	4.7
181 RQ	1	19.3	70	2.2	50	4.9
296 RQ	1	16.1	61	1.1	58	5
287 WT	1	9.8	70.2	0.6	73	3.8
301 WT	1	14	81	0.4	54	2.8
297 WT	1	9.1	72	0.2	68	3.3
586 WT	1	8.1	55	0.3	51	3
**587 WT	1	12	72	0.1	65	2.8

Table shows the number, amplitude, total duration, half-maximum amplitude duration, derivative, and speed of each CSD experimentally induced by inserting a pinprick in right frontal lobe of each transgenic R192Q and its wild type. *The incidence of 3 CSDs after just 1 pinprick in mouse number 394 from the R192Q group. **CSDs were monitored on both hemispheres with 2 electrodes simultaneously, with a very short delay the CSD wave was detected on the contralateral hemisphere to CSD induction side, but with lower amplitude compared to ipsilateral CSD.

Table 4.2. Electrophysiological Characteristics of 1 hr KCl-induced Multiple CSDs in R192Q strain HOM/HOM

1 hr KCl-induced multiple CSDs in R192Q strain HOM/HOM Mouse last 3 digits	Number of CSDs/hr	CSD Amplitude (mV)	CSD Total Duration (s)	Derivative (First CSD- Other CSDs) (mV/s)	CSD Half Maximum Duration (s)	Speed (mm/min)
330 RQ	12	8.8	78.67	First: 0.8 Other CSDs: 0.3	32.5	5
379 RQ	15	9.75	80	First: 0.5 Others:0.1	32.5	5.1
378 RQ	16	4	65.87	First: 0.8 Others: 0.2	33	5.3
623 RQ	11	11.2	71.32	First: 1.6 Others: 0.3	24.5	3.6
404 WT	6	1.78	56.87	-	49.5	1.9
360 WT	9	2.1	71	First: 0.1 Others:0.09	28	2.8
014 WT	4	3.7	53	-	61.5	2.3
625 WT	8	6.5	56.88	First: 0.8 Others: 0.4	43	2

Table shows the number, amplitude, total duration, half-maximum amplitude duration, derivative, and speed of CSDs experimentally induced by 1M KCl-cotton ball application on a bure hole on the right frontal lobe of each homozygous (HOM) and WT mice in R192Q strain.

Table 4.3. Electrophysiological Characteristics of 1 hr KCl- induced Multiple CSDs in S218L strain HET/WT

1 hr KCl- Induced Multiple CSDs in S218L strain HET/WT	Number of CSDs/hr	CSD Amplitude (mV)	CSD Total Duration (s)	Derivative (First CSD- Other CSDs) (mV/s)	CSD Half Maximum Duration (s)	Speed (mm/min)
KCl - 822 - SL/WT	18	10.6	80	First: 0.9 Other CSDs:0.3	26.5	5.8
KCl - 441 - SL/WT	11	11.2	72.8	First: 2 Others: 0.8	30	6.4
KCl - 435 - SL/WT	20	5.8	83	First:0.8 Others: 0.2	53.5	6
Sham - 386 - SL/WT	1	2.8	140	-	-	-
Sham - 815 - SL/WT	-	-	-	-	-	-
KCl - 523 - WT/WT	10	3.8	65	First: 0.2 Others: 0.1	45	1.7
KCl - 383 - WT/WT	9	2.7	74	First: 0.1 Others: 0.09	40	3.9
KCl - 816 - WT/WT	11	4.8	55	First: 0.6 Others: 0.08	43	2.8
Sham, 387, WT/WT	-	-	-	-	-	-
Sham, 821, WT/WT	-	-	-	-	-	-
Sham, 814, WT/WT	-	-	-	-	-	-

Table shows the number, amplitude, total duration, half-maximum amplitude duration, derivative, and speed of CSDs experimentally induced by 1M KCl-cotton ball application on a bore hole on the right frontal lobe of each heterozygous (HET) and WT mice in S218L strain.

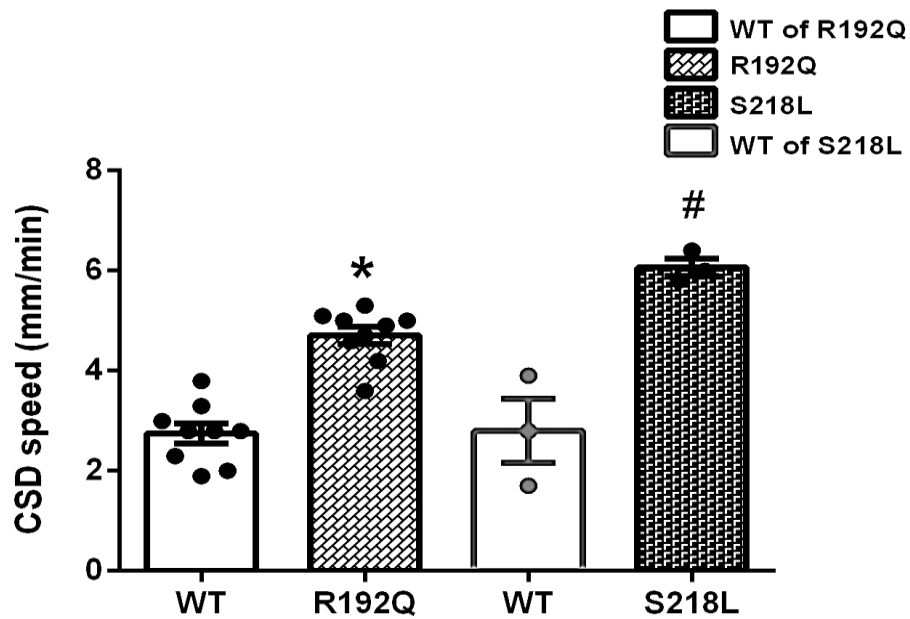
4.6.1. CSD amplitude was not significantly different in wild-type mice compared to that in R192Q or S218L mutant mice

When comparing the amplitude of CSD in WT and R192Q mutant mice, there was not a significant difference for the pinprick-induced CSD group (10.6 ± 1.06 mV, 17.14 ± 1.3 mV respectively) ($p=0.1$; $n=9$ /group); the same trend was followed for WT and S218L mutant mice (3.7 ± 0.6 mV, 9.2 ± 1.7 mV respectively) ($p=0.1$; $n=3$ /group). There was also no genotypic difference with respect to CSD amplitude for the KCl-induced multiple CSDs group ($p=0.14$).

4.6.2. Speed of CSD was higher in R192Q and S218L mutant mice compared to that in wild-type mice

When comparing CSD velocity in mutant and WT groups there was a significant difference with the speed being higher in R192Q mutant mice (4.7 ± 0.2 mm/min) compared to that in WT mice (2.7 ± 0.2 mm/min) ($p<0.0001$; $n=9$ /group). CSD speed in S218L mutant mice was also higher than in WT mice, but due to the low number of heterozygous S218L mutant mice tested ($n=3$ /group), no meaningful statistical analysis was obtained for this parameter. However, CSD velocity showed higher values for S218L mutant mice (6.0 ± 0.2 mm/min) compared to that in R192Q mutant mice (4.7 ± 0.2 mm/min) ($p=0.0091$) (Figure 4.26.).

CSD speed in R192Q and S218L mice compared to WT



4.26. CSD speed is increased in both R192Q and S218L mutant strains after both pinprick- and KCl-induced CSDs compared to WT mice. Bars show standard error of the mean (SEM). * $p < 0.0001$ versus WT; # $p = 0.009$ versus R192Q; $n = 9$ /group in R192Q and $n = 3$ /group in S218L experiments.

4.6.3. Total CSD duration was not significantly changed in R192Q and S218L mutant mice compared to that in wild-type mice

When comparing total CSD duration in mutant and WT groups, the results showed that in both the pinprick-induced CSD and the KCl-induced multiple CSDs experiments the total CSD duration in mutant mice was longer than in WT mice, although this difference did not reach statistical significance. In both the pinprick-induced CSD and the KCl-induced multiple CSDs experiments the total CSD duration in WT mice was 70.0 ± 4.2 seconds, and 59.4 ± 3.9 seconds, respectively, compared to 74.4 ± 7.5 seconds and 73.9 ± 3.3 seconds respectively in R192Q mutant mice, but this difference was not significant ($p=0.9$). A similar result was obtained for the heterozygous S218L mutant group. In KCl-induced multiple CSDs experiments the total CSD duration was 78.5 ± 3.1 seconds in S218L mutant mice and 64.6 ± 5.4 seconds in the respective WT group, and again the difference was not statistically significant ($p=0.2$).

4.6.4. CSD half-maximum duration was not statistically different in R192Q and S218L mutant mice compared to wild-type mice

When comparing CSD half-maximum amplitude duration in mutant and WT groups, results showed that in both the pinprick-induced CSD and the KCl-induced multiple CSDs experiments the half-maximum duration was longer in WT mice (62.2 ± 4.1 seconds and 45.5 ± 6.9 seconds, respectively) compared to that in R192Q mutant mice (51.2 ± 3.8 seconds and 30.6 ± 2.0 seconds, respectively) but these differences were not significant ($p=0.1$). A similar result was obtained for the heterozygous S218L group. In KCl-induced multiple CSDs experiments the half-maximum duration was longer in WT mice (42.6 ± 1.4 seconds) compared to that in S218L mutant mice (36.7 ± 8.5 seconds), and again the difference was not statistically significant ($p=0.7$).

4.6.5. Frequency of CSD events in R192Q and S218L mutant mice compared to that in wild-type mice

When comparing CSD frequency during 1-hour of KCl-application, the number of CSDs was increased in both the R192Q (13 ± 2) and S218L (16 ± 3) mutant mouse groups compared to the respective WT groups (7 ± 1 and 9 ± 1 , respectively), however, the differences were not statistically different ($p=0.1$), likely to the small group sizes ($n=4/\text{group}$ in R192Q experiments and $n=3/\text{group}$ in S218L experiments)(Figure 4.27.).

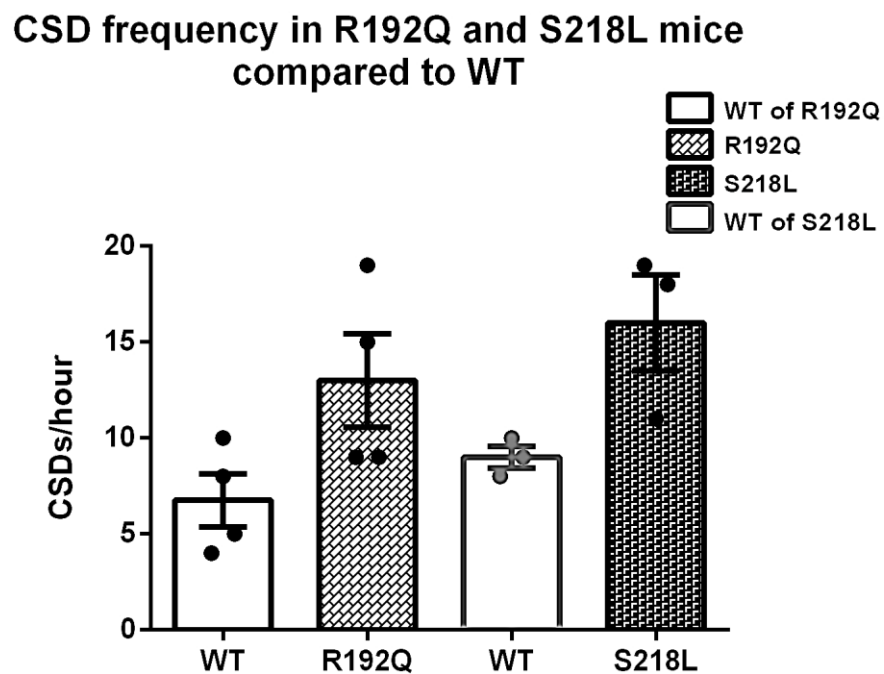


Figure 4.27. CSD frequency in R192Q and S218L mutant mice compared to WT mice. During 1-hour KCl-induced multiple CSDs, the DC recording shows an increase in the number of CSDs in mutant mice for both the R192Q and the S218L strain compared to WT mice, but this rise is not statistically significant. Bars show standard error of the mean (SEM). $n=4/\text{group}$ in R192Q mutant and $n=3/\text{group}$ in S218L mutant experiments.

4.6.6. CSD rising rate was higher in the first CSD event compared to subsequent events in R192Q and S218L mutant mice compared to that in wild-type mice

CSD rising rate, which is the first component (depolarizing phase) of the derivative of CSDs, indicating the depolarization rise amount, for the average of the first CSD in the R192Q mutant group was 1.13 ± 0.21 mV/s, which was considerably higher than that in the WT group (0.32 ± 0.06 mV/s)($p=0.0002$; $n=9$ /group). The average of the first CSD derivative was also higher in the S218L mutant group compared to WT but probably due to the low number of animals in the mutant group ($n=3$ /group) the difference did not reach statistical significance ($p=0.1$). After taking the average of the first component of derivative of other CSDs after the first one, during 1-hour KCl application, results showed that the average derivative of other CSDs in both the R192Q and S218L mutant mice was higher compared to that in WT mice but this was not significant ($p=0.08$, and $p=0.1$ respectively). In R192Q mutant mice, when we compared the average of the first CSD derivative (1.13 ± 0.21 mV/s) to the average derivative of other CSDs (0.22 ± 0.04 mV/s), there was a huge decrease of the subsequent CSDs derivative ($p=0.0028$; $n=9$ /group for first CSD and $n=4$ /group for other CSDs). The first CSD derivative was also higher compared to the average derivative of subsequent CSDs in the S218L mutant group, but this was not significant likely due to the small number of mice tested ($n=3$ /group). In WT mice, the derivative of the first CSD (0.32 ± 0.06 mV/s) was significantly higher than the average derivative of subsequent CSDs (0.09 ± 0.05)($p=0.025$; $n=7$ /group for first CSD and $n=3$ /group for other CSDs)(Figure 4.28.).

CSD rising rate difference between R192Q, S218L KI mice and WT

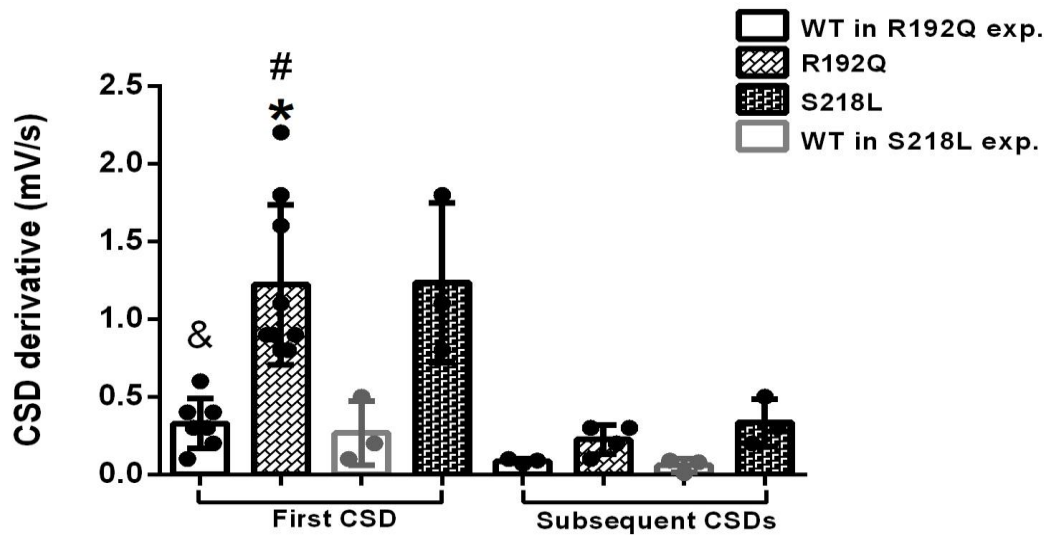


Figure 4.28. CSD derivatives (depolarizing phase) difference between WT, R192Q and S218L mutant mice. Bars show standard error of the mean (SEM). * $p=0.0002$ R192Q *versus* WT; & $p<0.05$ *versus* derivative of all CSDs in WT; # $p=0.002$ *versus* derivative of all CSDs in R192Q mutant mice; $n=9$ /group in R192Q and $n=3$ /group in S218L mutant mice

DISCUSSION

In WT mice, CSD has been shown to cause signaling between neurons, which are under stress, and trigeminal afferents via opening of neuronal Panx1 channels and subsequent activation of caspase-1 that is followed by the neuronal release of HMGB1 and NF- κ B activation in astrocytes (6). Therefore, in this thesis, both the basal parenchymal neuroinflammatory state, and CSD-induced parenchymal neuroinflammation, revealed by HMGB1 neuronal release and NF- κ B activation in astrocytes, was investigated deeply in a transgenic mouse model of migraine, namely in FHM1 mutant mice. We studied the female mice because migraine itself is more prevalent in females, and moreover, these FHM1 female mice have been studied vastly in the literature for electrophysiology and CSD threshold speed and also for the effect of female hormones on CSD characterizations.

This thesis data revealed not only a basal ongoing parenchymal neuroinflammatory signaling state in R192Q mutant mice but also a different regional distribution pattern in the inflammatory signaling upon CSD in the primary motor cortex and primary somatosensory cortex, and also striatum and thalamus of both R192Q mutant and WT mice. This neuroinflammatory pattern has a signature in FHM1 mutant mice in the sense that there is more HMGB1 release *contralateral* to the hemisphere in which CSD was induced. Such contralateral activation is not present with such intensity in WT mice. Moreover, our data showed a significant increase in HMGB1 release in subcortical areas of mutant mice compared to WT animals. The release was significantly higher in thalamus compared to striatum of R192Q mutant mice. Our findings indicate that (i) CSD triggers parenchymal inflammatory processes in both the WT and mutant mouse brains, (ii) this process is mostly ipsilateral to the side of CSD induction in WT mice, and (iii) that in mutant mice a bilateral inflammatory signature becomes expressed after CSD with a specific regional distribution pattern.

HMGB1 belongs to alarmin family and provides communication between the damaged and surrounding cells. There has been an increasing amount of evidence related to the role of HMGB1 in the CNS in recent years. Intracerebroventricular administration of HMGB1 increases Il-1 β and TNF- α concentration in brain tissue

(120). After the onset of ischemic stroke neurons release HMGB1 in experimental studies (121, 122) and it has biphasic actions in inflammation and recovery after stroke (123). In humans during the course of several neurological diseases like traumatic brain injury, subarachnoid hemorrhage, and meningitis, CSF HMGB1 level is increased at early time points (124). Cerebrospinal fluid levels of HMGB1 and cytochrome C predict the outcome after pediatric traumatic brain injury (125). Especially in experimental epilepsy models, HMGB1 contributes to disease progression, and consistent with animal data, there is an early expression of HMGB1 in patients with newly diagnosed epilepsy, and its persistence was associated with subsequent seizures (126). There are some hints about the close interplay between increased excitation and inflammation from epilepsy models (17, 18), which suggest that the elevated activity in glutamatergic pathways in R192Q mutant mice (16) being more pronounced during CSD episodes, may initiate a specific inflammatory response. On the other hand, it can be interpreted that the CSD-induced elevation of the inflammatory response can be the consequence of an already present pro-inflammatory state in the FHM1 mutant brain, which is present in naïve animals (96).

After CGRP receptor antagonists and monoclonal antibodies entering the migraine treatment market and following the studies related to neuroinflammation in migraine pathophysiology, the doubts over neuroinflammation hypothesis in migraine have been removed. Recent evidence for a pro-inflammatory profile came from studies of the same R192Q mutant strain namely from investigating trigeminal ganglia (TG) that showed signs of neuroinflammation in naïve animals (99). In TG, most of neurons co-express purinergic P2X3 and TNF α receptors making them susceptible to inflammation mediated by TNF α and related pain signaling (94, 95). R192Q mutant TG have been reported to be enriched in activated macrophages, as evidenced by both immunoreactivity to CD11b (an adhesion molecule marker that is expressed in microglia and macrophages that are active), Iba1 and macrophage antigen ED1, and by macrophage morphology, when compared to TG of WT mice (95). Besides, R192Q mutant TG expressed increased mRNA levels of IL6, IL1b, IL10 and TNF α cytokines. Intact TG of R192Q mutant mice appeared to be enriched in activated macrophages both in the absence and presence of a standard

inflammatory stimulus, LPS (95), however there are similar levels of inflammatory cytokines in TG extracts from WT and R192Q mutant mice (95). Similar to this study, in this thesis the amount of neuronal HMGB1 release is almost the same in both mutant and WT mice after CSD induction in the whole brain. In a study, a larger fraction of TG neurons has been shown to be immunoreactive for active phosphorylated CaMKII in intact ganglia and cultured TG neurons of R192Q mutant compared to WT mice (98). Blockage of P/Q channels in cultured TG neurons eliminated this difference in amount of phosphoprotein between the two genotypes, suggesting facilitation of basal $Ca_v2.1$ -dependent Ca^{2+} signaling (98). This may suggest that basal neuroinflammation accompanies facilitation of calcium signaling in TG of R192Q mutant mice. Here for the first time in the literature, we presented that there is a basal ongoing parenchymal neuroinflammatory signaling in R192Q mutant mice brain both in cortical and subcortical levels. In 2013, Karatas et al. suggested that CSD causes activation of parenchymal neuroinflammatory pathway which leads to trigeminovascular activation and head pain. In this thesis, this parenchymal neuroinflammatory signaling was seen in naïve FHM1 mutant mice at basal conditions. We showed that in the absence of any stimulus or CSD induction, both the basal HMGB1 release from neurons and NF- κ B activation in astrocytes are significantly higher in R192Q mutant compared to WT. These are the actual biomarkers of neuroinflammation that we investigated in the brain, in contrast to the above mentioned literature which indirectly studied and defined it as "pro-inflammatory state" by showing gene expression levels in caudal cortex and activated macrophages, microglia and increased cytokine expression levels in FHM1 mutant mice TG. We also checked if there has already been any HMGB1 release as a result of perfusion-hypoxia stress. Number of dysmorphic neurons in parietal cortex which indicates to the stressed neurons with HMGB1 release (127) was 1.65 % and 1.85 % for WT and FHM1 mutant mice groups respectively which both were below the 6 % threshold and indicated that cardiac perfusion was done well without any hypoxic effect on neurons and HMGB release. So, the release which we measured in this thesis belonged merely to the basal neuroinflammation or CSD-induced neuroinflammation in the mice (127). What we have shown in this thesis regarding the basal parenchymal neuroinflammatory state in the brain of R192Q mutant mice,

may further explain the facilitated CSD induction and propagation in these FHM1 mutant mice model, beside the evidence of basal $Ca_v2.1$ -channel gain of function.

The non-invasive stimulus of drilling the skull experiments, as a confounding factor, indicated that in the right frontal cortex on which the drilling was performed, HMGB1 release in R192Q mutant mice was more prominent than WT. However, this difference was not significant ($p=0.0571$) and the other regions of the brain act more or less the same in respect to HMGB1 release in mutant and WT mice. Therefore, drilling may not be a confounding factor in FHM1 mutant and WT mice experiments regarding to gene effect, but data showed that comparing naïve HMGB1 release to drilled groups, HMGB1 release was increased in both WT and R192Q mutant mice after drilling which was only significant in right cortex ($p=0.028$) compared to naïve mice.

Following pinprick-induced CSD and investigation of parenchymal neuroinflammation, our results showed that in R192Q mutant mouse brains, HMGB1 release was present in both hemispheres, so *bilateral*, whereas, in WT brains there was more HMGB1 release ipsilateral to the side of CSD induction compared to the contralateral side, in accordance with previous studies (6). Moreover, results demonstrated an increase in NF- κ B activation, which is downstream of neuroinflammatory signaling coming after HMGB1, in all investigated brain regions of R192Q mutant compared to WT mice. NF- κ B nuclear translocation was significantly higher in R192Q mutant ipsilateral frontal cortex compared to same area of WT mice. This result was obtained in R192Q mutant mice contralateral striatum compared to WT homolog region. It could reflect the activation of a signaling response in astrocytes that alarms the organism about the danger that is proceeding inside the brain. When we compared cortical areas in mutant and WT mice, our data demonstrated a significant increase in the amount of HMGB1 release from neurons in R192Q mutant contralateral frontal cortex compared to the same area in WT mice. In R192Q mutant mice neurons in frontal primary motor cortex released more HMGB1 compared to parietal cortex, the primary somatosensory area. This cortical parenchymal inflammatory pattern is in line with the motor symptoms of FHM1 mutants such as motor weakness during aura and headache. The bilateral HMGB1 release in FHM1 mutant mice has been reported for the first time in this

study. More studies are needed in the future to explain the reason of this bilaterality, to see if it can be related to the hyperexcitability of the whole brain in the FHM1 mutant mice, or to special mechanisms underlying the spread of parenchymal neuroinflammatory molecules such as HMGB1 as an alarmin molecule, independent of CSD. Another explanation may be the result of the CSD event, since the spreading of CSD to the contralateral hemisphere has not been reported with enough evidence, it also should be investigated if the CSD wave can reach to the contralateral hemisphere of the brain.

Comparing subcortical areas between R192Q mutant and WT mice revealed more pronounced increase in the amount of HMGB1 release from neurons in nearly all areas of R192Q mutant mice compared to that of WT mice except for right striatum. The fact that subcortical areas are affected in R192Q mutant mice is in accordance with earlier data showing that these areas are more easily affected as evidenced by the fact that CSD propagates readily into subcortical structures in the mutant mice (7). In R192Q mutant mice the amount of neuronal HMGB1 release was significantly more pronounced in the contralateral striatum compared to the homolog region of WT mice. This indicates again that parenchymal neuroinflammation in mutant mice is bilateral, also in subcortical structures. It has been reported that the facilitated spreading of subcortical CSD would not extent until thalamus in R192Q mutant mice (7), however, notably, our data revealed that the increase in HMGB1 release was significantly higher in thalamus, both at the ipsilateral and the contralateral side. This may be due to isoflurane anesthesia effect in the reported study which is a well-known anesthetic agent preventing CSD spreading; in our study we used urethane which is the most usable anesthetic in electrophysiological studies of the brain *in vivo* and has the least effect of anesthetic agent on neurophysiology of the brain. In WT mice, ipsilateral striatum had a higher amount of HMGB1 release than contralateral striatum which again confirms the unilateral parenchymal neuroinflammation shown for cortical areas of WT animals earlier (6). Altogether, our data revealed the increased susceptibility of FHM1 mutant mice to subcortical CSD and reverberating CSD waves as an increased parenchymal neuroinflammation in thalamus and striatum, in line with raised parenchymal neuroinflammation in cortical regions. This indicates that CSD-induced parenchymal

neuroinflammation spreads through cortex, striatum, and thalamus of both hemispheres in genetically susceptible brains, which may explain the prolonged hemiplegia, coma, and seizure phenotype in this variant of migraine with aura.

When we compared neuroinflammation in cortical and subcortical regions, data showed that in WT, ipsilateral frontal cortical and striatal HMGB1 release was higher than that in contralateral side; this indicates to the unilateral parenchymal neuroinflammation in CSD-side of WT mice. However, in R192Q mutant mice, the HMGB1 release was bilateral and more pronounced compared to WT for the contralateral side to CSD induction. R192Q mutant mice showed significantly more HMGB1 release in ipsilateral and contralateral striatum compared to ipsilateral and contralateral frontal cortices which may suggest that subcortical areas are more susceptible to CSD propagation in FHM1 mutant mice as discussed above.

NF- κ B activation in astrocytes after CSD events demonstrated a near to complete response in all astrocytes to parenchymal neuroinflammation compared to the CSD-induced neuronal HMGB1-release response in both WT and R192Q mutant mice. The lower number of astrocytes compared to neurons in mouse brain could be a possible explanation for this phenomenon.

In multiple CSD experiments during 1 hour, data indicated that there was higher HMGB1 amount compared to sham-operated mutant group in Western blotting of CSF of individual S218L mutant mice in CSD group. This was not significant possibly because of the insufficient number of mice used in these experiments ($n=2$ /group). Because collecting CSF from intracerebroventricular cannula is a quite complicated and difficult method, and the amount of CSF obtained is too low for being adequately detected in Western blot, more sensitive methods such as ELISA may be used in future for HMGB1 amount detection in the CSF of these mice. So, our goal is to repeat this set of experiments with more mice in near future. Notably, Western blotting of brains to check the amount of NF- κ B translocation from cytoplasm to the nucleus indicated that nuclear NF- κ B was higher in S218L sham-operated animals compared to those of the WT strain and in CSD groups compared to WT sham-operated mice. We might also take in to consideration the difference between immunohistochemistry and Western blotting techniques. For example in NF- κ B activation comparison, in immunohistochemistry experiments

astrocytes were marked specifically with S100-beta and nuclear NF- κ B translocation in astrocytes was determined accordingly, meaning that denominator was the number of astrocytes and this gives a more precise result; however, in Western blotting experiments in which a brain region such as frontal cortex was homogenized and processed according to the protocol, the denominator was the number of all the brain cells. Therefore, obtained band may reflect not only astrocytic NF- κ B but also the possible recruitment of other cells. This may dilute the result of Western blotting to show the actual NF- κ B relocation in astrocytes. However, even the current data of this thesis may suggest an increased neuroinflammation in the brain of FHM1 mutant mice as CSF is an indicator of the 'whole brain state' and not a specific brain area. If we consider all these together with more parenchymal neuroinflammation in naïve R192Q mutant mice compared to naïve WT animals revealed by more HMGB1 release from neurons and more NF- κ B activation in astrocytes in the mutants, two possible mechanisms may be important to speculate: (i) there is a possibility of spontaneous CSDs in naïve R192Q mutant mice, and (ii) HMGB1 may leak from neurons to the parenchyma in a more excitable brain in naïve mutant mice to alarm the organism of the possible dangers. In both scenarios neuronal HMGB1 pools may become depleted due to spontaneous release in naïve mutant mice, so no, or less HMGB1 can be released any more after a trigger like CSD. Moreover comparing immunohistochemistry of R192Q naïve mice with S218L sham-operated group in multiple CSD experiments may not be an option to check the basal level of neuroinflammation in these mutant mice, since firstly, we are talking about two different mutations which are S218L form, much more severe compared to R192Q, and secondly, for R192Q mice the un-touched naïve animal was sacrificed and studied for parenchymal neuroinflammatory signals but in S218L, the animal was under anesthesia and sham operation condition, drilled and opened skull for saline application, in any conditions the results of these two paradigms cannot be compared to each other, and we may expect to have more inflammatory signal by more HMGB1 release and NF- κ B relocation in sham S218L group compared to naïve R192Q group, that happened in this study too. Putting all these together, for detecting the real inflammatory signal in the basal state of these mice,

the naïve animal should be considered without the above-mentioned confounding factors.

Electrophysiological analysis of this thesis also showed interesting results. Comparing CSD velocity in R192Q and S218L mutant mice with the speed in WT groups showed a significant increase in R192Q mutants which was reported previously (14, 15). CSD velocity was significantly higher in S218L mutant mice compared to R192Q mutant animals showing more susceptible and hyperexcitable brain in S218L mutant compared to R192Q which is in accordance with their more severe phenotype. Total CSD duration in FHM1 mutants was longer than WT mice, but it was not significant. In this thesis for the first time, the first component of the derivative of CSDs was measured. This measure implies the depolarization rising rate; the higher the derivative, more neurons are recruited to the depolarization and more glutamate is released from neurons (108, 128). The rising rate of the first CSD in R192Q mutant mice was considerably higher than that in WT mice. The rising rate of the first CSD was also higher in S218L mutant mice compared to that in WT mice but probably due to the low number of mice in S218L/WT experiments (n=3/group), it was not significant. The average of derivatives of all subsequent CSDs, so after the first one, in both R192Q and S218L mutant mice, was higher compared to that in WT mice, but this was not significant. In R192Q mutant mice, when we compare the derivative of the first CSD to the average of derivatives of subsequent CSDs, a significant increase was shown for the first CSD derivative. The first CSD derivative was also increased compared to the average derivative of other CSDs in the S218L mutant mice. These data showed that the amount of depolarization, and the maximum amount of depolarized neurons and released glutamate at the beginning of a CSD wave could be increased in FHM1 mutant mice compared to WT, and also in the first CSD compared to all subsequent CSDs, so after the first one.

There are some limitations of this thesis study mainly related to the mouse numbers used in the experiments. It was because of our dependency to an abroad university for providing mice. Another one is performing immunohistochemistry experiments with R192Q mutant mice, however in Western blotting experiments S218L mutant mice were used. The reason was the breeding problem of R192Q mice. Although this limits the number of R192Q mutant mice, however, notably

working on different types of FHM1 mutants may display the results of two different genotypes and enrich our perspective on these mutant mice models. Besides, collaboration with a world-leading high-profile migraine group was a fruitful, productive and joyful experience. We believe that this and future collaborations will increase the visibility of our Institute around the World in migraine area.

Here, for the first time in the literature, we presented that there is a basal ongoing parenchymal neuroinflammatory signaling in R192Q mutant mice brain both in cortical and subcortical levels. Our findings indicate that CSD triggers parenchymal inflammatory processes in both WT and mutant mouse brains, this process is mostly ipsilateral to the side of CSD induction in WT, and bilateral in mutant mice. Future studies may indicate whether basal neuroinflammation contributes to cortical hyperexcitability seen in FHM1 mutants in addition to the increased neuronal calcium influx, or increased calcium and glutamate cause basal neuroinflammation. These findings indicate that CSD-induced parenchymal neuroinflammatory signaling spreads through cortex, striatum, and thalamus of both hemispheres in genetically susceptible brains, which may explain the prolonged hemiplegia, coma, and seizure phenotype in this variant of migraine with aura, and may highlight these areas as more particularly relevant to the disease pathology. This thesis study brings more questions about the pathophysiology of migraine. 1) More studies are needed to investigate the ways by which we can demonstrate more clearly the basal neuroinflammatory state with other inflammatory markers. 2) Future studies may reveal some insights regarding the basal parenchymal neuroinflammatory signaling which we observed both in R192Q and S218L mutant mice; it should be clarified if the anti-inflammatory mechanisms are also activated in these mice. This anti-inflammatory response may prevent further neuroinflammatory signaling like a ceiling effect. 3) More studies are needed to investigate more precisely the regional difference observed for parenchymal neuroinflammatory signaling in this study by other methods such as proteomic analysis. 4) The reason for significant bilateral neuronal HMGB1 release and astrocytic NF- κ B translocation in R192Q mutant should further be clarified; studies are needed to understand mechanism underlying the spreading of parenchymal proinflammatory signals to the other hemisphere in these FHM1 mutant mouse

model and to investigate if these mechanisms are induced and intensified in a CSD-independent manner or not. 5) If CSD can spread easily to the contralateral hemisphere to side of induction, and to understand the relation of this bilateral activation and stimulation to the specific mutation in FHM1 mice should be clarified. 6) Regarding the regional pattern of neuroinflammation observed here, future studies would be helpful why the thalamus was more stimulated and showed more HMGB1 release response in mutant mice, if it can be related to the pain perception role of the thalamus, or being a relaying site for projections of trigeminovascular second-order neurons to somatosensory and motor cortices. To our knowledge, there is no report till now about the HMGB1 distribution pattern in parenchymal neuroinflammation in the brain in other neurological diseases. 7) Moreover, studies needed to be done to see why some neurons have released HMGB1 after CSD and some not, we speculate this might be due to different type of neurons, principle neurons may be more sensitive to inflammatory signaling and may release HMGB1 more than interneurons, this could be in accordance with the fact that in FHM1 mutant mice pyramidal excitatory neurons are affected by the $Ca_v2.1$ -mutation and show increased Ca^{2+} current and glutamate release but inhibitory interneurons are unaffected and no GABA is released more as a result of this mutation.

In this study we investigated the time points of 30 minutes after CSD and 1 hour multiple CSDs effect on neuroinflammation, since HMGB1 is a low turn-over protein it is not replenished quickly in the tissue. So, after-CSD longer time points such as 6 hours or 24 hours should be studied to have a better understanding of this alarmin molecule action and behavior especially after proinflammatory signaling in the brain. Moreover, the effect of multiple CSDs is needed to be studied on HMGB1 release detected by immunohistochemistry and also the same procedure is needed to be performed to study these patterns in different areas of S218L mice. It is important to know in the absence of any invasive confounding stimulus such as drilling the skull, opening a bure hole, and anesthesia, in a condition of non-invasively induced CSD such as optogenetically-induced CSD in a freely moving mouse what will be the difference of the results regarding basal and CSD-induced neuroinflammatory signaling in these mutant and WT mice.

Here, we have studied the HMGB1 release from neurons and NF- κ B translocation in astrocytes which are considered in a "para inflammatory state" as can be explained as a transitory stage between basal normal brain state and pathologic inflammation. More studies should be done to make it clear what will happen after the activation of this para-inflammatory state in these FHM1 mutant mice and how can they be related to the pathological symptoms of the patients.

If HMGB1 is an alarmin proinflammatory molecule which may be released and spread independent of CSD event, the blocking of this pathway and molecule may have more implications for migraine comorbid diseases such as depression and epilepsy. As in depressive patients the incidence of migraine and epilepsy is common, more studies are needed to be done to see if common pathophysiology of these diseases is a neuroinflammatory-related mechanism as a key factor to all of them, and if by targeting HMGB1 molecule and its blockade we may find a common medication target for both migraine and its comorbid diseases. Besides, here we showed that neuroinflammatory signaling is bilaterally activated and it is highly significant in the R192Q mutant mice, if this pattern is not due to CSD spreading to the contralateral hemisphere of the brain, instead a neuroinflammatory signaling may spread to the contralateral side, the implications may also be useful in other diseases without CSD event, including migraine without aura, Alzheimer's disease, depression, and epilepsy.

CONCLUSION

- 1- There is a basal parenchymal neuroinflammatory state in R192Q mutant mice compared to WT as revealed by higher HMGB1 release from neurons and NF- κ B relocation in astrocytes.
- 2- There is a unique regional distribution pattern in the inflammatory signaling upon CSD in the frontal/parietal cortices and striatum/thalamus of both R192Q and wild-type mice.
- 3- This inflammatory pattern has its own signature in mutant mice based on more HMGB1 release contralateral to CSD induction side compared to WT.
- 4- This inflammatory process is mostly ipsilateral to the side of CSD induction in WT mice.
- 5- There is an increase in HMGB1 release in subcortical areas of FHM1 mutant animals compared to WT, which is significantly higher in the thalamus compared to striatum.
- 6- The amount of NF- κ B activation and translocation is higher in S218L sham-operated mice compared to WT sham-operated ones, and in S218L CSD group compared to WT CSD ones.
- 7- The derivative of the first CSD is significantly higher than the derivative of subsequent CSDs after the first one, in FHM1 mutant and WT mice, in a model of multiple CSDs.
- 8- The derivative of the first CSD is significantly higher in FHM1 mutant mice compared to that in WT. The same trend is followed for the derivatives of all other CSDs, subsequent to the first one.
- 9- Electrophysiological analysis showed that CSD speed is more in mutant groups, however CSD half maximum amplitude duration and CSD frequency did not change significantly between groups.
- 10- Future studies may indicate if basal neuroinflammation contributes to cortical hyperexcitability seen in FHM1 mutants in addition to the increased neuronal calcium influx or increased calcium and glutamate cause basal neuroinflammation.

REFERENCES

1. Vos T, Flaxman AD, Naghavi M, Lozano R, Michaud C, Ezzati M, et al. Years lived with disability (YLDs) for 1160 sequelae of 289 diseases and injuries 1990-2010: a systematic analysis for the Global Burden of Disease Study 2010. *Lancet*. 2012;380(9859):2163-96.
2. Bes A, Kunkel R, Lance JW, Nappi G, Pfaffenrath V, Rose FC, et al. The International Classification of Headache Disorders, 3rd edition (beta version). *Cephalalgia*. 2013;33(9):629-808.
3. Ferrari MD, Klever RR, Terwindt GM, Ayata C, van den Maagdenberg AMJM. Migraine pathophysiology: lessons from mouse models and human genetics. *Lancet Neurol*. 2015;14(1):65-80.
4. Tolner EA, Houben T, Terwindt GM, de Vries B, Ferrari MD, van den Maagdenberg AMJM. From migraine genes to mechanisms. *Pain*. 2015;156(4):S64-S74.
5. Lauritzen M. Pathophysiology of the Migraine Aura - the Spreading Depression Theory. *Brain*. 1994;117:199-210.
6. Karatas H, Erdener SE, Gursoy-Ozdemir Y, Lule S, Eren-Kocak E, Sen ZD, et al. Spreading Depression Triggers Headache by Activating Neuronal Panx1 Channels. *Science*. 2013;339(6123):1092-5.
7. Eikermann-Haerter K, Yuzawa I, Qin T, Wang YM, Baek K, Kim YR, et al. Enhanced Subcortical Spreading Depression in Familial Hemiplegic Migraine Type 1 Mutant Mice. *J Neurosci*. 2011;31(15):5755-63.
8. Bolay H, Reuter U, Dunn AK, Huang ZH, Boas DA, Moskowitz MA. Intrinsic brain activity triggers trigeminal meningeal afferents in a migraine model. *Nat Med*. 2002;8(2):136-42.
9. Lotze MT, Tracey KJ. High-mobility group box 1 protein (HMGB1): nuclear weapon in the immune arsenal. *Nat Rev Immunol*. 2005;5(4):331-42.
10. Brites D, Vaz AR. Microglia centered pathogenesis in ALS: insights in cell interconnectivity. *Front Cell Neurosci*. 2014;8:117.
11. Figuera-Losada M, Rojas C, Slusher BS. Inhibition of microglia activation as a phenotypic assay in early drug discovery. *J Biomol Screen*. 2014;19(1):17-31.
12. Wessman M, Terwindt GM, Kaunisto MA, Palotie A, Ophoff RA. Migraine: a complex genetic disorder. *Lancet Neurol*. 2007;6(6):521-32.
13. Ophoff RA, Terwindt GM, Vergouwe MN, vanEijk R, Oefner PJ, Hoffman SMG, et al. Familial hemiplegic migraine and episodic ataxia type-2 are caused by mutations in the Ca²⁺ channel gene CACNL1A4. *Cell*. 1996;87(3):543-52.
14. van den Maagdenberg AMJM, Pietrobon D, Pizzorusso T, Kaja S, Broos LAM, Cesetti T, et al. A Cacna1a knockin migraine mouse model with increased susceptibility to cortical spreading depression. *Neuron*. 2004;41(5):701-10.
15. Eikermann-Haerter K, Dilekoz E, Kudo C, Savitz SI, Waeber C, Baum MJ, et al. Genetic and hormonal factors modulate spreading depression and transient hemiparesis in mouse models of familial hemiplegic migraine type 1. *J Clin Invest*. 2009;119(1):99-109.
16. Tottene A, Conti R, Fabbro A, Vecchia D, Shapovalova M, Santello M, et al. Enhanced Excitatory Transmission at Cortical Synapses as the Basis for Facilitated

- Spreading Depression in Ca(v)2.1 Knockin Migraine Mice. *Neuron*. 2009;61(5):762-73.
17. Vezzani A, French J, Bartfai T, Baram TZ. The role of inflammation in epilepsy. *Nat Rev Neurol*. 2011;7(1):31-40.
 18. Vezzani A, Friedman A, Dingledine RJ. The role of inflammation in epileptogenesis. *Neuropharmacology*. 2013;69:16-24.
 19. Robbins MS, Lipton RB. The Epidemiology of Primary Headache Disorders. *Semin Neurol*. 2010;30(2):107-19.
 20. Bartleson JD, Cutrer FM. Migraine update. Diagnosis and treatment. *Minn Med*. 2010;93(5):36-41.
 21. Stovner LJ, Zwart JA, Hagen K, Terwindt GM, Pascual J. Epidemiology of headache in Europe. *Eur J Neurol*. 2006;13(4):333-45.
 22. Steiner TJ, Scher AI, Stewart WF, Kolodner K, Liberman J, Lipton RB. The prevalence and disability burden of adult migraine in England and their relationships to age, gender and ethnicity. *Cephalalgia*. 2003;23(7):519-27.
 23. Mortimer MJ, Kay J, Jaron A. Epidemiology of headache and childhood migraine in an urban general practice using Ad Hoc, Vahlquist and IHS criteria. *Dev Med Child Neurol*. 1992;34(12):1095-101.
 24. Lavados PM, Tenhamm E. Epidemiology of migraine headache in Santiago, Chile: a prevalence study. *Cephalalgia*. 1997;17(7):770-7.
 25. Wang SJ. Epidemiology of migraine and other types of headache in Asia. *Curr Neurol Neurosci Rep*. 2003;3(2):104-8.
 26. Rasmussen BK, Olesen J. Migraine with Aura and Migraine without Aura - an Epidemiologic-Study. *Cephalalgia*. 1992;12(4):221-8.
 27. Ottman R, Lipton RB. Comorbidity of Migraine and Epilepsy. *Neurology*. 1994;44(11):2105-10.
 28. Hughes DR. Digging up Bones - Brothwell,Dr. *Antiquity*. 1963;37(148):327-327.
 29. Brown-Sequard: An Improbable Genius Who Transformed Medicine [press release]. Oxford Univ Press 2010.
 30. MKv. B. Migräne: Ursachen, Formen, Therapie München: C. H. Beck Verlag 2007.
 31. Knapp RD, Jr. Report from the Past. 2. (Thomas Willis). Headache. 1963;3:112-22.
 32. R. E. From Hereditary Angioedema to Migraine [Vol Diploma]. Zurich: ETH Zurich. 2004.
 33. Wolff HG, Tunis MM. Analysis of cranial artery pressure pulse waves in patients with vascular headache of the migraine type. *Trans Assoc Am Physicians*. 1952;65:240-4.
 34. Torda C, Wolff HG. Experimental Studies on Headache: Pharmacodynamics of Urine Excreted during Migraine Headache and Its Relation to 17-Ketosteroid Content. *J Clin Invest*. 1943;22(6):853-8.
 35. Blau JN. Migraine: A vasomotor instability of the meningeal circulation. *Lancet*. 1978;2(8100):1136-9.
 36. Olesen J, Friberg L, Olsen TS, Iversen HK, Lassen NA, Andersen AR, et al. Timing and topography of cerebral blood flow, aura, and headache during migraine attacks. *Ann Neurol*. 1990;28(6):791-8.

37. Mayberg M, Langer RS, Zervas NT, Moskowitz MA. Perivascular meningeal projections from cat trigeminal ganglia: possible pathway for vascular headaches in man. *Science*. 1981;213(4504):228-30.
38. Tottene A, Fellin T, Pagnutti S, Luvisetto S, Striessnig J, Fletcher C, et al. Familial hemiplegic migraine mutations increase Ca²⁺ influx through single human Ca(V)_{2.1} channels and decrease maximal Ca(V)_{2.1} current density in neurons. *P Natl Acad Sci USA*. 2002;99(20):13284-9.
39. Goadsby PJ, Lipton RB, Ferrari MD. Migraine--current understanding and treatment. *N Engl J Med*. 2002;346(4):257-70.
40. Moskowitz MA, Macfarlane R. Neurovascular and molecular mechanisms in migraine headaches. *Cerebrovasc Brain Metab Rev*. 1993;5(3):159-77.
41. Moskowitz MA. Neurogenic versus vascular mechanisms of sumatriptan and ergot alkaloids in migraine. *Trends Pharmacol Sci*. 1992;13(8):307-11.
42. Waeber C, Moskowitz MA. Migraine as an inflammatory disorder. *Neurology*. 2005;64(10):S9-S15.
43. WHO. The Global Burden of Disease: 2004 Update. World Health Organization,; 2004.
44. Birringer C. ETH Zurich 2013.
45. Bloudek LM, Stokes M, Buse DC, Wilcox TK, Lipton RB, Goadsby PJ, et al. Cost of healthcare for patients with migraine in five European countries: results from the International Burden of Migraine Study (IBMS). *J Headache Pain*. 2012;13(5):361-78.
46. Hawkins K, Wang S, Rupnow MF. Indirect cost burden of migraine in the United States. *J Occup Environ Med*. 2007;49(4):368-74.
47. Headache Classification Committee of the International Headache Society (IHS) The International Classification of Headache Disorders, 3rd edition. *Cephalalgia*. 2018;38(1):1-211.
48. Eikermann-Haerter K, Lee JH, Yalcin N, Yu ES, Daneshmand A, Wei Y, et al. Migraine Prophylaxis, Ischemic Depolarizations, and Stroke Outcomes in Mice. *Stroke*. 2015;46(1):229-36.
49. De Fusco M, Marconi R, Silvestri L, Atorino L, Rampoldi L, Morgante L, et al. Haploinsufficiency of ATP1A2 encoding the Na⁺/K⁺ pump alpha 2 subunit associated with familial hemiplegic migraine type 2. *Nat Genet*. 2003;33(2):192-6.
50. Dichgans M, Freilinger T, Eckstein G, Babini E, Lorenz-Depiereux B, Biskup S, et al. Mutation in the neuronal voltage-gated sodium channel SCN1A in familial hemiplegic migraine. *Lancet*. 2005;366(9483):371-7.
51. Pietrobon D. Calcium channels and migraine. *Bba-Biomembranes*. 2013;1828(7):1655-65.
52. Mulleners WM, Chronicle EP, Vredeveld JW, Koehler PJ. Visual cortex excitability in migraine before and after valproate prophylaxis: a pilot study using TMS. *Eur J Neurol*. 2002;9(1):35-40.
53. Zhang X, Velumian AA, Jones OT, Carlen PL. Modulation of high-voltage-activated calcium channels in dentate granule cells by topiramate. *Epilepsia*. 2000;41 Suppl 1:S52-60.
54. Ayata C, Jin HW, Kudo C, Dalkara T, Moskowitz MA. Suppression of cortical spreading depression in migraine prophylaxis. *Ann Neurol*. 2006;59(4):652-61.

55. vanderKamp W, VandenBrink AM, Ferrari MD, vanDijk JG. Interictal cortical excitability to magnetic stimulation in familial hemiplegic migraine. *Neurology*. 1997;48(5):1462-4.
56. Brighina F, Bolognini N, Cosentino G, Maccora S, Paladino P, Baschi R, et al. Visual cortex hyperexcitability in migraine in response to sound-induced flash illusions. *Neurology*. 2015;84(20):2057-61.
57. Mulleners WM, Chronicle EP, Palmer JE, Koehler PJ, Vredeveld JW. Visual cortex excitability in migraine with and without aura. *Headache*. 2001;41(6):565-72.
58. Thomsen LL, Ostergaard E, Olesen J, Russell MB. Evidence for a separate type of migraine with aura - Sporadic hemiplegic migraine. *Neurology*. 2003;60(4):595-601.
59. Catterall WA. Structure and function of neuronal Ca²⁺ channels and their role in neurotransmitter release. *Cell Calcium*. 1998;24(5-6):307-23.
60. Adams PJ, Rungta RL, Garcia E, van den Maagdenberg AMJM, MacVicar BA, Snutch TP. Contribution of calcium-dependent facilitation to synaptic plasticity revealed by migraine mutations in the P/Q-type calcium channel. *P Natl Acad Sci USA*. 2010;107(43):18694-9.
61. Stam AH, Luijckx GJ, Poll-The BT, Ginjaar IB, Frants RR, Haan J, et al. Early seizures and cerebral oedema after trivial head trauma associated with the CACNA1A S218L mutation. *J Neurol Neurosurg Ps*. 2009;80(10):1125-9.
62. Tavraz NN, Friedrich T, Durr KL, Koenderink JB, Bamberg E, Freilinger T, et al. Diverse Functional Consequences of Mutations in the Na⁺/K⁺-ATPase alpha(2)-Subunit Causing Familial Hemiplegic Migraine Type 2. *J Biol Chem*. 2008;283(45):31097-106.
63. Pisano T, Spiller S, Mei D, Guerrini R, Cianchetti C, Friedrich T, et al. Functional characterization of a novel C-terminal ATP1A2 mutation causing hemiplegic migraine and epilepsy. *Cephalalgia*. 2013;33(16):1302-10.
64. D'Ambrosio R, Gordon DS, Winn HR. Differential role of KIR channel and Na⁺/K⁺-pump in the regulation of extracellular K⁺ in rat hippocampus. *J Neurophysiol*. 2002;87(1):87-102.
65. Riant F, De Fusco M, Aridon P, Ducros A, Ploton C, Marchelli F, et al. ATP1A2 mutations in 11 families with familial hemiplegic migraine. *Hum Mutat*. 2005;26(3):281.
66. Vanmolkot KR, Kors EE, Turk U, Turkdogan D, Keyser A, Broos LA, et al. Two de novo mutations in the Na, K-ATPase gene ATP1A2 associated with pure familial hemiplegic migraine. *Eur J Hum Genet*. 2006;14(5):555-60.
67. Echenne B, Ducros A, Rivier F, Joutel A, Humbertclaude V, Roubertie A, et al. Recurrent episodes of coma: An unusual phenotype of familial hemiplegic migraine with linkage to chromosome 1. *Neuropediatrics*. 1999;30(4):214-7.
68. Spadaro M, Ursu S, Lehmann-Horn F, Liana V, Giovanni A, Paola G, et al. A G301R Na(+)/K(+)-ATPase mutation causes familial hemiplegic migraine type 2 with cerebellar signs. *Neurogenetics*. 2004;5(3):177-85.
69. Jurkat-Rott K, Freilinger T, Dreier JP, Herzog J, Gobel H, Petzold GC, et al. Variability of familial hemiplegic migraine with novel A1A2 Na⁺/K⁺-ATPase variants. *Neurology*. 2004;62(10):1857-61.
70. Vanmolkot KRJ, Kors EE, Hottenga JJ, Terwindt GM, Haan J, Hoefnagels WAJ, et al. Novel mutations in the Na⁺,K⁺-ATPase pump gene ATP1A2 associated

with familial hemiplegic migraine and benign familial infantile convulsions. *Ann Neurol.* 2003;54(3):360-6.

71. Castro MJ, Stam AH, Lemos C, de Vries B, Vanmolkot KR, Barros J, et al. First mutation in the voltage-gated Nav1.1 subunit gene SCN1A with co-occurring familial hemiplegic migraine and epilepsy. *Cephalalgia.* 2009;29(3):308-13.
72. Vahedi K, Depienne C, Le Fort D, Riant F, Chaine P, Trouillard O, et al. Elicited repetitive daily blindness A new phenotype associated with hemiplegic migraine and SCN1A mutations. *Neurology.* 2009;72(13):1178-83.
73. Parihar R, Ganesh S. The SCN1A gene variants and epileptic encephalopathies. *J Hum Genet.* 2013;58(9):573-80.
74. Cestele S, Labate A, Rusconi R, Tarantino P, Mumoli L, Franceschetti S, et al. Divergent effects of the T1174S SCN1A mutation associated with seizures and hemiplegic migraine. *Epilepsia.* 2013;54(5):927-35.
75. Kahlig KM, Rhodes TH, Pusch M, Freilinger T, Pereira-Monteiro JM, Ferrari MD, et al. Divergent sodium channel defects in familial hemiplegic migraine. *P Natl Acad Sci USA.* 2008;105(28):9799-804.
76. Pietrobon D, Moskowitz MA. Pathophysiology of Migraine. *Annu Rev Physiol.* 2013;75:365-91.
77. Nosedà R, Burstein R. Migraine pathophysiology: Anatomy of the trigeminovascular pathway and associated neurological symptoms, cortical spreading depression, sensitization, and modulation of pain. *Pain.* 2013;154:S44-S53.
78. van den Maagdenberg AMJM, Pizzorusso T, Kaja S, Terpolilli N, Shapovalova M, Hoebeek FE, et al. High Cortical Spreading Depression Susceptibility and Migraine-Associated Symptoms in Ca(V)2.1 S218L Mice. *Ann Neurol.* 2010;67(1):85-98.
79. Eikermann-Haerter K, Baum MJ, Ferrari MD, van den Maagdenberg AMJM, Moskowitz MA, Ayata C. Androgenic Suppression of Spreading Depression in Familial Hemiplegic Migraine Type 1 Mutant Mice. *Ann Neurol.* 2009;66(4):564-8.
80. Eikermann-Haerter K, Ayata C. Cortical Spreading Depression and Migraine. *Curr Neurol Neurosci.* 2010;10(3):167-73.
81. Vecchia D, Tottene A, van den Maagdenberg AMJM, Pietrobon D. Mechanism underlying unaltered cortical inhibitory synaptic transmission in contrast with enhanced excitatory transmission in Ca(V)2.1 knockin migraine mice. *Neurobiol Dis.* 2014;69:225-34.
82. Vecchia D, Tottene A, van den Maagdenberg AMJM, Pietrobon D. Abnormal cortical synaptic transmission in Ca(V)2.1 knockin mice with the S218L missense mutation which causes a severe familial hemiplegic migraine syndrome in humans. *Front Cell Neurosci.* 2015;9.
83. Dilekoz E, Houben T, Eikermann-Haerter K, Balkaya M, Lenselink AM, Whalen MJ, et al. Migraine Mutations Impair Hippocampal Learning Despite Enhanced Long-Term Potentiation. *J Neurosci.* 2015;35(8):3397-402.
84. Mathew R, Andreou AP, Chami L, Bergerot A, van den Maagdenberg AMJM, Ferrari MD, et al. Immunohistochemical characterization of calcitonin gene-related peptide in the trigeminal system of the familial hemiplegic migraine 1 knock-in mouse. *Cephalalgia.* 2011;31(13):1368-80.
85. Fioretti B, Catacuzzeno L, Sforna L, Gerke-Duncan MB, van den Maagdenberg AMJM, Franciolini F, et al. Trigeminal ganglion neuron subtype-

- specific alterations of CaV2.1 calcium current and excitability in a Cacna1a mouse model of migraine. *J Physiol-London*. 2011;589(23):5879-95.
86. Ceruti S, Villa G, Fumagalli M, Colombo L, Magni G, Zanardelli M, et al. Calcitonin Gene-Related Peptide-Mediated Enhancement of Purinergic Neuron/Glia Communication by the Allogenic Factor Bradykinin in Mouse Trigeminal Ganglia from Wild-Type and R192Q Ca(v)2.1 Knock-In Mice: Implications for Basic Mechanisms of Migraine Pain. *J Neurosci*. 2011;31(10):3638-49.
87. Eikermann-Haerter K, Arbel-Ornath M, Yalcin N, Yu ES, Kuchibhotla KV, Yuzawa I, et al. Abnormal synaptic Ca²⁺ homeostasis and morphology in cortical neurons of familial hemiplegic migraine type 1 mutant mice. *Ann Neurol*. 2015;78(2):193-210.
88. Shyti R, Eikermann-Haerter K, van Heiningen SH, Meijer OC, Ayata C, Joels M, et al. Stress hormone corticosterone enhances susceptibility to cortical spreading depression in familial hemiplegic migraine type 1 mutant mice. *Exp Neurol*. 2015;263:214-20.
89. Klychnikov OI, Li KW, Sidorov IA, Loos M, Spijker S, Broos LAM, et al. Quantitative cortical synapse proteomics of a transgenic migraine mouse model with mutated Ca(v)2.1 calcium channels. *Proteomics*. 2010;10(13):2531-5.
90. Di Guilmi MN, Wang TT, Inchauspe CG, Forsythe ID, Ferrari MD, van den Maagdenberg AMJM, et al. Synaptic Gain-of-Function Effects of Mutant Ca(v)2.1 Channels in a Mouse Model of Familial Hemiplegic Migraine Are Due to Increased Basal [Ca²⁺]_i. *J Neurosci*. 2014;34(21):7047-58.
91. Inchauspe CG, Urbano FJ, Di Guilmi MN, Ferrari MD, van den Maagdenberg AMJM, Forsythe ID, et al. Presynaptic Ca(v)2.1 calcium channels carrying familial hemiplegic migraine mutation R192Q allow faster recovery from synaptic depression in mouse calyx of Held. *J Neurophysiol*. 2012;108(11):2967-76.
92. Inchauspe CG, Urbano FJ, Di Guilmi MN, Forsythe ID, Ferrari MD, van den Maagdenberg AMJM, et al. Gain of Function in FHM-1 Ca(v)2.1 Knock-In Mice Is Related to the Shape of the Action Potential. *J Neurophysiol*. 2010;104(1):291-9.
93. Shu YS, Hasenstaub A, McCormick DA. Turning on and off recurrent balanced cortical activity. *Nature*. 2003;423(6937):288-93.
94. Hullugundi SK, Ansuini A, Ferrari MD, van den Maagdenberg AMJM, Nistri A. A Hyperexcitability Phenotype in Mouse Trigeminal Sensory Neurons Expressing the R192q Cacna1a Missense Mutation of Familial Hemiplegic Migraine Type-1. *Neuroscience*. 2014;266:244-54.
95. Franceschini A, Vilotti S, Ferrari MD, van den Maagdenberg AMJM, Nistri A, Fabbretti E. TNF alpha Levels and Macrophages Expression Reflect an Inflammatory Potential of Trigeminal Ganglia in a Mouse Model of Familial Hemiplegic Migraine. *Plos One*. 2013;8(1).
96. Eising E, Shyti R, 't Hoen PAC, Vijfhuizen LS, Huisman SMH, Broos LAM, et al. Cortical Spreading Depression Causes Unique Dysregulation of Inflammatory Pathways in a Transgenic Mouse Model of Migraine. *Mol Neurobiol*. 2017;54(4):2986-96.
97. Wang IM, Zhang B, Yang X, Zhu J, Stepaniants S, Zhang CS, et al. Systems analysis of eleven rodent disease models reveals an inflammatome signature and key drivers. *Mol Syst Biol*. 2012;8.
98. Nair A, Simonetti M, Birsa N, Ferrari MD, van den Maagdenberg AMJM, Giniatullin R, et al. Familial hemiplegic migraine Ca(V)2.1 channel mutation R192Q

- enhances ATP-gated P2X₃ receptor activity of mouse sensory ganglion neurons mediating trigeminal pain. *Mol Pain*. 2010;6.
99. Franceschini A, Hullugundi SK, van den Maagdenberg AMJM, Nistri A, Fabbretti E. Effects of LPS on P2X₃ receptors of trigeminal sensory neurons and macrophages from mice expressing the R192Q Cacna1a gene mutation of familial hemiplegic migraine-1. *Purinerg Signal*. 2013;9(1):7-13.
100. Franceschini A, Nair A, Bele T, van den Maagdenberg AMJM, Nistri A, Fabbretti E. Functional crosstalk in culture between macrophages and trigeminal sensory neurons of a mouse genetic model of migraine. *Bmc Neurosci*. 2012;13.
101. Alle H, Roth A, Geiger JR. Energy-efficient action potentials in hippocampal mossy fibers. *Science*. 2009;325(5946):1405-8.
102. Rolfe DF, Brown GC. Cellular energy utilization and molecular origin of standard metabolic rate in mammals. *Physiol Rev*. 1997;77(3):731-58.
103. Dreier JP. The role of spreading depression, spreading depolarization and spreading ischemia in neurological disease. *Nat Med*. 2011;17(4):439-47.
104. Kraig RP, Nicholson C. Extracellular ionic variations during spreading depression. *Neuroscience*. 1978;3(11):1045-59.
105. Canals S, Makarova I, Lopez-Aguado L, Largo C, Ibarz JM, Herreras O. Longitudinal depolarization gradients along the somatodendritic axis of CA1 pyramidal cells: a novel feature of spreading depression. *J Neurophysiol*. 2005;94(2):943-51.
106. Leão AAP. Spreading depression of activity in the cerebral cortex. *J Neurophysiol*. 1944;7:359-90.
107. Takano T, Tian GF, Peng W, Lou N, Lovatt D, Hansen AJ, et al. Cortical spreading depression causes and coincides with tissue hypoxia. *Nat Neurosci*. 2007;10(6):754-62.
108. Kager H, Wadman WJ, Somjen GG. Conditions for the triggering of spreading depression studied with computer simulations. *J Neurophysiol*. 2002;88(5):2700-12.
109. Leao AA. Further observations on the spreading depression of activity in the cerebral cortex. *J Neurophysiol*. 1947;10(6):409-14.
110. Zhang XC, Levy D, Kainz V, Nosedá R, Jakubowski M, Burstein R. Activation of Central Trigeminal Vascular Neurons by Cortical Spreading Depression. *Ann Neurol*. 2011;69(5):855-65.
111. Yang H, Wang H, Czura CJ, Tracey KJ. The cytokine activity of HMGB1. *J Leukoc Biol*. 2005;78(1):1-8.
112. Zhang CC, Krieg S, Shapiro DJ. HMG-1 stimulates estrogen response element binding by estrogen receptor from stably transfected HeLa cells. *Mol Endocrinol*. 1999;13(4):632-43.
113. Maroso M, Balosso S, Ravizza T, Liu J, Aronica E, Iyer AM, et al. Toll-like receptor 4 and high-mobility group box-1 are involved in ictogenesis and can be targeted to reduce seizures. *Nat Med*. 2010;16(4):413-U91.
114. Qiu J, Nishimura M, Wang Y, Sims JR, Qiu S, Savitz SI, et al. Early release of HMGB-1 from neurons after the onset of brain ischemia. *J Cereb Blood Flow Metab*. 2008;28(5):927-38.
115. Wang H, Bloom O, Zhang M, Vishnubhakat JM, Ombrellino M, Che J, et al. HMG-1 as a late mediator of endotoxin lethality in mice. *Science*. 1999;285(5425):248-51.

116. Mogensen TH. Pathogen recognition and inflammatory signaling in innate immune defenses. *Clin Microbiol Rev.* 2009;22(2):240-73, Table of Contents.
117. Gilmore TD. Introduction to NF-kappa B: players, pathways, perspectives. *Oncogene.* 2006;25(51):6680-4.
118. Perkins ND. Integrating cell-signalling pathways with NF-kappaB and IKK function. *Nat Rev Mol Cell Biol.* 2007;8(1):49-62.
119. Barnes PJ. Nuclear factor-kappa B. *Int J Biochem Cell Biol.* 1997;29(6):867-70.
120. O'Connor KA, Hansen MK, Pugh CR, Deak MM, Biedenkapp JC, Milligan ED, et al. Further characterization of high mobility group box 1 (HMGB1) as a proinflammatory cytokine: central nervous system effects. *Cytokine.* 2003;24(6):254-65.
121. Faraco G, Fossati S, Bianchi ME, Patrone M, Pedrazzi M, Sparatore B, et al. High mobility group box I protein is released by neural cells upon different stresses and worsens ischemic neurodegeneration in vitro and in vivo. *J Neurochem.* 2007;103(2):590-603.
122. Qiu J, Nishimura M, Wang Y, Sims JR, Qiu S, Savitz SI, et al. Early release of HMGB-1 from neurons after the onset of brain ischemia. *J Cerebr Blood F Met.* 2008;28(5):927-38.
123. Hayakawa K, Qiu JH, Lo EH. Biphasic actions of HMGB1 signaling in inflammation and recovery after stroke. *Ann Ny Acad Sci.* 2010;1207:50-7.
124. Asano T, Ichiki K, Koizumi S, Kaizu K, Hatori T, Mashiko K, et al. High Mobility Group Box 1 in Cerebrospinal Fluid From Several Neurological Diseases at Early Time Points. *Int J Neurosci.* 2011;121(8):480-4.
125. Sokol B, Wozniak A, Jankowski R, Jurga S, Wasik N, Shahid H, et al. HMGB1 Level in Cerebrospinal Fluid as a Marker of Treatment Outcome in Patients with Acute Hydrocephalus Following Aneurysmal Subarachnoid Hemorrhage. *J Stroke Cerebrovasc Dis.* 2015;24(8):1897-904.
126. Walker LE, Frigerio F, Ravizza T, Ricci E, Tse K, Jenkins RE, et al. Molecular isoforms of high-mobility group box 1 are mechanistic biomarkers for epilepsy. *J Clin Invest.* 2017;127(6):2118-32.
127. Dehghani A, Karatas H, Can A, Erdemli E, Yemisci M, Eren-Kocak E, et al. Nuclear expansion and pore opening are instant signs of neuronal hypoxia and can identify poorly fixed brains. *Sci Rep.* 2018;8(1):14770.
128. Somjen GG. Mechanisms of spreading depression and hypoxic spreading depression-like depolarization. *Physiol Rev.* 2001;81(3):1065-96.

ADDITORY**Add-1: Ethical Approval-1**

T.C.
HACETTEPE ÜNİVERSİTESİ
Hayvan Deneyleri Yerel Etik Kurulu

Sayı : 52338575 -89

HAYVAN DENEYLERİ YEREL ETİK KURUL KARARI

TOPLANTI TARİHİ	: 29.08.2016 (PAZARTESİ)
TOPLANTI SAYISI	: 2016/06
DOSYA KAYIT NUMARASI	: 2016/42
KARAR NUMARASI	: 2016/42 - 3
ARAŞTIRMA YÜRÜTÜCÜSÜ	: Doç. Dr. Hülya Karataş KURŞUN
HAYVAN DENEYLERİNDEN SORUMLU ARAŞTIRMACI	: Doç. Dr. Hülya Karataş KURŞUN, Anisa Dehghani, Buket Dönmez DEMİR
YARDIMCI ARAŞTIRMACILAR	: Prof. Dr. Turgay DALKARA, Sinem Yılmaz ÖZCAN
ONAYLANAN HAYVAN TÜRÜ ve SAYISI	: 72 Adet Swiss Albino (25-30 g), 24 Adet C57 (25-30 g), 38 Adet Transgenik (25-30 g)

Üniversitemiz Tıp Fakültesi Nörolojik Bilimler ve Psikiyatri Enstitüsü öğretim üyelerinden Doç. Dr. Hülya Karataş KURŞUN' un araştırma yürütücüsü olduğu 2016/42 kayıt numaralı "*Inflammasome Activation Is Increased In Familial Hemiplegic Migraine Type1 Transgenic Mouse Model After Cortical Spreading Depression*" isimli çalışma Hayvan Deneyleri Yerel Etik Kurulu Yönergesi'ne göre uygun bulunarak oy birliği ile onaylanmasına karar verilmiştir.

Sorumlu araştırmacı deneylere başlangıç tarihini Etik Kurula bildirmekle yükümlüdür.

Prof. Dr. Mehmet Ali ONUR
Etik Kurul Başkanı V.

Add-2: Ethical Approval-2



T.C.
HACETTEPE ÜNİVERSİTESİ
Hayvan Deneyleri Yerel Etik Kurulu

Sayı : 52338575 -111

HAYVAN DENEYLERİ YEREL ETİK KURUL KARARI

TOPLANTI TARİHİ : 18.09.2018 (SALI)
TOPLANTI SAYISI : 2018/09
DOSYA KAYIT NUMARASI : 2018/57
KARAR NUMARASI : 2018/57 – 07
ARAŞTIRMA YÜRÜTÜCÜSÜ : Doç. Dr. Hülya Karataş KURŞUN
HAYVAN DENEYLERİNDE : Anisa DEHGHANI, Doç. Dr. Hülya Karataş
GÖREVLİ ARAŞTIRMACILAR : KURŞUN, Dr. Buket Nebiye DEMİR, Dr. Sinem
Yılmaz ÖZCAN
DİĞER YARDIMCI : Prof. Dr. Turgay DALKARA
ARAŞTIRMACILAR :
ONAYLANAN HAYVAN TÜRÜ ve : 24 Adet C57 Fare (25-30g)
SAYISI :

Üniversitemiz Nörolojik Bilimler ve Psikiyatri Enstitüsü öğretim üyelerinden Doç. Dr. Hülya Karataş KURŞUN'un araştırma yürütücüsü olduğu 2018/57 kayıt numaralı "*Familiyal Hemiplejik Migren Tip 1 S218L Transgenik Farede Kortikal Yayılan Depresyona Bağlı İnflamasyon Aktivasyonu*" isimli çalışma Hayvan Deneyleri Yerel Etik Kurulu Yönergesi'ne göre uygun bulunarak oy birliği ile onaylanmasına karar verilmiştir.

Araştırma yürütücüsü Kurulumuza araştırma projesinin bitiş tarihini bildirmek ve proje sonuç raporunu sunmak ile yükümlüdür.

Prof. Dr. Nüket Örnek BÜKEN
Etik Kurul Başkan Vekili

Add-3: Turnitin Ekran görüntüsü

Doküman Görüntüleyici

Turnitin Orijinallik Raporu

İşleme kondu: 15-Oca-2019 11:16 +03
 NUMARA: 1064323062
 Kelime Sayısı: 26367
 Gönderildi: 1

Benzerlik Endeksi	Kaynağa göre Benzerlik
%14	İnternet Sources: %10 Yayınlar: %9 Öğrenci Ödevleri: %1

PARENCHYMAL NEUROINFLAMMATION IN FAMILIAL HEM... Anisa Dehghani Mohammadi tarafından

alintıları çıkar bibliyografyayı dahil et 1% > eşleşmeleri çıkar İndir yenile yazdır

nod: raporlu hızlı görüntüle (klasik)

4% match (yayınlar)	✕
Shih-Pin Chen, Else A Tolner, Katharina Eikermann-Haerter. "Animal models of monogenic migraine", Cephalalgia, 2016	
4% match (02-Kas-2015 tarihli internet)	✕
http://e-collection.library.ethz.ch	
1% match (yayınlar)	✕
Kivilcim Kilic, Hulya Karatas, Buket Dönmez-Demir, Emine Eren-Kocak et al. "Inadequate brain glycogen or sleep increases spreading depression susceptibility", Annals of Neurology, 2018	
1% match (14-Oca-2019 tarihli internet)	✕
https://repository.tudelft.nl/islandora/object/uuid:eeffef50-8828-4fc3-b4e8-89a51715a20c/datastream/OBJ/download	
1% match (04-Mar-2015 tarihli internet)	✕
http://www.ncbi.nlm.nih.gov	
1% match (08-May-2016 tarihli internet)	✕
http://journal.frontiersin.org	
1% match (yayınlar)	✕
Michel D Ferrari, Roselin R Klever, Gisela M Terwindt, Cenk Ayata, Arn M J M van den Maagdenberg. "Migraine pathophysiology: lessons from mouse models and human genetics". The Lancet Neurology, 2015	

Add-4: Digital Makbuz



Dijital Makbuz

Bu makbuz ödevinizin Turnitin'e ulaştığını bildirmektedir. Gönderiminize dair bilgiler şöyledir:

Gönderinizin ilk sayfası aşağıda gönderilmektedir.

Gönderen: Anisa Dehghani Mohammadi
 Ödev başlığı: PARENCHYMAL NEUROINFLAMMA...
 Gönderi Başlığı: PARENCHYMAL NEUROINFLAMMA...
 Dosya adı: Anisa_DM_Ph.D._Thesis_afterdef...
 Dosya boyutu: 28.7M
 Sayfa sayısı: 125
 Kelime sayısı: 26,367
 Karakter sayısı: 150,108
 Gönderim Tarihi: 15-Oca-2019 11:06AM (UTC+0300)
 Gönderim Numarası: 1064323062



Academic CV

MSc thesis, Baha'i Institute for Higher Education (BIHE), Tehran, Iran

Memory & Learning after Temporal Lobe Surgery: Effects of hemispheric side and extent of surgical removal.

Supervisor: Professor Faraneh Vargha-Khadem, University College London, London, UK

BSc thesis, BIHE

The effect of water pollution on the population of Ephemeroptera (mayfly) larvae as a bio-indicator, in Darband River in Tehran; and identification to the genus stage.

Supervisor: Dr. Naim Khazei, BIHE, Tehran

Education and qualifications

- | | |
|-----------|---|
| 2014-2018 | Basic Neuroscience, PhD, Hacettepe University Medical School, Institute of Neurological Sciences and Psychiatry, Ankara, Turkey |
| 2010-2013 | Neuroscience, MSc, BIHE, Tehran, Iran |
| 2009 | Completion of the Internship Connections program of AED/CIEV in South Africa. This program is an exchange program that aims to build technical, leadership, and management skills of young professional working in social services such as health, children's issues and poverty alleviation. |
| 2008 | Completion of DSA (Discourse on Social Action) Program in India. |
| 2002-2007 | Biology, BSc, BIHE, Tehran, Iran |

Teaching experience

Teaching assistant

- | | |
|-----------|--|
| 2011-2013 | “Evolution”, Department of Biology, BIHE, Tehran, Iran |
| 2009 | “Neuroscience”, Department of Biology, Neuroscience master program, BIHE, Tehran, Iran |
| 2007-2008 | “Embryology”, Department of Biology, BIHE, Tehran, Iran |
| 2006-2007 | “Histology laboratory techniques”, Department of Biology, BIHE, Tehran, Iran |

Tutorship

- | | |
|------------|--|
| 2009, 2012 | Discourse on social Action, BIHE, Tehran, Iran |
|------------|--|

Work experience

2014-present Full-time PhD student Dalkara lab. Neuroscience program, Institute of Neurological Sciences and Psychiatry, Hacettepe University, Ankara, Turkey

Voluntary works

2010 Voluntary work in Identification and Classification Center of Butterflies in Insect Museum of Agricultural and Health Ministry, Tehran, Iran

2007-2009 Women Society for Protesting Against Environment Pollution, Tehran, Iran

2007-2010 A Better World for Children NGO, Child Labor, Tehran, Iran

2006-2007 Institute for Cancerous Children (MAHAK), Tehran, Iran

Skills

- 1- *In vivo* stereotaxic craniotomy and surgery in rodents
- 2- *In vivo* electrophysiology
- 3- Intra-cerebro-ventricular (i.c.v) injection
- 4- Intra-cortical (i.c.) injection
- 5- Cerebrospinal fluid collection from cisterna magna and i.c.v. cannula
- 6- Different sectioning methods for cryopreserved frozen sections, free floating sections and paraffin embedded sections
- 7- Immunohistochemistry and Western blotting
- 8- Bright-field, phase-contrast, fluorescent, and laser-scanning confocal microscopy
- 9- Scoring Pain Grimace Scale (PGS) in mice
- 10- Working knowledge to use ImageJ, cell quantification and signal analysis

Awards & Achievements

- International Headache Society (IHS) fellowship award 2018, to do a postdoc in Leiden University Medical School
- 31st International League Against Epilepsy (ILAE) Young Investigator's Awards, 5-9 September 2015, Istanbul, Turkey

Forthcoming Publication

- Parenchymal neuroinflammation in FHM1 mouse model after CSD (Ready to be submitted)
- Mice pain behavior with artificial intelligence (Ready to be submitted)

- Familial Hemiplegic Migraine mouse models for studying migraine pathophysiology, A Review (Ready to be submitted)

Publications and conference presentations

Dehghani A, Karatas H, Can A, Erdemli E, Yemisci M, Eren-Kocak E, Dalkara T. Nuclear expansion and pore opening are instant signs of neuronal hypoxia and can identify poorly fixed brains. *Scientific Reports*. 2018 Oct 3; 8 (1):14770.doi: 10.1038/s41598-018-32878-1. PMID: 30282977

A. Dehghani, E. Isaacs, A.I. Della Rocchetta, G. Pitts, C.E. Polkey, M. Mishkin, F. Vargha-Khadem. Memory and Learning after Temporal Lobe Surgery: Effects of Hemispheric sides and extent of surgical removal. 31th International Epilepsy Congress, 2015 September. *Epilepsia*, Volume 56, p3–263, IssueS1, 2015. DOI:10.1111/epi.13241

Anisa Dehghani, Hülya Karataş-Kurşun, Alp Can, Müge Yemişçi-Ozkan, Emine Eren-Kocak, Turgay Dalkara. Investigation of a Marker for the Quality of Transcardial Perfusion in Frozen Brain Section in Mice. Oral presentation at: National Neuroscience Congress, May 7-10; 2017; Sakarya, Turkey.

Anisa Dehghani, Hülya Karataş-Kurşun, Alp Can, Müge Yemişçi-Ozkan, Emine Eren-Kocak, Turgay Dalkara. Fluorescent biomarkers as reporters of poor quality transcardial perfusion-fixation in frozen brain sections: A much needed tool for experimental neuroscience. *Staining and Imaging Techniques*, poster#436.03. 2017 Neuroscience Meeting Planner. Washington, DC: Society for Neuroscience (SFN), 2017. Online.
